[redacted]

[redacted]

Westinghouse Advanced Reactors Division

[redacted]

P-1417

DISCLAIMER

WARD-4135-13
UC-25 Metals, Ceramics, and Materials

MASTER

OXIDE FUEL ELEMENT DEVELOPMENT

QUARTERLY PROGRESS REPORT

FOR THE PERIOD ENDING SEPTEMBER 30, 1970

Approved by: A. Boltax
A. Boltax
Principal Investigator

P. Murray
Project Manager
P. Murray

Contract AT(30-1)-4135
U. S. Atomic Energy Commission

Submitted to AEC-NYOO in January 1971

Westinghouse Electric Corporation
Advanced Reactors Division
P. O. Box 158
Madison, Pennsylvania 15663

Printed in the United States of America
Available from
National Technical Information Service
Springfield, Virginia 22151
Price: Printed Copy $3.00; Microfiche $0.65

CONTENTS

CONTENTS (CONTINUED)

CONTENTS (CONTINUED)

CONTENTS (CONTINUED)

LIST OF FIGURES

LIST OF FIGURES (CONTINUED)

LIST OF FIGURES (CONTINUED)

LIST OF TABLES

LIST OF TABLES (CONTINUED)

SECTION 1
INTRODUCTION

1.0 GENERAL

This is the ninth quarterly progress report and covers the work performed during the first quarter of FY-1971.

2.0 SUMMARY OF OBJECTIVES

The overall program approach is to conduct parallel analytical and experimental studies on mixed-oxide fuel pins with close liaison and feedback between the two activities. In the analytical work, the initial efforts will be directed to compiling all pertinent data on the irradiation behavior of austenitic stainless steel cladding, mixed-oxide fuel pins. A similar effort will be directed toward compiling data on the behavior of Type 316 austenitic stainless steel cladding - in particular on high-burnup fuel pins. These data will be analyzed by current theoretical models, and where required, new models and computer codes will be devised. These analytical techniques will be used to provide the technical basis for the experimental irradiation programs. This procedure, in turn, will permit reliable parametric studies of design variables of interest to FFTF and LMFBR.

3.0 SUMMARY OF PRIOR WORK

All work related to the present investigations and performed prior to the present period has been fully reported in:

WARD-3791-28 "Oxide Fuel Element Development Quarterly Progress Report for the Period Ending September 30, 1968."

WARD-3791-32 "Oxide Fuel Element Development Quarterly Progress Report for the Period Ending December 31, 1968."

WARD-3791-37 "Oxide Fuel Element Development Quarterly Progress Report for the Period Ending March 31, 1969."

WARD-3791-39 "Oxide Fuel Element Development Quarterly Progress Report for the Period Ending June 30, 1969."

WARD-4135-1 "Oxide Fuel Element Development Quarterly Progress Report for the Period Ending September 30, 1969."

WARD-4135-4 "Oxide Fuel Element Development Quarterly Progress Report for the Period Ending December 31, 1969."

WARD-4135-8 "Oxide Fuel Element Development Quarterly Progress Report for the Period Ending March 31, 1970."

WARD-4135-11 "Oxide Fuel Element Development Quarterly Progress Report for the Period Ending June 30, 1970."

4.0 SUMMARY OF CURRENT PROGRESS

OFBA-210

Two additional models were incorporated into the OLYMPUS-II code. The models permit calculation of the cladding strain upon heat-up as a result of differential thermal expansion of the cladding and fuel and the cladding deformation controlled by fuel swelling when the fuel reaches a limiting hot-pressing density. Detailed analysis of the EBR-II pin F2H was conducted using the OLYMPUS-II A code. Studies of the effects of neutron spectrum on irradiation-induced creep and cladding swelling were initiated.

OFBA-211

The CYGRO-F code was modified to include irradiation-induced creep effects in the stainless steel cladding. The modified code was used to examine the effects of irradiation-induced creep on total diametral strain, internal stress relaxation, and the amount of thermal creep strain. Preliminary results indicate that the code is performing satisfactorily. Detailed comparisons of CYGRO-F and OLYMPUS-II results are being planned.

OFBA-310

A re-evaluation of the WSA-1 and -2 series fuel pins was completed using the OLYMPUS-IIB code. Preliminary design of the WSA-5 series fuel pins was completed and a request for "Approval-in-Principle" for irradiation in EBR-II was submitted to the AEC. The primary objective of the WSA-5 experiment is to obtain quantitative information on cladding strain mechanisms.

OFBA-311

The final design analyses for the WSA-3 subassembly have been completed and prepared for the data package to be submitted to the EBR-II Project. Recent work includes thermal, hydraulic, stress-strain, and safety analysis. Major experimental objectives for the WSA-4 subassembly have been identified and preliminary design work initiated. The WSA-3 mockup flow test assembly was shipped to the EBR-II site and was received in good condition.

OFBA-312

The bases for the choice of selected hot spot factors were reviewed and compared with the results of the subchannel analyses performed with the

COBRA code. Analyses were made of channel closing by simultaneous displacement (towards the center) of the rods forming a flow channel and of flow and temperature redistribution by modification of side channel flow resistance by changes in either the flow area or the grid support strap thickness.

Flow-induced vibration analyses were performed of the rod assembly with honeycomb grids for end-of-life-conditions. With the assumed grid span lengths, the maximum vibrational amplitude was found well below the allowable limit of 0.001 inch. The possible variation in rod spacing produced by tolerance stackup was examined and used as a basis for specifying the dimensional tolerances for the honeycomb grid. Maximum fuel rod bowing by the simultaneous effect of thermal gradients and axial loading was calculated and the margin of stability and the amount of channel closing determined. The amount of thermal ratcheting was calculated based on a strain analysis. The smallest margin of safety of 60% occurred near the core outlet.

A preliminary design was evolved for three capsules in one subassembly each containing about 12 grids and seven non-fuel carrying rods making up seven unit cells. Feasibility studies revealed no basic problems. A test description was written and submitted to Argonne National Laboratories (ANL) for comment.

OFBA-313

The fabrication of the fretting test 37-pin subassembly was completed. Details on the grid dimensions and fuel pin loading operations are described. The DFAT test section in the GPL-1 test cubicle was modified for the fretting test. Installation of the subassembly in the test section was completed and testing will begin in the next quarter.

OFBA-410

During the quarter 20 inner grid assemblies and support strap assemblies were fabricated for use in welding trials and the WSA-3 fuel assembly. Detailed procedures were prepared and issued to control fabrication operations. Liners and the inner can for WSA-3 have been machined and inspected. The dimensional stability of the liners and samples of the inner can was acceptable after three thermal cycles to 1100°F.

OFBA-411

All objectives related to grid fabrication for the WSA-3 fuel assembly have been accomplished. Hardware design for WSA-4 is being planned. The flow test objectives for WSA-3 have been completed. The results of the flow tests were evaluated and prepared for incorporation in the WSA-3 data package.

OFBA-510

Additional process investigations were performed to improve control of fuel fabrication. Large batches of pellets, approximately 1.6 kg quantities, were manufactured during the period with sufficient fuel being made to meet the WSA-3 requirements. Additonal PuO_2 and UO_2 were procured for future irradiation tests.

OFBA-511

Characterization of the raw materials for fuel to be used in WSA-5 was completed. Acceptance analyses for the plutonium nitrate and enriched uranium dioxide showed them to be satisfactory from a chemical standpoint. The progression of the methods of adjusting the O/M of large $(U,Pu)O_2$ fuel batches for WSA-3 was evaluated. With the fabrication route currently used, O/M gradients in the sintering boats are no longer a problem. Considerable effort was spent in evaluating the effects of different binder additions and pelletizing procedures on the sintered microstructures of pellets. A chemical etching technique was developed giving much clearer grain delineation than was previously possible. Detailed metallographic evaluation was completed on the high density fuel batches.

OFBA-512

All of the high density fuel pellets required for Group I and Group II experiments (24 pins) have passed all inspection requirements and are being fabricated into fuel pins. All 13 of the Group II pins have been fabricated and the 11 Group I pins will be completed by October 15. About half of the low density fuel pellets for Group III and Group IV experiments (21 pins) have been characterized and approved for loading. Xenon tagging has been successfully carried out on fuel pins. The process and procedure was witnessed and approved by EBR-II personnel.

OFBA-513

Density variation histograms have been constructed for 14 different fuel pellet batches. The dimensions and density of each of about 5300 pellets are key punched and pellet storage locations maintained. Computer generated information and listings have been supplied for use in pellet selection for pin loading.

SECTION 2

OFBA-110 PROJECT ADMINISTRATION

F. A. Brassart, W. B. Heubel, and P. Murray

1.0 OBJECTIVES

The objectives of this task are to assure that the project is successfully completed, on schedule within budget, and to the satisfaction of the Atomic Energy Commission; to assure compliance with contracted obligations; and to coordinate this project with other AEC-sponsored and Westinghouse-sponsored LMFBR development projects.

Overall project direction and day-to-day administration will be provided under this task. Plans and controls will be established and maintained; periodic reviews will be held with the Commission; correspondences and reports will be coordinated; and day-to-day technical and administrative liason with the Commission will be provided.

2.0 PRIOR WORK

Schedule 189a/Work Plans for FY-1971 were prepared and submitted to the New York Operations Office.

For FY-1971 administrative control, the project is divided into the following tasks:

OFBA-110	Project Administration
OFBA-210	Fuel Performance Analysis
OFBA-211	Improvement of Analytical Methods and Fuel Lifetime Codes
OFBA-310	Encapsulated Mixed-Oxide Fuel Pin Irradiation Tests
OFBA-311	Mixed-Oxide Irradiation Tests in Grid-Type Subassemblies
OFBA-312	217-Pin Grid-Type Fuel Assembly Design and Development
OFBA-313	Grid-Type Subassembly Development and Testing
OFBA-410	Fabrication Development of EBR-II Grid-Type Subassemblies
OFBA-411	Subassembly Design and Hardware
OFBA-510	Pellet Fabrication
OFBA-511	Fuel Characterization
OFBA-512	Fuel Element Fabrication
OFBA-513	Product Control and Documentation

3.0 CURRENT PROGRESS

Project administration and day-to-day liaison with the customer continued.

WARD-4135-6, the final report for FY-1970 Task OFBA-212 ("Design Limit and Transient Survival Testing of Fuel Element"), was prepared and distributed.

SECTION 3

OFBA-210 FUEL PERFORMANCE ANALYSIS

A. Biancheria, A. Boltax, F. Garner,
A. Rowcliffe, T. Soffa, and W. Wolfer

1.0 OBJECTIVES

The maximum utilization of expensive and limited irradiation test data is achieved by continuing analysis of the data. The objectives of this task are to provide analyses of the effects of irradiation on the properties and structure of cladding materials and the interrelationship of these processes with the stresses imposed by fuel swelling. The technical approach involves the development of analytical models and appropriate computer codes. The basic objective is to provide an understanding of the behavior of stainless steel cladding mixed-oxide fuel elements exposed to fast neutron flux.

2.0 PRIOR WORK

An analytical model for fission gas release was developed and correlated with experimental data. The effects of sodium corrosion and fuel cladding reactions were studied and analytical expressions prepared to describe cladding wastage. An expression for the stress-induced swelling of stainless steel was derived based on the growth of voids under stress. Computational procedures for all these models were incorporated into the OLYMPUS II code, resulting in two versions (OLYMPUS-II A and OLYMPUS-II B) which are identical except for the stress-induced swelling in OLYMPUS-II B.

3.0 CURRENT PROGRESS

3.1 OLYMPUS-II Development

Two additional models have been incorporated into the OLYMPUS-II code to account for the following phenomena:

1. Cladding strains upon heat-up of the fuel-pin as a result of differential thermal expansion of the cladding and fuel.

2. Cladding deformation controlled by fuel swelling which occurs when the fuel reaches a limiting hot-pressing density of approximately 98% or higher.

3.2 Calculation of Cladding Strains Upon Heat-Up

Three approaches were taken to calculate cladding strains on heat-up:

1. Hot-pressing of the fuel and cladding creep during the heat-up period.

2. Elastic compression of the fuel and elastic-plastic strain of the cladding.

3. Elastic-plastic compression of the fuel and elastic-plastic deformation of the cladding.

Calculations of cladding heat-up strains, based on the steady-state hot-pressing behavior of the fuel for heat-up periods of 10 to 100 hours at typical cladding operating temperatures, invariably resulted in cladding strains equal to the differential thermal expansion between the cladding and fuel. This model is considered too conservative and inadequate, because, essentially, no fuel deformation occurred.

In the second approach, the fuel is considered as an elastic body. The elastic modulus of the fuel is known as a function of porosity and temperature [1] ($UO_{2.00}$ properties are used in place of $(U,Pu)O_2$ fuel), and evaluated at the volumetric mean temperature of the fuel and the as-fabricated fuel porosity. The expression for the elastic modulus is given by:

$$E(T,Po) = \left\{ [32.0 - 1.45 \times 10^{-2} \; T] \; [1 - 2.27 \; Po] \right\} \; 10^6 \qquad (1)$$

where: T = Temperature (°C)

Po= Porosity Fraction

The elastic-plastic tensile properties of the cladding as a function of temperature are expressed in array form in a subroutine STRAIN. The method of solving for the strain imposed on the cladding by the fuel involves an iterative procedure to simultaneously solve the following equations for the equilibrium interfacial pressure, $P_{eq} = P_{ic} = P_{if}$.

$$P_{ic} = 2 \; t \; \sigma h \; (\varepsilon c, T)/d \qquad (2)$$

$$P_{if} = E(T,Po) \; \varepsilon f \qquad (3)$$

$$\varepsilon f + \varepsilon c = \left\{ \frac{RFH-RCH}{RCH} \right\} 100 \qquad (4)$$

where: d = inside diameter cladding

P_{ic} = interfacial cladding pressure

P_{if} = interfacial fuel pressure

t = cladding thickness

$\sigma h(\varepsilon c,T)$ = cladding hoop stress as a function of cladding strain and temperature

εf = fuel strain, %

εc = cladding strain, %

RFH = radius of the hot fuel

RCH = radius of the hot cladding

A sample calculation of the cladding strain on heat-up was made on a fuel pin which operated under the following hypothetical conditions:

Power Rating =	14 kw/ft
Cladding Temperature =	522°C
Pellet Density =	96.6%
Cladding =	solution-treated 316 stainless steel
Fuel Surface Temperature =	1010°C
Fuel Center Temperature =	2497°C
Cold Gap =	1 mil

The calculated strain in the cladding was 0.66% with 0.03% in the fuel.

A sample calculation of the cladding strain on heat-up was also made for the same conditions defined above except that the fuel was considered as an elastic-plastic body. The elastic-properties of the fuel were obtained from compressive tests [2] and are in array form in subroutine FSTRAIN. Using this method in the above example, the strain associated with the cladding was 0.375% and with the fuel 0.315%. Methods 2 and 3 are available for use in OLYMPUS II-A and II-B.

3.3 Calculation of Cladding Strains Controlled by Fuel Swelling

Analysis of EBR-II fuel pins of high fuel density and small cold gap, operating at high power levels (> 11 kw/ft), shows that the fuel is hot pressed to theoretical density early in life. At this point cladding strains are considered to be controlled by fuel swelling. The procedure for solving the stresses and strains associated with fuel swelling involves solving the fuel swelling rate and cladding strain rate equation simultaneously by an iterative technique.

The fuel swelling rate designated, FSR, in the diametral direction is equal to:

$$FSR = \frac{1}{2}\left[\left(\frac{\Delta V}{V}\right)_{FS} - \left(\frac{\Delta V}{V}\right)_{CS}/3 - \left(\frac{\Delta L}{L}\right)_{IC} - \left(\frac{\Delta L}{L}\right)_{TS}\right] \quad (5)$$

where: $\left(\frac{\Delta V}{V}\right)_{FS}$ = volumetric fuel swelling rate

$\left(\frac{\Delta V}{V}\right)_{CS}$ = volumetric cladding swelling rate

$\left(\frac{\Delta L}{L}\right)_{IC}$ = axial irradiation-induced creep rate of cladding

$\left(\frac{\Delta L}{L}\right)_{TS}$ = axial thermal strain rate of cladding

The total cladding deformation in the axial direction is considered small and is neglected. Future studies will account for axial deformation and its effect on the diametral fuel swelling rate.

Cladding deformation in the diametral direction consists of three components:

1. Cladding swelling (with or without stress-enhanced swelling)
2. Irradiation-induced creep
3. Thermal deformation

The cladding strain rate, designated by CSR, is given by:

$$CSR = \left(\frac{\Delta D}{D}\right)_{CS} + \left(\frac{\Delta D}{D}\right)_{IC} + \left(\frac{\Delta D}{D}\right)_{TC} \quad (6)$$

where: $\left(\frac{\Delta D}{D}\right)_{CS} = \left(\frac{\Delta V}{V}\right)_{CS}/3$ = diametral cladding swelling rate

$\left(\frac{\Delta D}{D}\right)_{IC}$ = diametral irradiation-induced creep rate

$\left(\frac{\Delta D}{D}\right)_{TS}$ = diametral cladding thermal strain rate

An iteration procedure is used to simultaneously solve equation 5 and 6 for stress.

3.4 Application of Models to Experimental Fuel Pins

An OLYMPUS II-A code analysis was made on GE pin F2H [3] which operated under the following conditions.

Cladding	= Solution-treated Type 316 stainless steel, 0.250 inch OD, 15 mil wall thickness
Cladding Temperature	= 520°C
Power Rating	= 14 kw/ft
Cold Gap	= 2 mils
Pellet Density	= 96.6% T.D.
Flux (E>0.1 Mev)	= 1.4×10^{15} n/cm^2 sec.

The strain component due to cladding swelling was evaluated using the recent HEDL swelling equation [4] for solution-treated Types 304 or 316 stainless steel as given by:

$$\%\frac{\Delta V}{V} = (\phi t)^{2.05 - 27/\theta + 78/\theta^2} [\,(T-40) \times 10^{-10}] \times \exp(-0.015T - 5100/T + 32.6) \quad (7)$$

where: ϕt = fast fluence (E>0.1Mev) $\times 10^{-22}$

T = temperature, (°K)

θ = T - 623

The results of the OLYMPUS-IIA analysis of the F2H pin are given in Figure 3-1 and 3-2. Figure 3-1 and 3-2 illustrate the cladding strain components using an empirical fuel swelling model and two levels of irradiation-induced creep. The fuel swelling model was normalized to the observed total diametral strain of 1.7% at 7.3% burnup.

Figure 3-1 shows the diametral strain prediction versus burnup for the irradiation-induced creep strain model previously reported. [5] An initial thermal strain of 0.03% was calculated for the heat-up period. Hot-pressing of the fuel continued to 2.9% burnup producing an additional thermal strain of 0.03%. At 3% burnup the fuel attained the limiting hot-pressing density (presently defined as 98% T.D.). Above 3% burnup, irradiation-induced creep and thermal strain occur at approximately equal rates. The code predicts 3.1% total strain at 10% burnup.

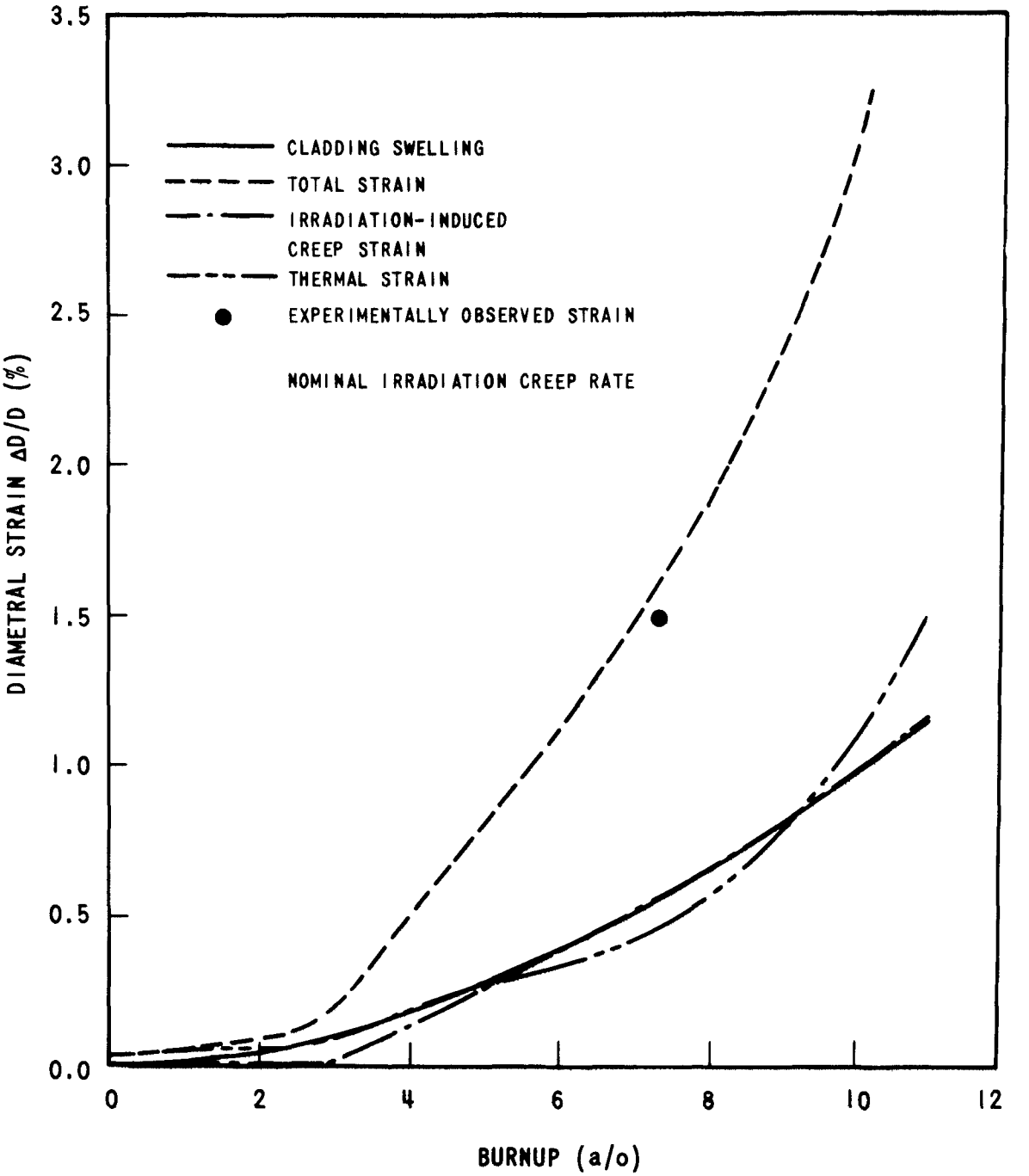

Figure 3-1. OLYMPUS 2A Analysis of EBR-II Pin F2H

3937-1

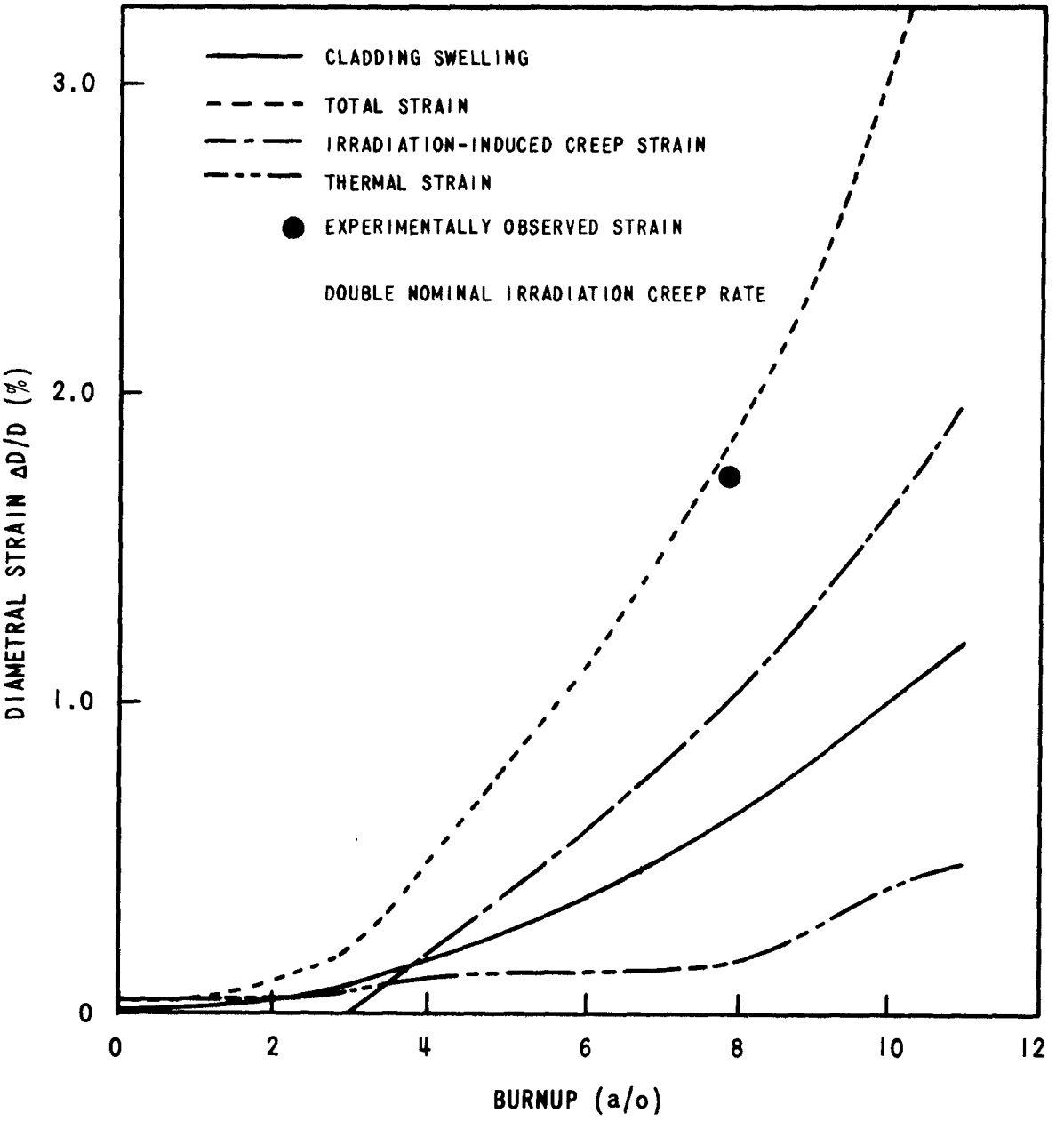

Figure 3-2. OLYMPUS 2A Analysis of EBR-II Pin F2H

3937-2

A limited sensitivity study was made on pin F2H involving variations of irradiation-induced creep. Figure 3-2 shows the results obtained at double the level of irradiation-induced creep used to obtain Figure 3-1. The irradiation-induced creep strain is 0.57% at 7.3% burnup in Figure 3-1 and the comparable irradiation-induced creep strain is 0.88% in Figure 3-2. Furthermore, the thermal strain showed a reduction from 0.47% to 0.16% as a consequence of doubling the irradiation-induced creep. Also, it was noted that the factor of 2 increase in irradiation-induced creep gave rise to large reductions in cladding hoop stress.

3.5 Irradiation-Induced Creep

The irradiation-induced creep equations for solution-treated and 20% cold-worked Type 316 stainless steel previously given [5] are being reviewed to determine the effects of neutron spectrum variation. Preliminary results indicate that the previously reported equations should be used with total fluence for mixed-oxide reactors such as FFTF, but these equations will underestimate the irradiation-induced creep in EBR-II central core locations.

3.6 Stainless-Steel Swelling

Investigation of the effects of neutron spectrum on irradiation-induced property changes was extended to include swelling of stainless steel. Although detailed results are not yet available, it appears that the current swelling equations for solution-treated (the θ equation) and 20% cold-worked (the 1.5 equation) Type 316 stainless steel overestimate swelling for the softer neutron spectra typical of mixed oxide reactors. Sensitivity analysis studies are in progress to evaluate the effects of reduced swelling on the design of fuel pins for mixed-oxide cores.

3.7 Hot-Pressing of Fuel

A theoretical correlation between the hot-pressing constant, K, used in OLYMPUS-II and the creep properties of oxide fuel was established on the basis that K is simply related to the viscosity (defined as σ/ε) of the fuel. Under low stresses, the fuel viscosity, KETA, may be determined as a function of linear power and surface temperature.

Comparison of the magnitude and temperature dependency of KETA with empirical K values shows reasonable agreement in the range where most of the irradiation data were obtained. This agreement lends verification to the physical interpretation attached to the empirically generated K values. Further analysis concerning the hot-pressing correlation is in progress.

4.0 REFERENCES

1. R. J. Forlano, A. W. Allen, and R. J. Beals, "Elasticity and Anelasticity of Uranium Oxides at Room Temperature," ANL-7101, December 1965.

2. J. F. Byron, "Yield and Flow of Polycrystalline Uranium Dioxide," J. Nucl. Mater. 27, pp. 48-53 (1968).

3. C. N. Craig, R. R. Asamoto, and R. N. Duncan, "Fast Reactor (Pu, U)O_2 Fuel Pin Irradiation in EBR-II to 75,000 MWd/Te," Trans. Am. Nucl. Soc. 12, p. 566 (1969).

4. T. T. Claudson, Personal Communication, July 1970.

5. "Oxide Fuel Element Development Quarterly Progress Report for the Period Ending March 31, 1970," WARD-4135-8, July 1970.

SECTION 4

OFBA-211 DEVELOPMENT OF ANALYTICAL METHODS AND FUEL LIFETIME CODES

B. L. Harbourne, M. S. Beck, J. P. Foster, A. Biancheria, and A. Boltax

1.0 OBJECTIVES

The overall objective of this task is to develop detailed design codes for performance of mixed-oxide fuel rods over the range of parameters characteristic of the LMFBR. This task is closely related to Task OFBA-210. The major emphasis of Task OFBA-211 is the development of the CYGRO code for fast reactor applications.

The activities of Task OFBA-211 can be divided into four areas with initial emphasis on the first three areas:

1. Development of analytical methods to predict steady state behavior of the fuel rod system.
2. Identification of information needed to improve the models.
3. Development of integrated design codes.
4. Development of design models to predict off-normal transient behavior of the fuel system.

The starting point for this program is the CYGRO-2 code developed at Bettis Atomic Power Laboratory. The modifications of CYGRO-2 for application to fast reactor fuel pin studies are called the CYGRO-F series codes.

2.0 PRIOR WORK

Analysis of the performance of representative experimental fuel pins gave mixed results with the predicted cladding strains being substantially higher than were observed in a number of cases. These errors were attributed to the ommission of irradiation effects on the fuel and cladding mechanical properties.

A sensitivity study on FFTF pin design parameters showed that in many cases cladding deformation was controlled by internal stresses built up as a result of differential swelling across the cladding thickness.

3.0 CURRENT PROGRESS

3.1 CYGRO-F Irradiation-Induced Creep Analysis

A critical feature of fuel pin behavior, as described by CYGRO-F, is the build-up of internal stresses in the cladding by thermally-induced differential swelling. The internal stresses significantly enhance cladding deformation due to internal gas pressure and fuel-cladding mechanical interaction. These effects are maximized by combinations of high flux and low-moderate temperatures. Under these same conditions, irradiation-induced creep is expected to be substantial and would act to relieve the internal stesses.

The main problem in incorporating irradiation-induced creep analysis into CYGRO-F is to obtain a compatible model. The stress-strain analysis is dependent on both stress-rate and strain-rate and therefore requires a partial differential form of the creep equation. If the irradiation-induced creep equation with a time-dependent stress is differentiated with respect to time, the following equations are obtained:

$$\varepsilon = K\sigma\phi t \tag{1}$$

$$\dot{\varepsilon} = K\sigma\phi + K\phi t \frac{d\sigma}{dt} \tag{2}$$

$$\dot{\varepsilon} = K\sigma\phi + \frac{\varepsilon}{\sigma} \frac{d\sigma}{dt} \tag{3}$$

Equation 3 indicates that the instantaneous strain rate is a function of the strain at that time. The second term in Equation 3 is significant during rapid loading conditions and is of lesser significance during steady state conditions. For initial CYGRO-F studies involving irradiation-induced creep, the second term in Equation 3 was neglected. This assumption gives rise to an underestimation of irradiation-induced creep during rapid loading conditions, such as occur at the start of fuel-cladding interaction. The irradiation-induced creep equation used in CYGRO-F is:

$$\dot{\varepsilon} = [1.224 \times 10^{-29} \exp(-\phi t/6.37 \times 10^{20}) + 1.86 \times 10^{-30}] \alpha \bar{\sigma} \phi \tag{4}$$

where $\dot{\varepsilon}$ is the instantaneous irradiation-induced creep strain rate, ϕt the total fluence, $\bar{\sigma}$ the average stress during a given time increment, and $\alpha = \exp(1.405 - 0.027T)$ with T in °K.

Equation 4 relates only to the shear mode of irradiation-induced creep and is used in CYGRO-F with the deviatoric stresses. It should be noted that the irradiation-induced creep component due to hydrostatic stress is not presently incorporated in the CYGRO-F code. Thus, the results discussed below reflect only the smaller shear stress irradiation-induced creep component. Preliminary studies are in progress which mock-up the hydrostatic component by the use of appropriate multiplying factors to Equation 4.

The principle strain rates are calculated from the Prandtl-Reuss relation :

$$\dot{\varepsilon}_i = \frac{3}{2} \frac{\varepsilon}{\bar{\sigma}} (\sigma_i - \sigma_m) , i = 1,2,3 \qquad (5)$$

where σ_m is the hydrostatic stress and $\varepsilon/\bar{\sigma}$ is given by Equation 4. A similar relation is used to determine the thermal creep rate, and the total strain rate is then the arithmetic sum of the irradiation-induced and thermal creep rates. Strain hardening is computed from the thermal creep strain alone.

The influence of the irradiation-induced creep model has been examined using the analysis of several sections of a hypothetical fuel pin with and without the irradiation-induced creep model operating. The pin had a peak rating of 12.5 kw/ft and maximum cladding temperature of 650°C. Cases with peak fluxes of 3.6×10^{15} and 1.8×10^{15} n . cm^{-2} . sec^{-1} were examined.

Detailed evaluation of the results remains to be completed, however, the following tentative conclusions are indicated:

1. The increase in total diametral strain due to irradiation-induced creep is small, usually less than 10%.

2. Maximum and average generalized stresses in the cladding are reduced by small but significant amounts by irradiation-induced creep. The reductions in maximum stresses are greater than that of the average stresses, signifying internal stress relaxation, and are more marked at intermediate burnups (Figure 4-1).

3. At low-moderate temperatures irradiation-induced creep strain reduces the amount of thermal creep strain (Figure 4-2); but at high temperatures the thermal creep is not reduced by the irradiation-induced creep components (Figure 4-3).

4. Prior to fuel-cladding contact when average cladding stresses are low, irradiation-induced creep causes a marked relaxation of internal stresses; but after contact, internal stresses may be virtually eliminated by thermal creep alone (Figure 4-4).

It is planned to compare the treatment of irradiation-induced creep and its effects in OLYMPUS-II with those obtained from CYGRO-F.

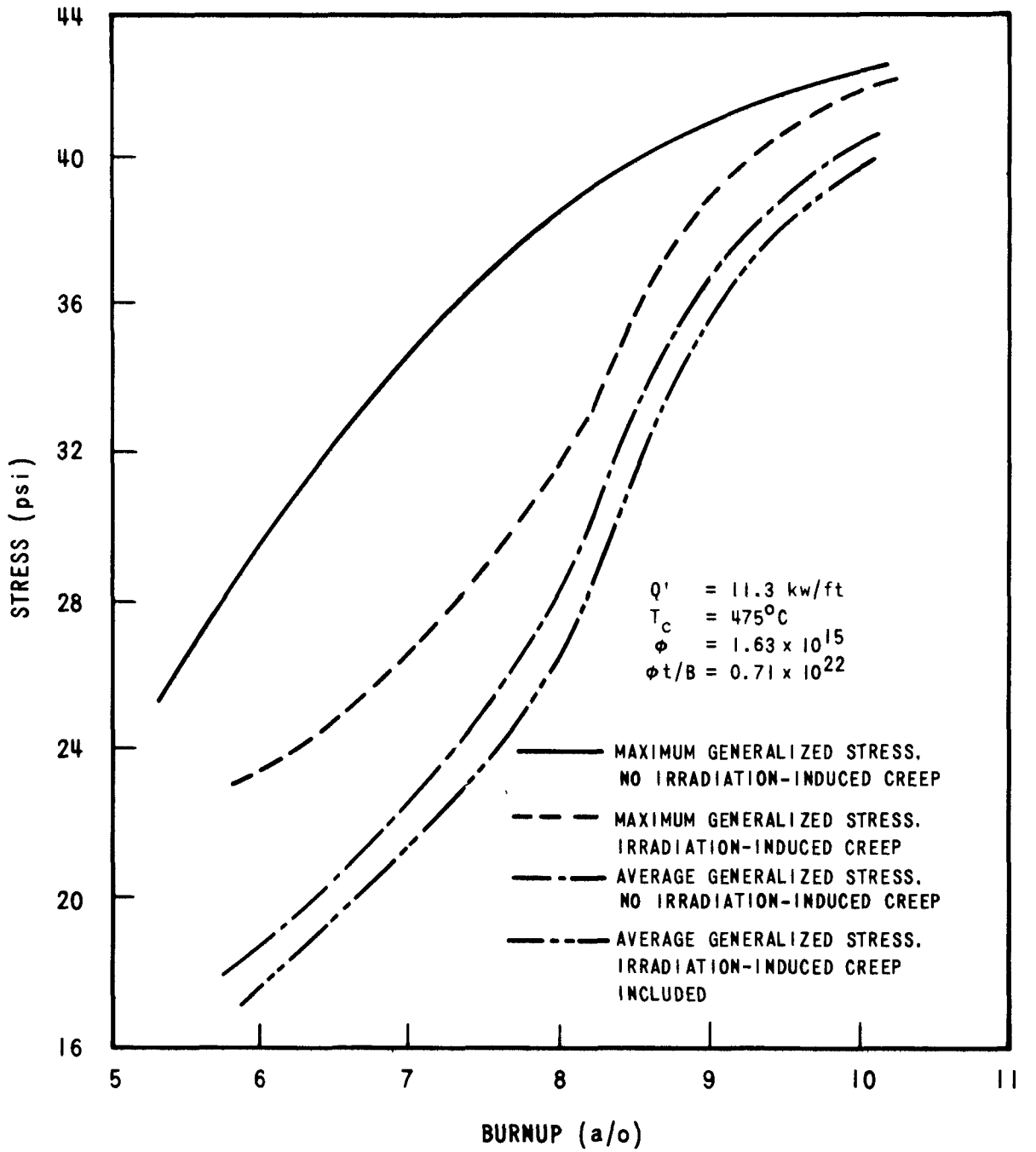

Figure 4-1. Effect of Irradiation-Induced Creep on Cladding Stresses at Low Temperatures

3937-3

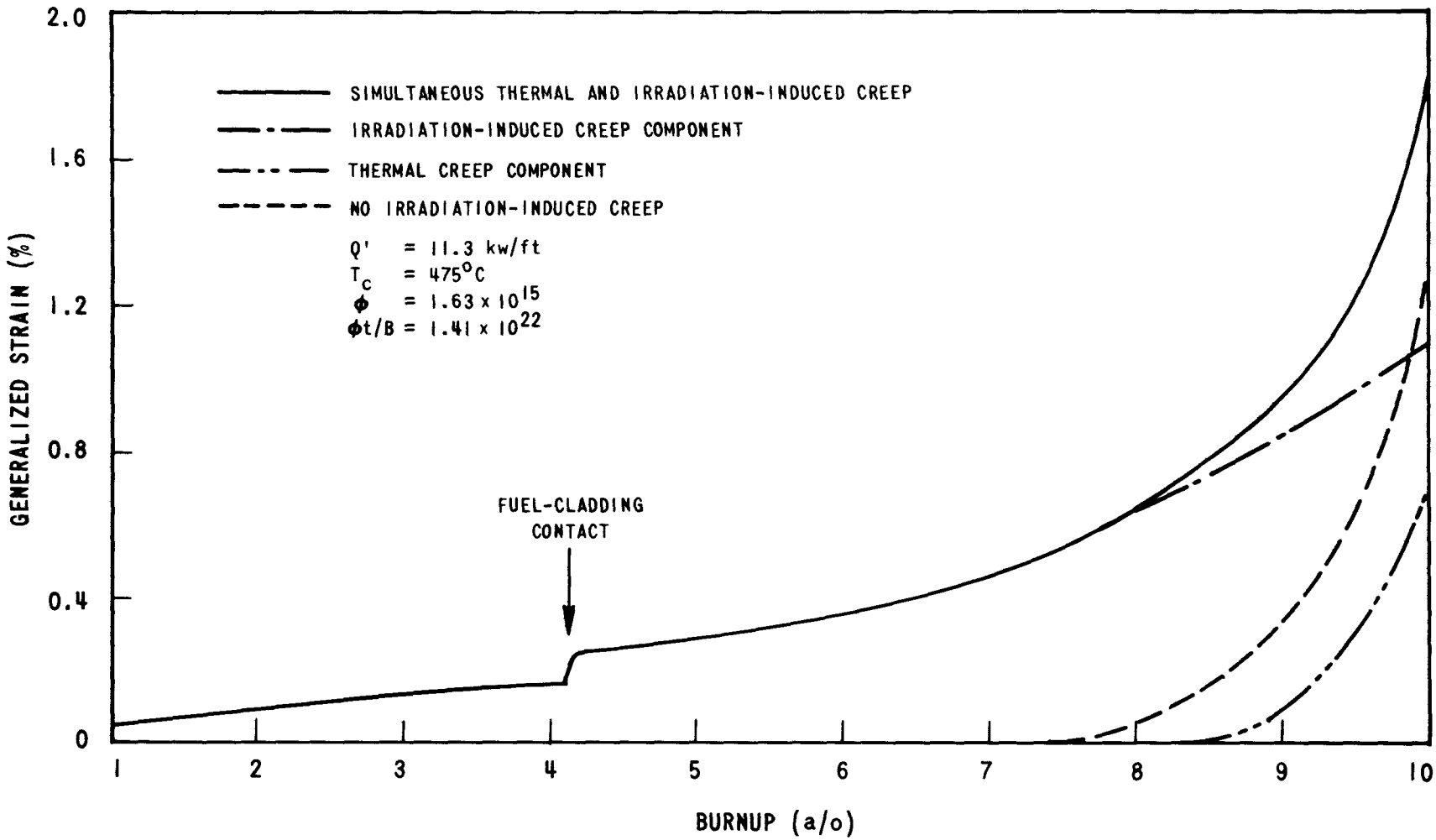

Figure 4-2. Effect of Irradiation-Induced Creep on Generalized Cladding Strain at Low Temperature

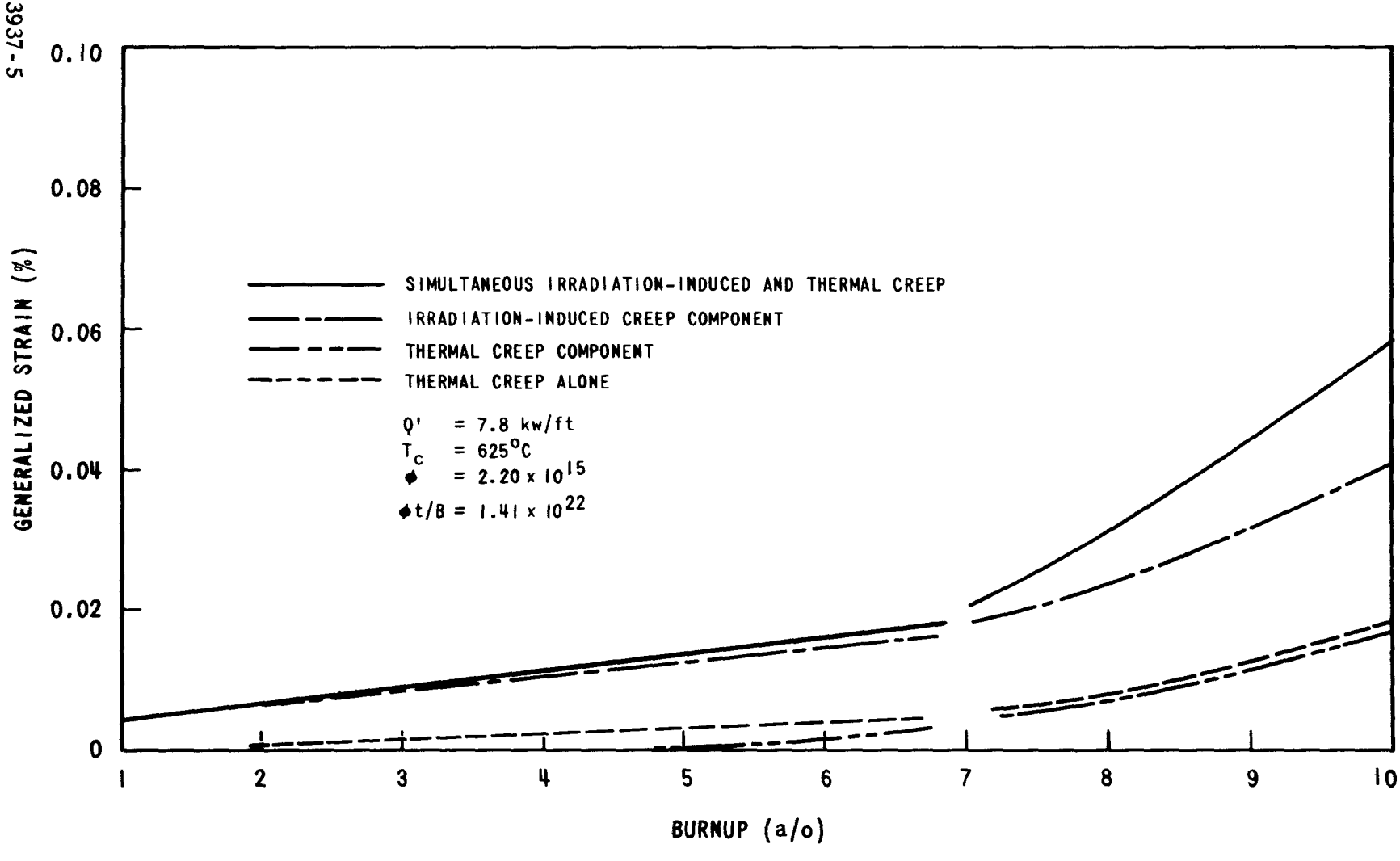

Figure 4-3. Effect of Irradiation-Induced Creep on Generalized Cladding Strain at High Temperature

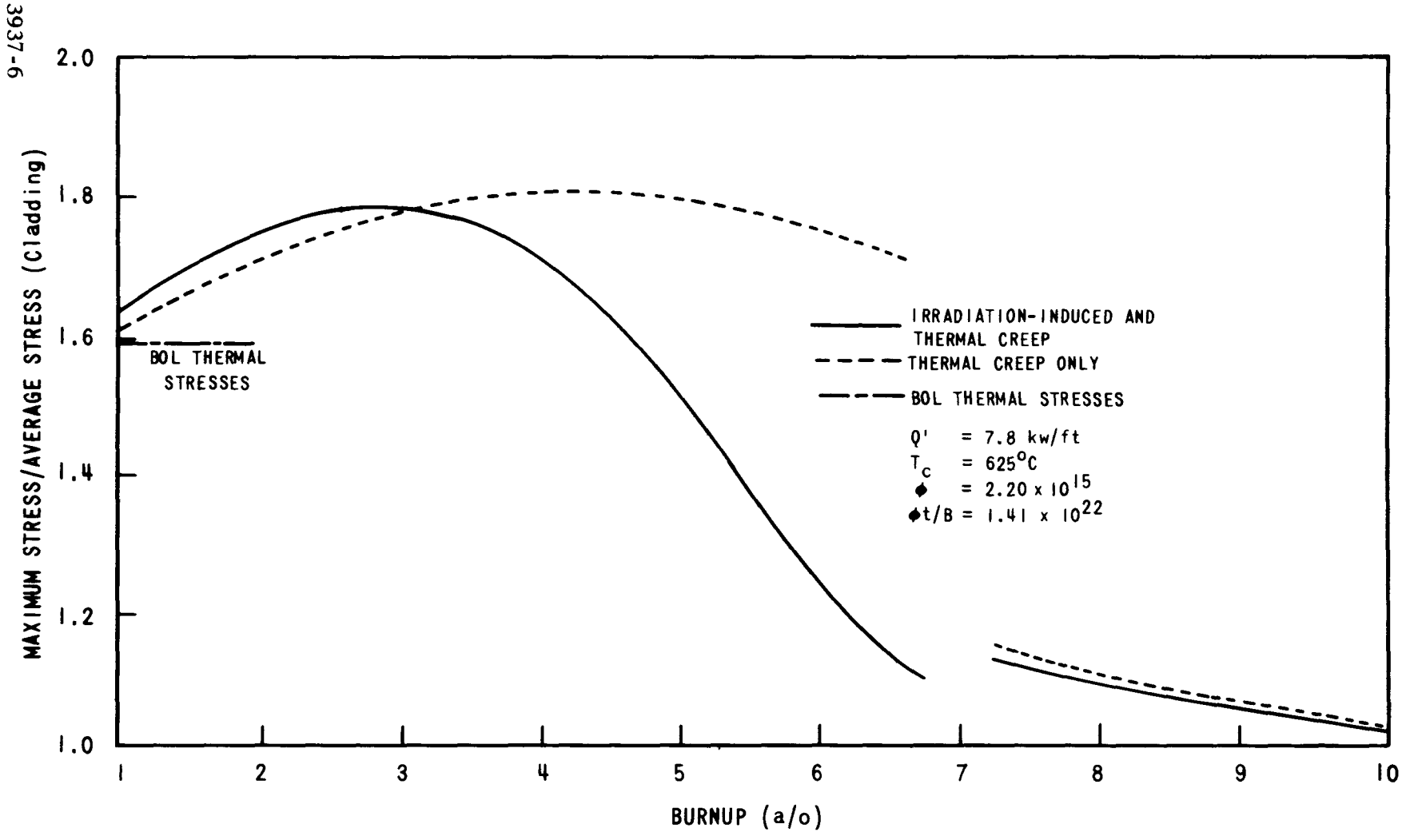

Figure 4-4. Relaxation of Internal Cladding Stresses at High Temperature

SECTION 5

OFBA-310 ENCAPSULATED MIXED-OXIDE FUEL PIN IRRADIATION TESTS

A. Biancheria, B. L. Harbourne, U. P. Nayak,
R. K. Dawless, and T. A. Damico

1.0 OBJECTIVES

The objectives of this task are to plan, conduct, and evaluate in-reactor experiments of critical areas of special sensitivity to fuel-pin behavior analysis.

2.0 PRIOR WORK

Work on subassemblies WSA-1 and -2 was completed, and these were inserted in the EBR-II reactor. A re-analysis on WSA-1 and -2 was started using the OLYMPUS-IIA code to provide a basis for the design of the WSA-5 Series fuel pins. The WSA-5 Series fuel pins form replacements for WSA-1 and -2 to be removed at the interim examination. Experimental planning for the WSA-5 Series was initiated.

3.0 CURRENT PROGRESS

The status of WSA-1 and -2 subassemblies at the end of EBR-II Run 45 (September 10, 1970) is summarized in Table 5-1. Starting with Run 46, EBR-II full power will be 62.5 MWt. To maintain similar irradiation conditions, subassembly WSA-1 has been relocated from position 6F4 to 7C4 and WSA-2 from 7D3 to 7D1. Re-evaluation of the WSA-1 and -2 series fuel pins using the OLYMPUS-IIB code was completed. The results are shown in Tables 5-2 and 5-3. Strain profiles for pin W1-13 after 20,000 and 27,500 MWd exposure are shown in Figures 5-1 and 5-2, respectively. The cladding strain calculations include stress effects on stainless steel swelling.

Table 5-1. Status of ARD Encapsulated Subassemblies At The End Of Run 45

Fuel Pin	EBR-II S/A	Reactor Position	Accumulated Exposure (MWd)	BU (a/o)
WSA-1	X088	6F4	4051	0.6
WSA-2	X076	7D3	5552	1.8

Table 5-2. OLYMPUS-II Analysis of WSA-1 Pin Behavior

Pin No.	Original Target Exposure (Mwd)	Peak BU (a/o)	Max. (ΔD/D) (%)	Thermal Creep (ΔD/D) (%)	Increased Target Exposure (Mwd)	Peak BU (a/o)	Max. (ΔD/D) (%)	Thermal Creep (ΔD/D) (%)	Comments
1	12,500	3.0	0.47	0.15	N.C.	---	---	---	Interim Discharge
2	"	3.0	0.43	0.09	"	---	---	---	" "
3	"	2.9	0.36	0.11	"	---	---	---	" "
4	20,000	4.9	0.69	<0.01	27,500	6.7	1.23	0.01	Retain to 27,500 Mwd
5	"	4.6	1.02	0.20	"	6.3	1.62	0.20	" "
6	"	4.8	0.23	<0.01	"	6.6	0.44	0.05	" "
7	"	4.7	0.63	0.07	"	6.5	1.02	0.07	" "
8	12,500	3.2	0.94	0.50	N.C.	---	---	---	Interim Discharge
9	"	3.3	0.49	0.09	"	---	---	---	" "
10	"	3.1	0.82	0.41	"	---	---	---	" "
11	20,000	5.2	0.71	<0.01	27,500	7.2	1.39	0.03	Retain to 27,500 Mwd
12	"	5.3	0.46	0.07	"	7.3	1.01	0.08	" "
13	"	5.0	1.27	0.29	"	6.9	2.01	0.41	" "
14	"	5.2	1.06	0.14	"	7.2	1.79	0.14	" "
15	"	5.1	0.69	<0.01	"	7.0	1.27	0.03	" "
16S	12,500	3.0	0.45	0.13	N.C.	---	---	---	Interim Discharge
17S	20,000	4.8	1.10	0.18	"	---	---	---	Discharge at 20,000 Mwd
18S	"	4.6	1.00	0.17	"	---	---	---	" "
19S	"	4.8	1.15	0.21	"	---	---	---	" "

Table 5-3. OLYMPUS-II Analysis of WSA-2 Pin Behavior

Pin No.	Original Target Exposure (Mwd)	Peak BU (a/o)	Max. (ΔD/D) (%)	Thermal Creep (ΔD/D) (%)	Increased Target Exposure (Mwd)	Peak BU (a/o)	Max. (ΔD/D) (%)	Thermal Creep (ΔD/D) (%)	Comments
1	15,000	3.4	0.48	0.17	N.C.	---	---	---	Interim Discharge
2	"	3.4	0.29	0.07	"	---	---	---	" "
3	25,000	6.1	0.50	0.07	35,000	8.5	0.90	0.07	Retain to 35,000 Mwd
4	"	5.9	0.82	0.11	"	8.3	1.39	0.14	" "
5	"	5.6	1.38	0.51	"	7.8	2.12	0.53	" "
6	"	5.9	0.82	0.11	"	8.3	1.39	0.14	" "
7	15,000	4.8	0.27	<0.01	N.C.	---	---	---	Interim Discharge
8	"	3.7	1.01	0.60	"	---	---	---	" "
9	"	3.8	0.46	0.09	"	---	---	---	" "
10	25,000	6.7	1.25	0.18	35,000	9.4	2.23	0.18	Retain to 35,000 Mwd
11	"	6.5	1.49	0.35	"	9.1	2.47	0.35	" "
12	"	8.2	0.99	0.08	"	11.5	2.24[a]	0.09[a]	" "
13	"	6.1	1.50	0.52	"	8.5	2.5	0.87	Discharge at 25,000 Mwd
14	15,000	4.1	1.38	0.99	N.C.	---	---	---	Interim Discharge
15	"	4.1	0.11	<0.01	"	---	---	---	" "
16	25,000	8.4	1.61	0.62	35,000	11.8	2.51[a]	0.9[a]	Discharge at 25,000 Mwd
17	"	8.7	1.2	0.50	"	12.2	2.76[a]	1.2[a]	" "
18	"	6.4	1.08	0.33	"	9.1	1.78	0.36	Retain to 35,000 Mwd
19	"	8.2	0.79	0.07	"	11.5	1.82[a]	0.08[a]	" "

[a]Values are reported at 10 a/o BU.

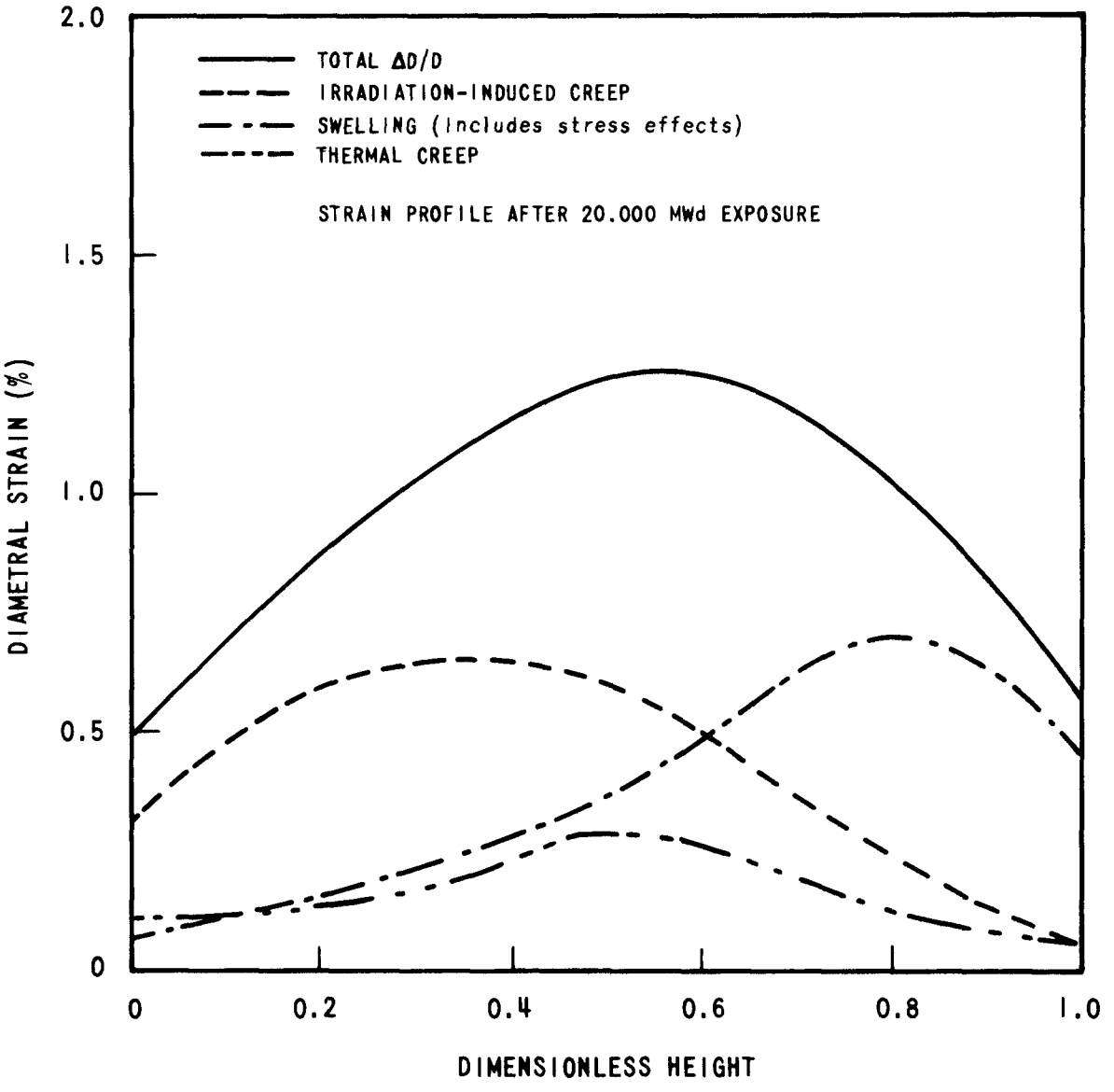

Figure 5-1. OLYMPUS-II Calculated Strain Profiles, Pin WSA-1/13

3937-7

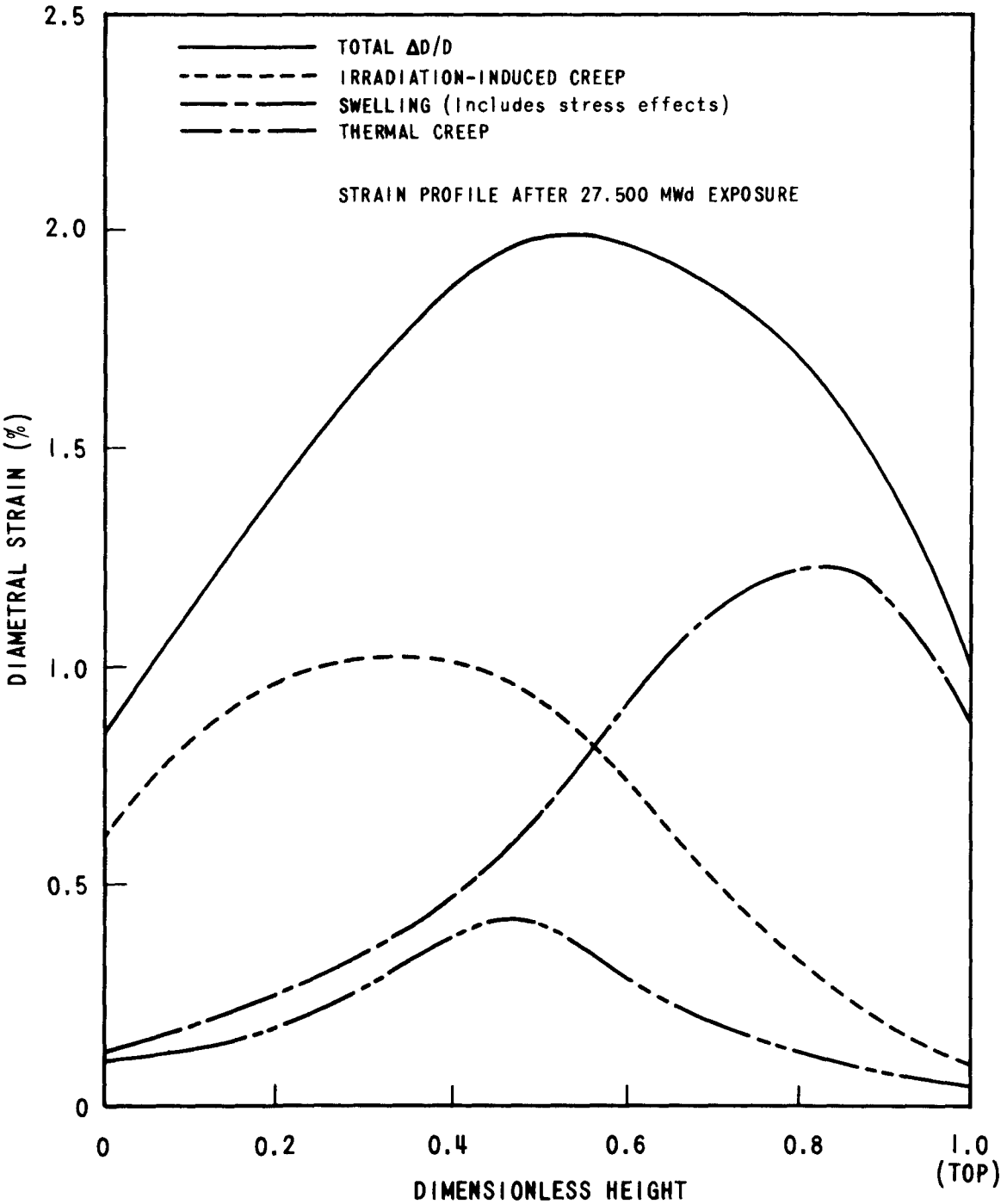

Figure 5-2. OLYMPUS-II Calculated Strain Profiles, Pin WSA-1/13

3937-8

Preliminary design of the WSA-5 series fuel pins was completed during this quarter, and a request for "Approval-In-Principle" for irradiation in EBR-II was submitted to the AEC. These mixed-oxide, stainless steel clad, encapsulated fuel pins form replacements for fourteen fuel pins which will be removed from WSA-1 and -2 for destructive examination at the programmed interim discharge. The primary objective of the WSA-5 experiment is to obtain quantitative information on the various types of cladding strain mechanisms and relate them to test operating conditions.

The engineering designs and target operating conditions for WSA-5 fuel pins have been selected to yield specific data in the following critical areas:

1. The influence of stress and temperature on cladding swelling.
2. Irradiation-induced creep deformation of cladding at low and high temperatures.
3. The effect of internal stresses on cladding deformation.
4. The effect of fuel-cladding mechanical interaction on cladding deformation.
5. The effects of gas pressure stresses on cladding deformation.

A study of cladding deformation characteristics requires variations in temperature, stress level, cladding loading method, flux level and fluence. As this experiment is constrained to the ambient operating conditions of subassemblies WSA-1 and -2, only small variations in flux and fluence will be possible. Variations in the other three variables will be emphasized.

Cladding temperature in a given pin will be controlled by the total heat output and the disposition of the fuel column relative to the EBR-II core length. A parametric study was performed using the SPACER code to determine the fuel column disposition and cladding temperatures required.

Stress levels in the cladding will be controlled by adjustment of the plenum to fuel volume ratio and by selecting fuel-cladding gap sizes and smear densities to promote or minimize fuel-cladding mechanical interaction.

Cladding stresses will be imposed by internal gas pressure, a combination of gas pressure and fuel-cladding mechanical interaction, and by thermal-induced internal stresses. Internal stresses result from the heat flux and are due initially to differential thermal expansion, while later in life they are caused by the differential in cladding swelling rate. Cladding behavior in the absence of these internal stresses will be studied by incorporating unfueled regions in some fuel pins.

Cladding swelling behavior will be determined on unstressed cladding samples located within some fuel pins. These samples will not be subject to gas pressure loading or to internal stresses.

Plenum volumes will be sized to produce life-averaged gas pressures of 600 and 1000 psi. Preliminary estimates show that fuel/plenum volume ratios of $\sim$3 and $\sim$5 will be required. The feasibility of pressurizing the pins to about 10 atmospheres will also be investigated. If a filling pressure of 10 atmospheres can be attained, the fuel/plenum volume ratios may be reduced to $\sim$2 and $\sim$3 for the low and high pressure pins, respectively.

Design details and preliminary operating conditions for the fourteen WSA-5 fuel pins are presented in Table 5-4. Pins W5-1 through W5-7 will be irradiated with the remaining WSA-1 pins, and pins W5-8 through W5-14 with the remaining WSA-2 pins. All pins will be contained in Mk-A capsules and assembled into MkA-19 subassemblies. Fuel column distribution for these pins is shown in Figure 5-3.

Figure 5-4 shows the general arrangement of two basic fuel pin types, and Figure 5-5 shows the axial temperature profiles of the two types. From the region "E" of the two pins (Figure 5-5), data will be obtained on:

1. The swelling behavior of unstressed cladding samples.
2. Swelling and deformation of stressed cladding with internal stresses.
3. Swelling and deformation of stressed cladding without internal stresses.

Adjustment of the fuel column positioning in pin B (Figure 5-4) will vary the temperature and flux in region "E." Mean cladding temperatures in the range 475-600°C will be studied in this way. Preliminary estimates of these conditions are shown in Table 5-4.

A detailed design and analysis effort on these fuel pins has been started. The smaller gas plenums to produce large internal gas pressures requires removal of connecting plugs used in WSA-1 and -2 series fuel pins and a new design for end plugs. A review of bowing analysis of WSA-1 and -2 fuel pins is in progress to establish end plug designs which can effectively control the bow without the connecting plugs.

Fuel pellet requirements and specifications will be established during the next quarter. Fuel and fuel element fabrication will be initiated shortly thereafter. The fabrication schedule for WSA-5 fuel pins is based on interim discharge of WSA-1 and -2 subassemblies in April 1971.

Table 5-4. Design Parameters and Operating Conditions, WSA-5

Pin No.	Cladding	Pellet Density (%)	Fuel Clad Gap (mils)	Smear Density (%)	Fuel Column Length (in)	Fuel Column Location[a]	Fuel Vol. Plenum Vol.	Peak Rating (kw/ft)	Cladding Temp. (°C) Peak	Cladding Temp. (°C) "E"	Fluence(>.1) ($n.cm.^{-2} \times 10^{-22}$) Peak	Fluence(>.1) ($n.cm.^{-2} \times 10^{-22}$) "E"	Exposure (MWd)
1	WSA-1 Replacements 0.243 in OD, 0.010 in wall,	90-92	6	85.2-87.1	7	B	5	13.2	645	515	4.0	3.9	15,000
2		93-95	3	90.5-92.5	9	B	5	"	660	570	"	3.3	"
3		90-92	6	85.2-87.1	11	B	5	"	690	600	"	3.1	"
4		90-92	6	85.2-87.1	9	B	3	"	660	570	"	3.3	"
5		93-95	3	90.5-92.5	11	B	3	"	690	600	"	3.1	"
6		90-92	6	85.2-87.1	8	T	5	"	620	(b)	"	(b)	"
7		93-95	3	90.5-92.5	8	T	3	"	620	(b)	"	(b)	"
8	WSA-2 Replacements CW Type 316 Stainless Steel	90-92	6	85.2-87.1	6.5	B	3	10.6	550	475	4.0	4.0	20,000
9		93-95	3	90.5-92.5	9	B	3	"	595	515	"	3.7	"
10		90-92	6	85.2-87.1	11	B	3	"	615	550	"	3.1	"
11		93-95	3	90.5-92.5	6.5	B	5	"	550	475	"	4.0	"
12		93-95	3	90.5-92.5	11	B	5	"	615	550	"	3.1	"
13		93-95	3	90.5-92.5	8	T	5	"	560	(c)	"	(c)	"
14		90-92	6	85.2-87.1	8	T	3	"	560	(c)	"	(c)	"

(a) Fuel column location: one end of column in line with bottom (B) or top (T) of EBR-II core

(b) 515,570, and 600°C

(c) 475,515, and 550°C

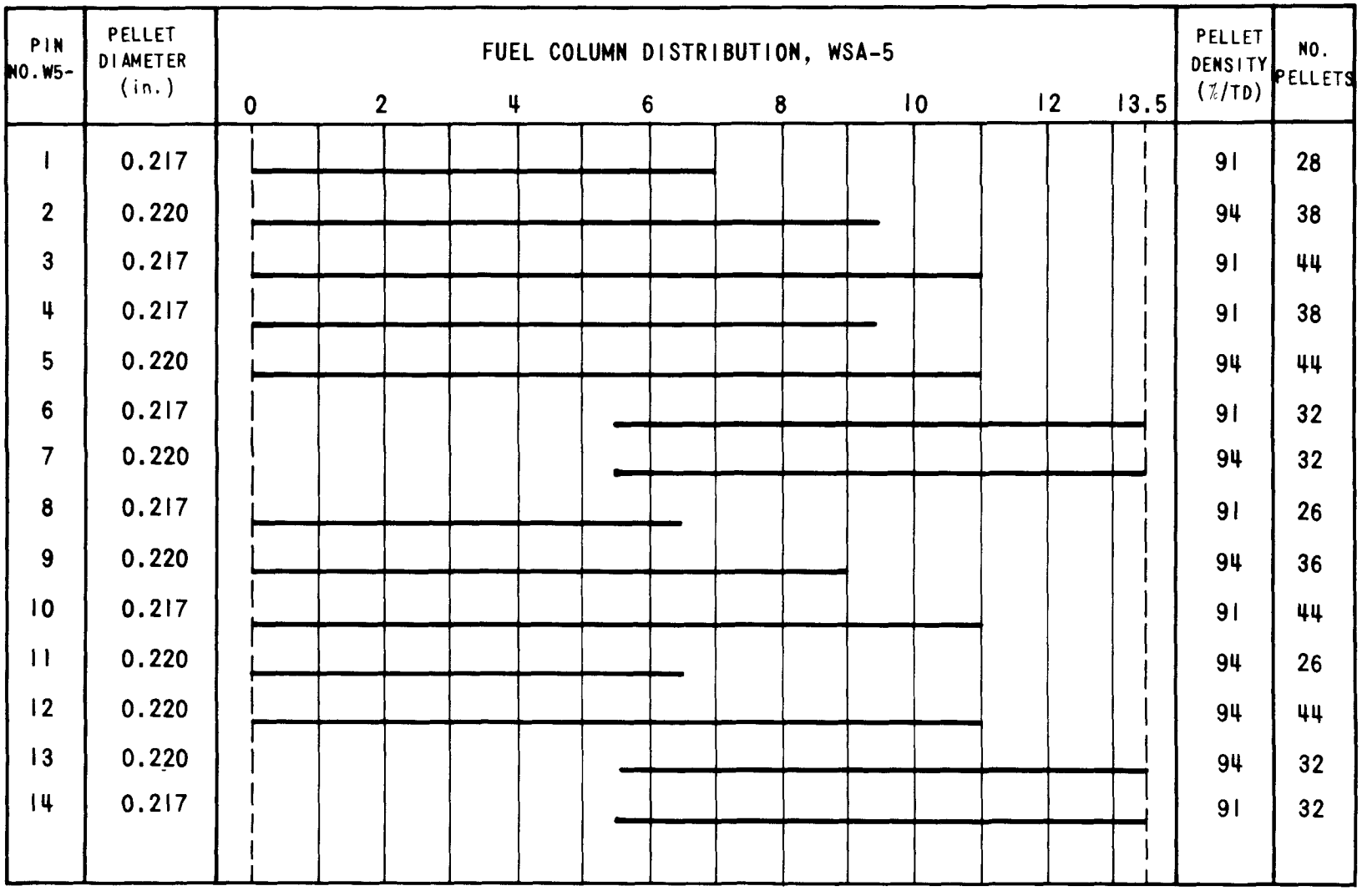

Figure 5-3. Fuel Column Distribution, WSA-5

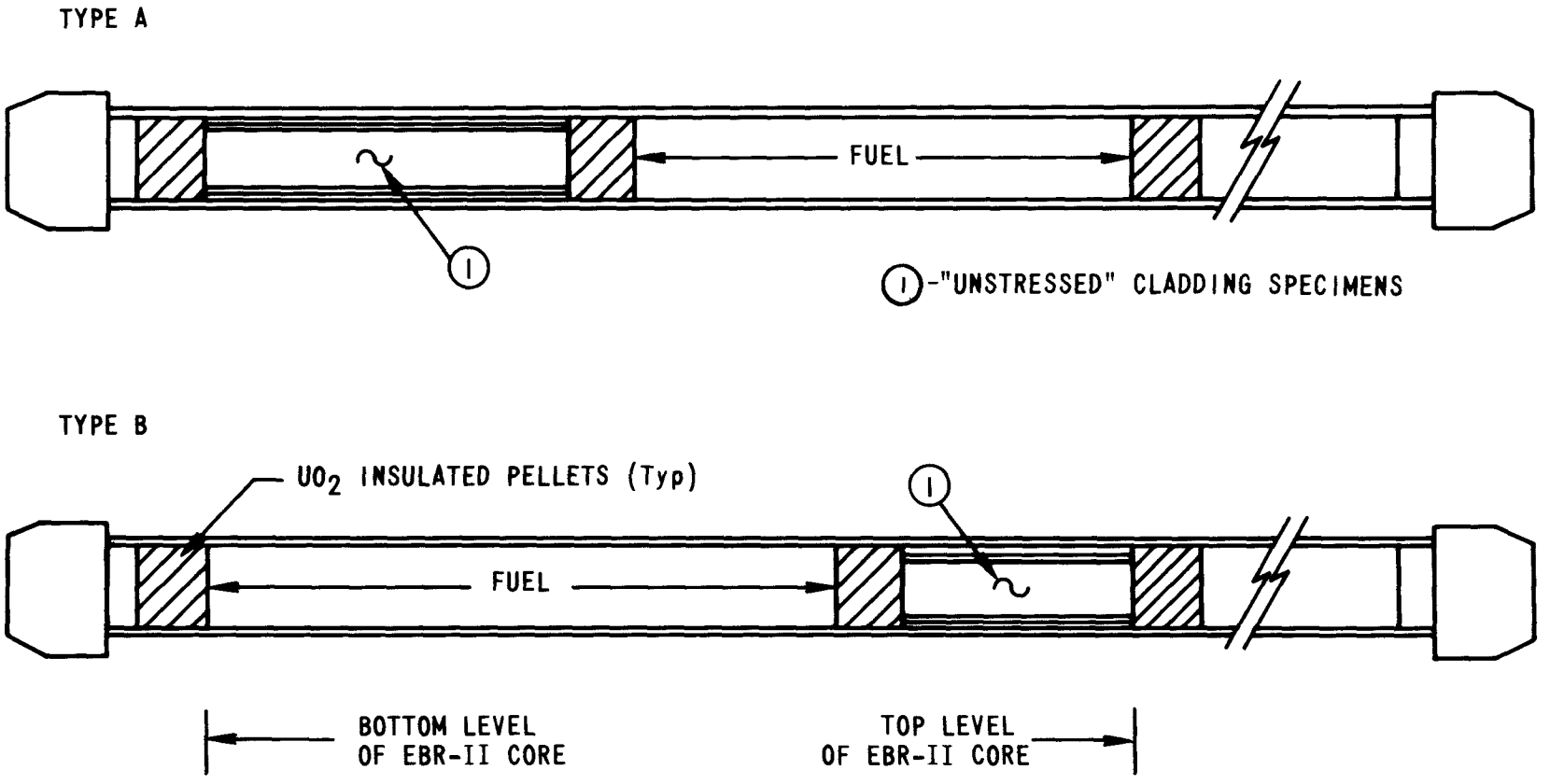

Figure 5-4. Schematic Fuel Pin Designs - WSA-5

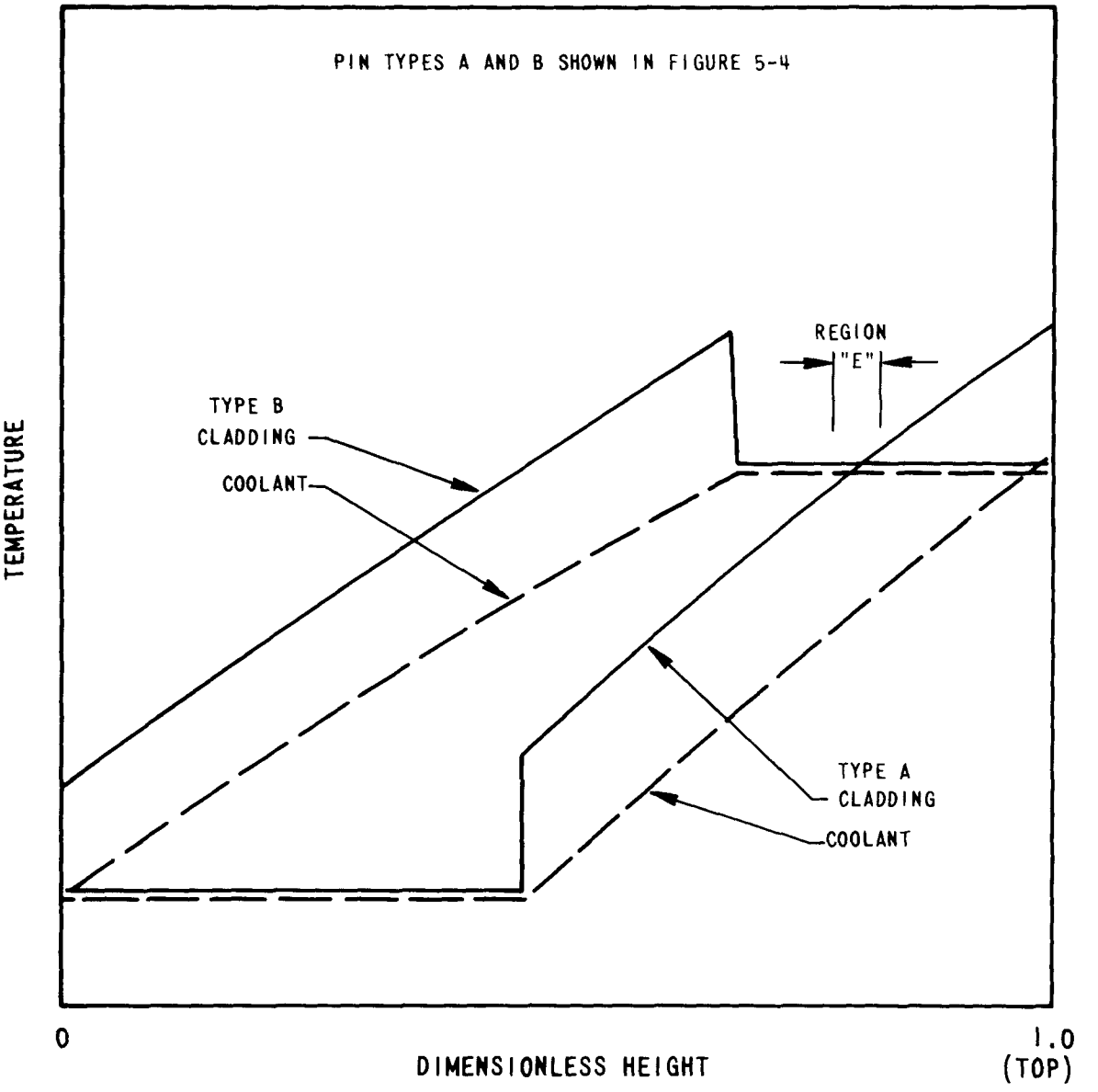

Figure 5-5. Axial Temperature Profiles - WSA-5

3937-11

4.0 REFERENCES

1. "Oxide Fuel Element Development Quarterly Progress Report for the Period Ending June 30, 1970," WARD-4135-11, September 1970.

SECTION 6

OFBA-311 UNENCAPSULATED MIXED-OXIDE FUEL PIN IRRADIATION TESTS

A. Biancheria, J. M. Aldeanueva, R. K. Dawless
P. J. Levine, R. A. Markley, U. P. Nayak, and J. F. Patterson

1.0 OBJECTIVES

This task is part of the overall irradiation program on mixed-oxide fuel to study special areas of fuel-rod behavior and assembly performance. The specific objectives are to design, irradiate, and evaluate grid-type subassemblies with unencapsulated mixed-oxide fuel pins for the following purposes:

1. Demonstrate satisfactory performance of Type 316 stainless steel grid-type subassemblies in a fast reactor environment.

2. Investigate the combined effects of radiation, flowing sodium, stress, and temperature on the mechanical and corrosion properties of grid material and on pin-grid interaction.

3. Develop statistically significant design information on mixed-oxide fuel pin performance.

The grid-type subassembly is further intended to provide an irradiation vehicle which will minimize the interaction between individual pins.

2.0 PRIOR WORK

The first of a series of grid-type subassemblies was designed for irradiation in EBR-II. Approval-in-principle was received and detailed design drawings were completed for WSA-3. Thermal, mechanical, and nuclear analyses were initiated, and safety analyses were completed for this subassembly. All materials have been received, and fabrication of fuel and subassembly hardware was started. A mock-up flow test subassembly of WSA-3 was fabricated and tested satisfactorily. The fuel pin shipping container was partially completed. Experimental planning for the second subassembly, WSA-4, was initiated.

3.0 CURRENT PROGRESS

3.1 WSA-3 Design

The final design analyses for WSA-3 have been completed and prepared in written form for the required data package to be submitted to the EBR-II Project. A brief summary of the analyses completed this quarter follows.

3.1.1 Thermal Analysis

Following the re-evaluation of uncertainty factors,[1] peak fuel pin operating temperatures and power ratings were determined with the factors included. The resultant values are summarized in Table 6-1. The corresponding axial temperature profile for the highest rated pin, W3-1, is shown in Figure 6-1.

3.1.2 Stress-Strain Analysis

Fission gas release rates and internal pressures at the end-of-life were calculated for each fuel pin with uncertainty factors applied. These results, obtained with the NICE code, were used in the CAPSTR code to determine the cladding strains exclusive of fuel-cladding interaction and cladding swelling. The values are tabulated in Table 6-2. To account for the exclusions from CAPSTR, the fuel pin behavior analysis code, OLYMPUS-II, was used to determine the maximum total strains. The results obtained from OLYMPUS-II A and II B indicate the total diametral increase for any pin does not exceed 0.3% $\Delta D/D$ at 5% burnup. The axial profile of the highest rated pin, W3-1, is shown in Figure 6-2.

3.1.3 Safety Analysis

Analyses of a fuel pin failure were made to determine the extent of coolant and cover gas contamination and the possibility of gas blanketing. The activities of gaseous isotopes ^{85}Kr, ^{88}Kr, ^{133}Xe, and ^{135}Xe were calculated assuming failure occurred in the highest rated pin, W3-1, after 5% burnup was achieved. Activity levels of the released fission gases and products in the coolant and cover gas were calculated as a function of time after subassembly removal. Also, the primary loop activity due to non-gaseous fission product dispersion in the coolant was determined.

The gas blanketing analysis concluded that failure propagation by this means is unlikely except for the case where a jet of released gas impinges on an adjacent pin. In this instance, failure would be limited to the adjacent pin.

3.1.4 Hydraulic Analysis

This analysis was performed to determine the effect of end-of-life dimensional changes in fuel pins and subassembly hardware on coolant flow. Calculations including pin diameter increases and liner swelling result in a 1% flow area increase and less than a 0.1% decrease in hydraulic diameter. The overall result is a small increase in flow rate and a decrease in average outlet temperature. Translating these data to a subchannel coolant temperature analysis, the results shown in Figure 6-3 were obtained for end-of-life conditions. The corner channel temperatures increased up to 23°F with inboard channels decreasing no more than 5°F.

Table 6-1. Peak Operating Conditions with Uncertainty Factors for WSA-3 Pins

Pin Number	Linear Rating (kw/ft)	Total Pin Heat Generation (kw)	Coolant Outlet Temp. (°F)	Cladding Outer Surface Temp. (°F)	Mean Cladding Temp. (°F)	Cladding Inner Surface Temp. (°F)	Fuel Surface Temp. (°F)	Fuel Centerline Temp. (°F)	Burnup (%)
W3-1	13.55	13.17	1151	1184	1214	1244	1975	4653	5.54
W3-2	12.35	12.00	1146	1176	1203	1231	1888	4212	5.43
W3-3	12.81	12.45	1136	1167	1224	1195	1913	4465	5.21
W3-4	11.89	11.55	1121	1149	1176	1202	2096	4474	5.10
W3-5	13.10	12.73	1156	1187	1216	1245	1947	4379	5.54
W3-6	13.21	12.83	1156	1187	1216	1246	1954	4573	5.43
W3-7	12.06	11.72	1146	1175	1201	1228	1867	4149	5.21
W3-8	12.46	12.11	1133	1163	1191	1218	1886	4373	5.10
W3-9	11.51	11.18	1114	1142	1167	1193	2056	4370	4.88
W3-10	12.99	12.62	1151	1183	1212	1241	2220	4775	5.54
W3-11	12.77	12.41	1156	1186	1214	1243	1924	4308	5.43
W3-12	12.86	12.49	1151	1182	1211	1239	1927	4486	5.21
W3-13	11.68	11.35	1135	1163	1189	1214	1832	4058	5.10
W3-14	11.65	11.32	1120	1147	1173	1199	1819	4045	4.88
W3-15	11.21	10.89	1102	1128	1153	1178	1775	3936	4.77
W3-16	12.70	12.34	1142	1172	1200	1229	1909	4288	5.54
W3-17	12.67	12.31	1150	1180	1208	1236	2189	4692	5.43
W3-18	12.34	11.99	1149	1178	1206	1233	2157	4607	5.21
W3-19	12.46	12.11	1140	1170	1198	1225	1891	4377	5.10
W3-20	11.56	11.23	1122	1150	1175	1201	2066	4387	4.88
W3-21	11.17	10.85	1107	1133	1158	1183	2019	4273	4.77
W3-22	10.74	10.43	1085	1110	1134	1158	1964	4139	4.55
W3-23	12.73	12.37	1140	1171	1199	1228	1911	4294	5.43
W3-24	12.44	12.09	1140	1170	1198	1225	1889	4229	5.21
W3-25	11.68	11.35	1131	1158	1184	1210	1829	4056	5.10
W3-26	12.05	11.71	1121	1149	1176	1203	1848	4263	4.88
W3-27	11.26	10.94	1108	1135	1160	1185	1783	3950	4.77
W3-28	10.50	10.20	1088	1113	1136	1159	1715	3764	4.55
W3-29	12.29	11.94	1133	1163	1190	1218	2142	4586	5.21
W3-30	12.46	12.11	1131	1160	1188	1215	1883	4372	5.10
W3-31	11.30	10.67	1120	1146	1171	1197	1795	3965	4.88
W3-32	11.65	11.32	1108	1136	1162	1187	1810	4149	4.77
W3-33	11.19	10.87	1096	1123	1148	1172	1770	4021	4.55
W3-34	11.62	11.29	1117	1145	1170	1196	1815	4037	5.10
W3-35	12.00	11.66	1114	1143	1169	1196	1840	4246	4.88
W3-36	10.87	10.56	1102	1128	1152	1176	1752	3858	4.77
W3-37	10.82	10.51	1085	1110	1134	1158	1736	3839	4.55

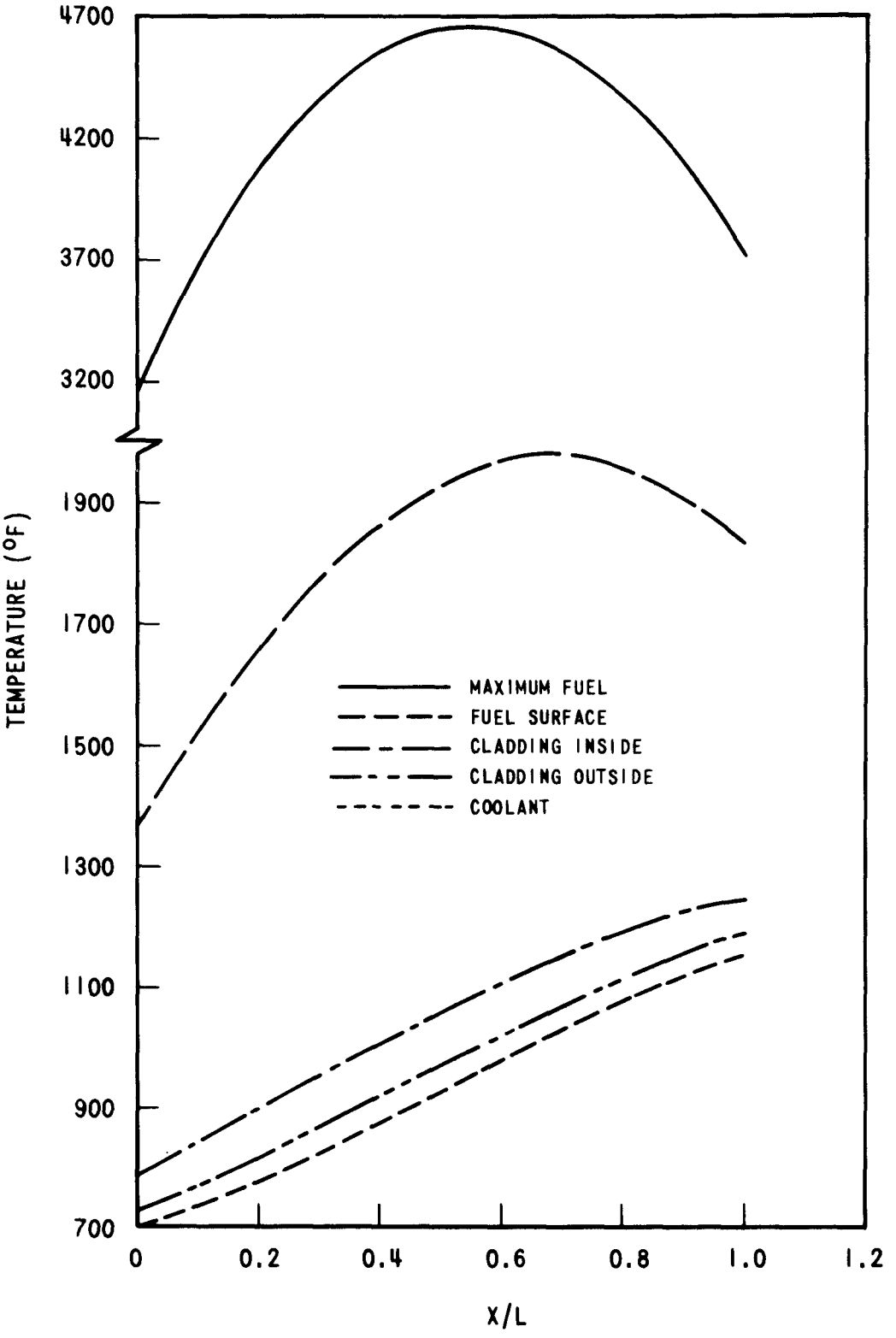

Figure 6-1. W3-1 Axial Temperature Profiles (Uncertainty factors included)

3937-12

Table 6-2. Stress-Strain Results

Pin Number	Nominal Fractional Fission Gas Release at C	Nominal Initial Pressure (psi)	Nominal End of Life Pressure	End of Life Pressure (UFI)	Fuel Pin Cladding Hoop Pressure Stress at Core Outlet (psi)	Fuel Pin Cladding Thermal Stress at Core C, (psi)	Total Forced Strain at C % (UFI)	Total Forced Strain at Core Outlet (UFI)	Fuel Clad. Effective Thickness End of Life at Core Outlet (in.)
W3-1	0.64	75	301	369	2740	14,000	0.054	0.042	0.0118
W3-2	0.73	73	314	381	2800	12,800	0.050	0.040	0.0119
W3-3	0.62	75	279	341	2460	13,200	0.050	0.039	0.0125
W3-4	0.61	73	261	318	2270	12,300	0.046	0.036	0.0121
W3-5	0.74	75	331	402	3000	13,500	0.054	0.043	0.0118
W3-6	0.63	76	297	361	2680	13,600	0.052	0.041	0.0118
W3-7	0.72	74	301	364	2670	12,500	0.049	0.038	0.0119
W3-8	0.61	75	273	332	2400	12,900	0.049	0.038	0.0120
W3-9	0.60	73	248	301	2110	11,900	0.044	0.034	0.0121
W3-10	0.64	74	291	356	2620	13,400	0.051	0.040	0.0118
W3-11	0.73	75	325	394	2940	13,200	0.052	0.041	0.0118
W3-12	0.62	76	282	344	2520	13,300	0.051	0.039	0.0118
W3-13	0.72	73	293	354	2570	12,100	0.047	0.037	0.0120
W3-14	0.70	73	284	343	2460	12,100	0.046	0.036	0.0121
W3-15	0.70	73	274	331	2330	11,600	0.044	0.034	0.0122
W3-16	0.74	73	320	389	2880	13,100	0.052	0.041	0.0119
W3-17	0.63	74	286	348	2560	13,100	0.050	0.039	0.0118
W3-18	0.62	74	272	331	2410	12,700	0.048	0.038	0.0119
W3-19	0.61	75	274	333	2420	12,900	0.049	0.038	0.0119
W3-20	0.60	73	250	303	2150	12,000	0.045	0.034	0.0121
W3-21	0.59	73	242	293	2050	11,600	0.043	0.033	0.0122
W3-22	0.58	72	226	274	1880	11,200	0.041	0.031	0.0123
W3-23	0.73	74	321	390	2870	13,200	0.052	0.041	0.0119
W3-24	0.72	74	309	373	2740	12,900	0.050	0.039	0.0119
W3-25	0.72	73	292	353	2560	12,100	0.047	0.037	0.0120
W3-26	0.60	74	259	313	2230	12,500	0.047	0.036	0.0121
W3-27	0.70	73	276	332	2360	11,700	0.045	0.035	0.0121
W3-28	0.69	71	253	304	2100	10,900	0.041	0.032	0.0123
W3-29	0.62	74	269	328	2360	12,700	0.048	0.037	0.0120
W3-30	0.61	75	273	331	2390	12,900	0.049	0.038	0.0120
W3-31	0.70	73	277	334	2390	11,700	0.045	0.035	0.0121
W3-32	0.59	74	250	303	2140	12,100	0.045	0.034	0.0121
W3-33	0.58	73	236	385	1960	11,600	0.043	0.033	0.0122
W3-34	0.72	72	289	350	2520	12,000	0.046	0.036	0.0121
W3-35	0.60	74	257	312	2200	12,400	0.046	0.036	0.0121
W3-36	0.70	72	267	323	2260	11,300	0.043	0.032	0.0122
W3-37	0.69	72	259	311	2170	11,300	0.042	0.032	0.0123

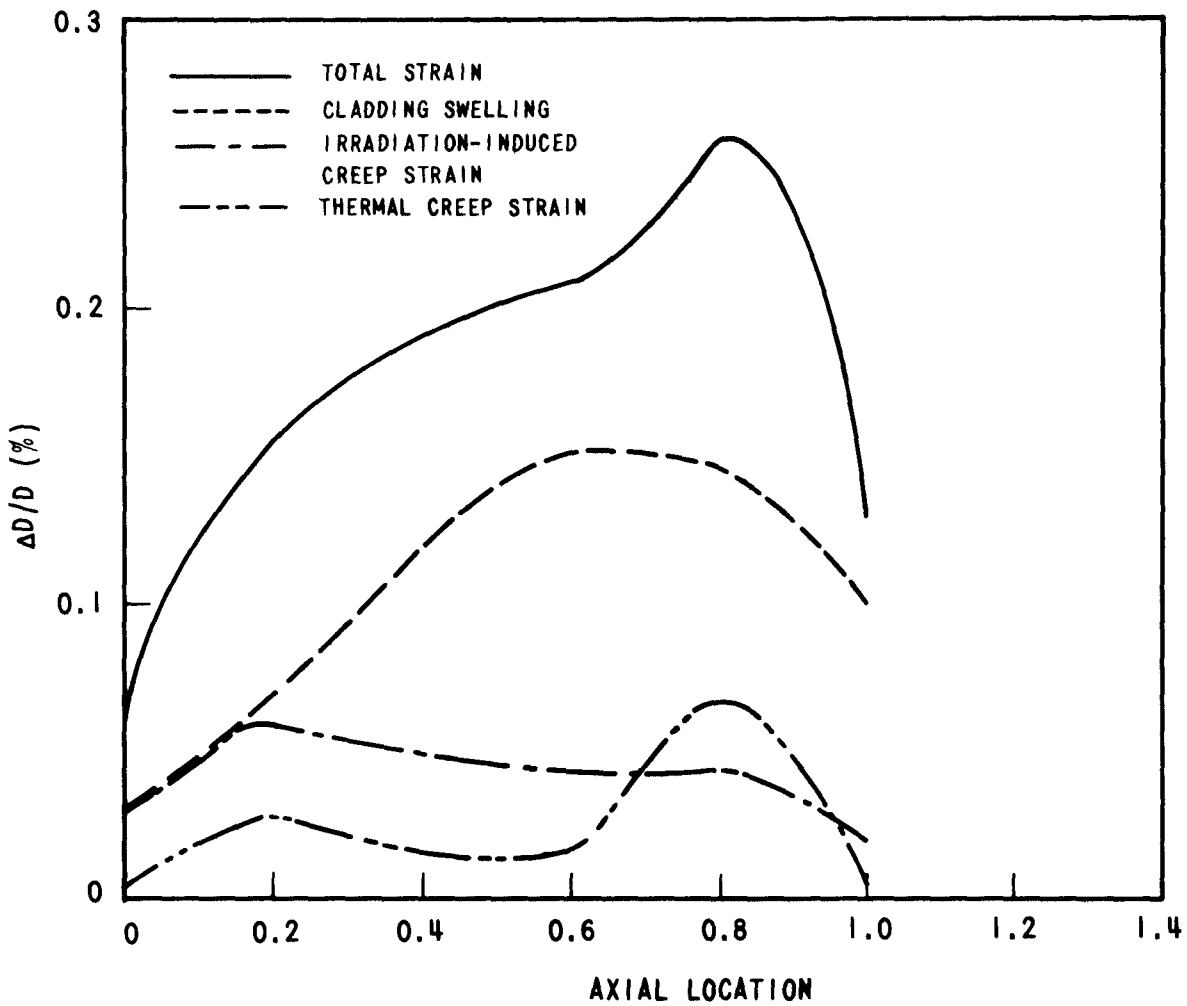

Figure 6-2. Diametral Cladding Strains From Olympus-IIA Pin W3-1

3937-13

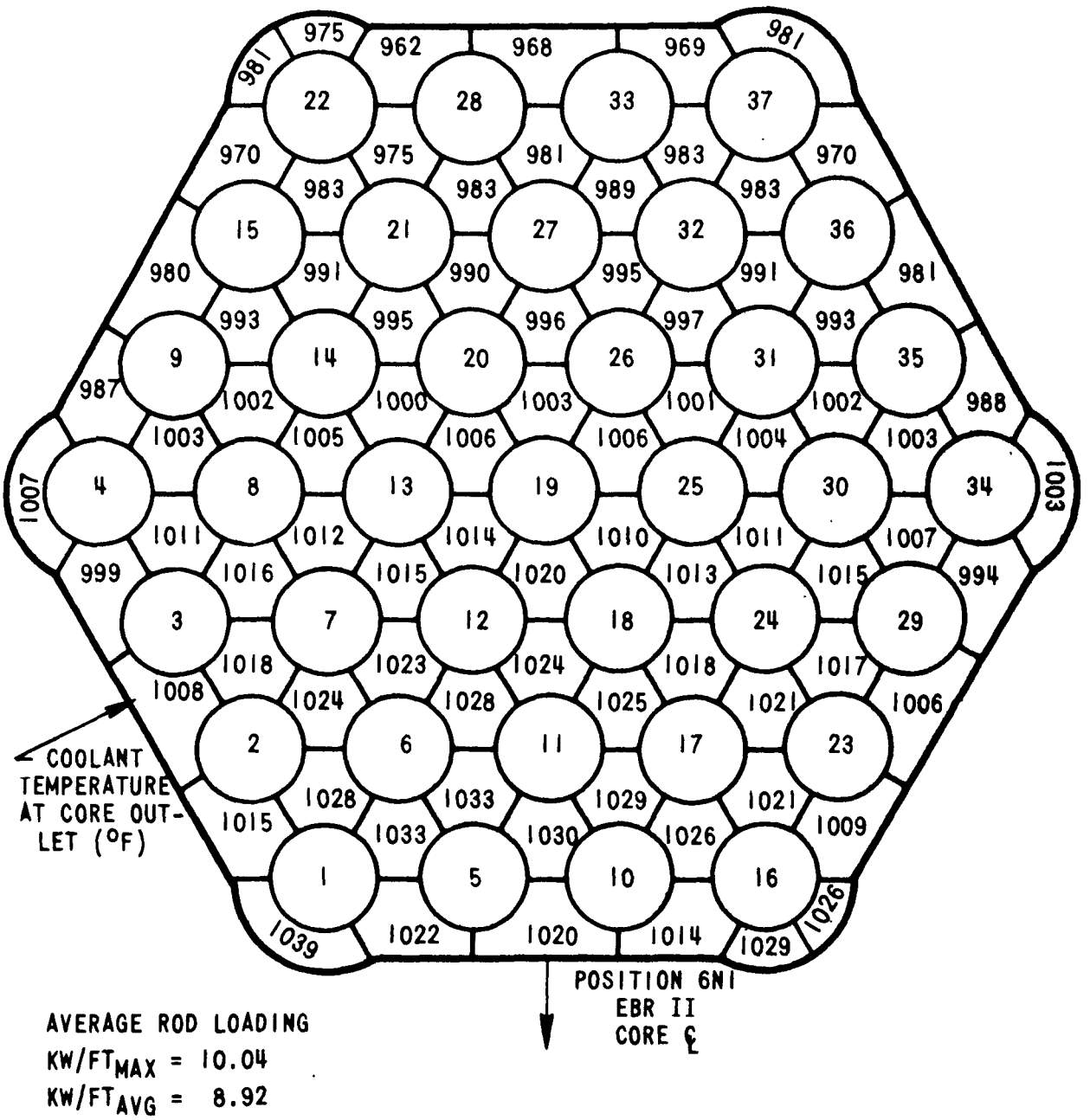

Figure 6-3. Outlet Coolant Temperature Distribution at End of Life

3937-14

3.2 WSA-3 Fabrication

All fuel pin hardware has been received. Fuel fabrication is nearing completion, and fuel pin assembly is in progress; as reported under Tasks 510 and 512, respectively. The initial xenon tagging of fuel pins was accomplished in the presence of an EBR-II Project representative. Approval was granted to complete all 37 pins and the 8 spare pins. Subassembly hardware fabrication is in progress with several inner grid assemblies completed as discussed in the Task 410 report (Section 9). During this quarter an AEC quality assurance audit was conducted of the fabrication areas involved in the irradiation programs. Many procedures and operations were documented to comply with RDT directives, causing some delays in several areas of the fabrication effort.

3.3 WSA-4 Design

Major experimental objectives for the WSA-4 subassembly have been identified, and design concepts capable of meeting these objectives have been proposed for evaluation by preliminary analysis. The objectives include:

1. Interference fit between fuel pins and grid cells early in life.
2. Increased temperature gradients (as compared to WSA-3) in the peripheral region to assess the effect on channel closing.
3. Higher cladding temperatures ($\sim$1250°F) to evaluate high temperature swelling phenomenon.
4. Capability of individual pin removal without disturbing pin-grid relationship of other locations. Improved inspectability of subassembly peripheral region prior to extensive disassembly.

Two design concepts or modifications of WSA-3 are being considered to provide the second and third objectives for WSA-4. The first concept allows large amounts of bypass flow between the inner and outer hex cans. Reasonably high gradients across the can walls and peripheral regions are possible with this method. Some cladding temperatures as high as 1300°F with an acceptable mixed mean outlet temperature and 13.5 kw/ft linear power ratings are feasible. The second concept makes use of flow maldistribution within the rod bundle caused by removal of the liners from the WSA-3 design. Through proper design, the outer region is overcooled still keeping the subassembly within the mixed mean outlet temperature criterion. Preliminary subchannel analyses using COBRA are in progress to determine the feasibility and conditions available for this concept. Results of an initial preliminary run for the core region not including the effect of grids is shown in Figure 6-4. The maximum coolant temperature of 1206°F is in the acceptable range, but the outer region temperature gradients appear excessive. These can be reduced by proper design of the grid and flow tabs to induce cross flow. Studies on these concepts are continuing.

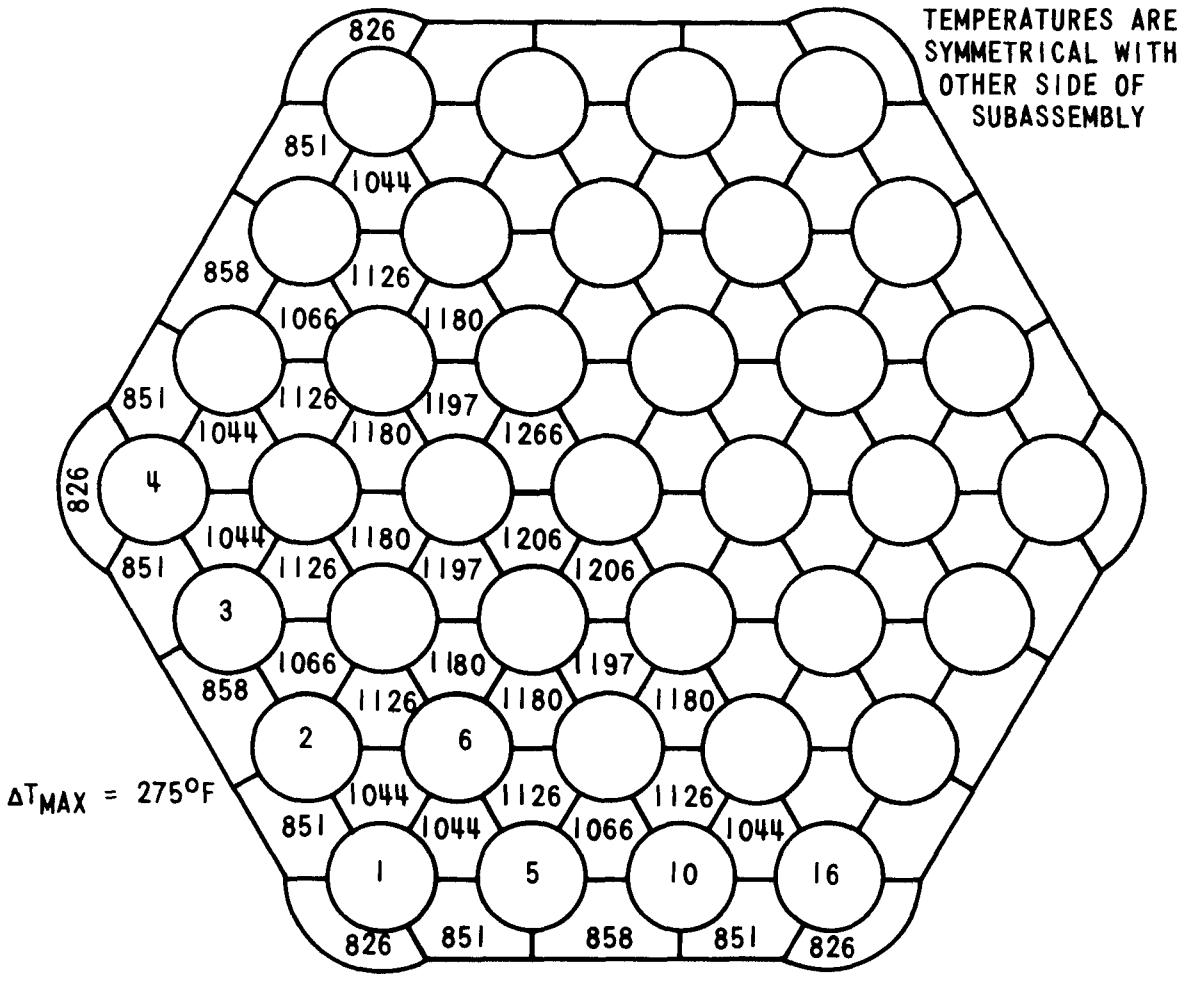

AVERAGE ROD LOADING

KW/FT_{MAX} = 13.0

KW/FT_{AVG} = 11.56

W = 21,190 lb/hr

T_{AVG} = 955°F

Figure 6-4. Coolant Outlet Temperatures for WSA-4 Concept

3937-15

3.4 Program Activities

The data package draft for WSA-3 is nearing completion. A final draft for review and comment should be finished by mid-October and ready for submittal shortly thereafter.

The mockup flow test subassembly was received at the EBR-II Site in good condition. Tests on the mockup will commence soon.

A request for "Approval-in-Principle" of the WSA-4 experiment has been prepared. It will be sent to RDT within the next month.

4.0 REFERENCES

1. "Oxide Fuel Element Development Quarterly Progress Report for the Period Ending June 30, 1970," WARD-4135-11, September 1970.

SECTION 7

OFBA-312 217-ROD GRID-TYPE FUEL ASSEMBLY DESIGN AND DEVELOPMENT

P. Arnsberger, B. Bishop, R. Borst, F. Engel,
A. Krebs, R. Markley, and J. Patterson

1.0 OBJECTIVES

The overall objective of this program is to develop a grid-type fuel assembly for the LMFBR program and to provide a backup for the FFTF reactor. This program will include the design, development, and evaluation of the grid and grid-type assembly.

2.0 PRIOR WORK

The work program was specified. A preliminary analysis was made of grid types, grid stresses, rod vibration, and grid strap wastage. Manufacturability studies were initiated. A thermal and hydraulic parameter study was made for determination of fuel rod and grid design limits within the constraints of the FFTF geometry and coolant flow conditions. Preliminary thermal and hydraulic subchannel analyses were initiated with the aim of determining the effects of variations in geometry on flow and temperature distribution due to tolerances or predicted changes during operation.

Design of capsules for grid specimen irradiation tests in EBR-II was started.

3.0 CURRENT PROGRESS

3.1 Preliminary Thermal and Hydraulic Design

3.1.1 Hot Spot Factors

The methods of attaining the best estimates of the hot spot factors were reviewed, and the effect of their individual contribution to the temperature rise was examined. The results are summarized in Table 7-1. These values that represent the best current estimates of the uncertainty values in the T&H design will form the basis for the initiation of preliminary design. These factors will be continually reassessed during preliminary design of the grid-type fuel assembly.

The semi-statistical method which was employed is discussed below. In determining the maximum probable cladding temperature, the effects of the enthalpy rise factors far overshadow those of the film and cladding temperature rise contributions. Use of the semi-statistical method requires the separation of the variables that cause the hot spot temperatures into two principal groups: one of the statistical origin and the other non-statistical. The two categories are defined below.

Table 7-1. Effect of Hot Spot Factors On Temperature Distribution

	$F_{\Delta H}$		F_{θ}		$F_{Cladding}$		F_{Gap}		F_{Fuel}	
	Value	°F	Value	°F	Value	°F	Value	°F	Value	°F
Non-Statistical										
Power control band	1.02	9	1.02	1	1.02	2	1.02	11	1.02	48
Inlet flow maldistribution	1.05	22	--	--	--	--	--	--	--	--
Intra-assy. flow maldistribution	1.03	13	--	--	--	--	--	--	--	--
Local channel closing	1.05	22	1.08	3	--		--		--	
Circumference temperature variation	--	--	1.30 1.10(a)	13 4(a)	--		--		--	
Direct Combination	1.158	66	1.432 1.212(a)	18 9(a)	1.02	2	1.02	11	1.02	46
Statistical										
Power level measurement	1.09	40	1.09	4	1.09	6	1.09	42	1.09	224
Orificing Uncertainties and assembly tol. effect on flow	1.05	22	1.02	1	--		--		--	
Unit cell flow area	1.04	18	1.075	3	--		--		--	
Fuel fissile content & length	1.02	9	1.035	1.5	1.035	2.5	1.035	16	1.035	84
Material properties, thickness & heat transfer coefficients	1.04	18	1.15	6.5	1.12	9	1.20	92	1.10	238
Statistical Combination	1.119	53	1.195	8.5	1.154	11	1.22	101	1.139	337
Total Hot Spot Factor	1.296	124	1.711	30	1.177	13	1.25	112	1.162	385

(a) For fuel temperature only.

A non-statistical uncertainty is defined as a variable, the exact value of which cannot be predicted in advance but is not subject to random occurrence. Computationally, the non-statistical factors represent multipliers applied to the nominal magnitudes of the variables to provide the worst possible values which can be assumed. A variable which has a frequency distribution of occurrence due to its random character is treated statistically. In addition, experimental data (e.g., fuel and cladding properties) are treated statistically, since their evaluation by experiment implies some statistical behavior.

Figure 7-1 illustrates the method of combining hot spot factors. The nominal temperature difference $\Delta T_{j,nom}$ of component j is increased by the cumulative or non-statistical effects to the new corrected cumulative temperature difference $\Delta T_{j,cum}$. This new actual cumulative component temperature $T_{j,cum}$ represents the mean value for the statistical temperature distribution caused by the variables of random origin.

The bases for arriving at the individual assembly hot spot factors are discussed in the following.

3.1.1.1 Non-Statistical Uncertainties

1. Power Control Band--A long-term steady state power control band of 2% was adopted. This is the reference FFTF reactor design value. This determines the maximum deviation in power level to be applied in considering the reactor long term behavior (e.g., in consideration of creep, swelling, corrosion, etc.).

2. Steady State Overpower Margin--For control system failure and power transients, a steady state overpower margin is required between the reactor nominal design conditions and fuel melting. The corresponding temperatures of the structural materials will be used for primary stress evaluations. This margin (i.e., the 15% value) includes the 2% variation for power control band. This overpower margin defines the reactor short term design conditions.

3. Local Power Density (Nuclear Calculation and Control Rod Effects)--The axial and radial flux and power distribution were provided by the nuclear calculations of FFTF. The non-statistical uncertainties in the calculational procedures are assumed to be included in the values quoted for F_Z^N and F_R^N.

4. Inlet Flow Maldistribution (Effect of Vessel and Internals)--The flow distribution in the lower and upper plenum is determined mainly by the vessel inlet and outlet flow arrangements as well as the internal structure. Therefore, the static pressure distribution might not be ideal and the flow distribution between assemblies, partially determined by that static pressure profile, could deviate from the desired condition.

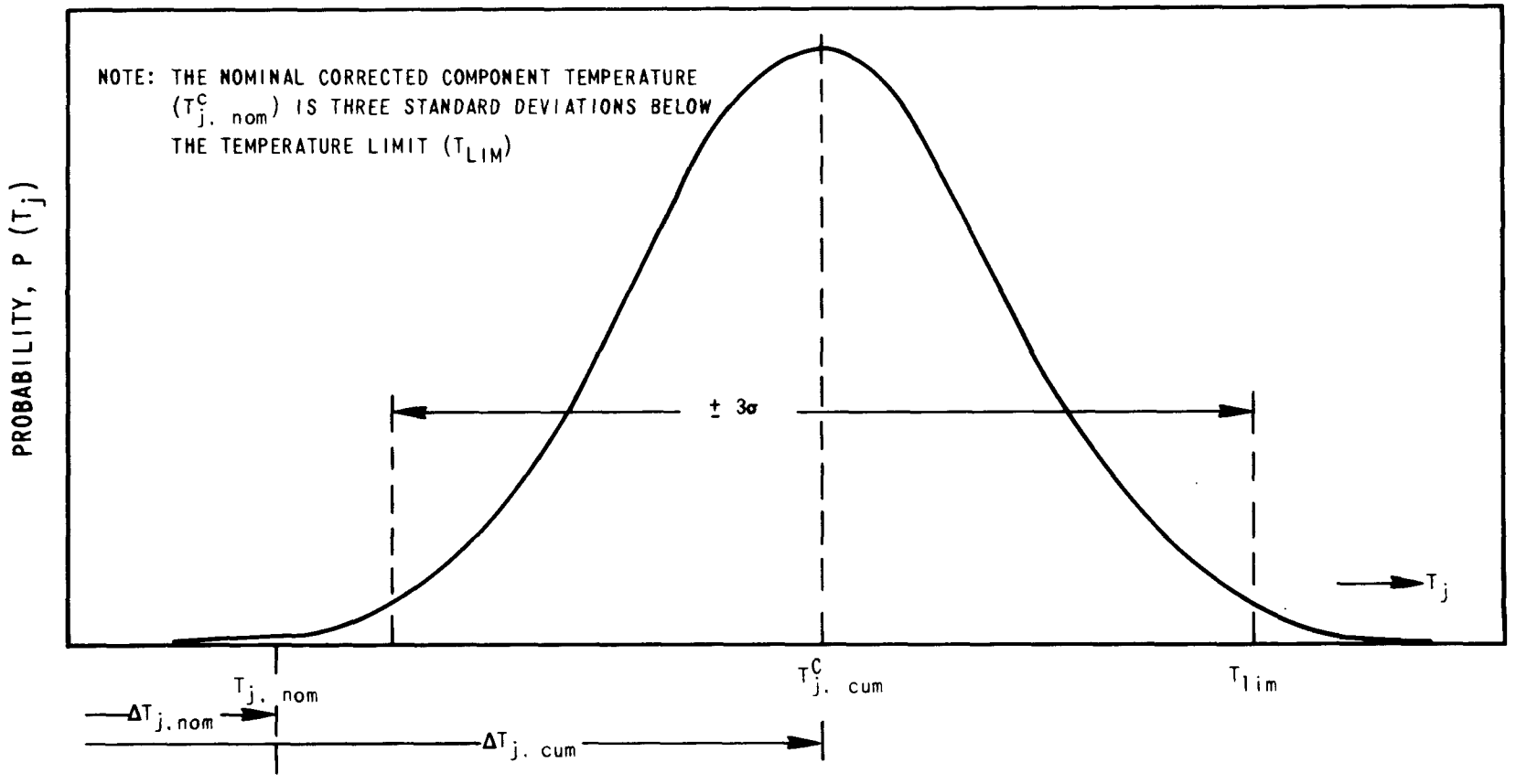

Figure 7-1. Application of Semi-Statistical Method

A further flow shift between assemblies could be caused by differential swelling due to irradiation. Three facts cause this to appear as minor:

a. The fuel rod spacers (grids) swell at approximately the same rate as the assembly duct, so that the ratio of free stream area to blocked flow area would remain approximately constant.

b. The swelling rates of grids and fuel rods are very similar, so that the relative change in coolant channel geometry is negligible.

c. The previously described swelling effect is only present in approximately one-third of the total assembly height. This reduces its influence on the total assembly pressure drop.

Based on FTR design value, a 5% maldistribution is adopted.

5. Intra-Subassembly Flow Distribution--The flow distribution within the grid-type fuel assembly is calculated by means of the subchannel analysis code, COBRA, using the nominal channel and grid dimensions. The effects of cross flow, mixing, and conduction between adjacent channels are taken into account in this code. In a Westinghouse proprietary study, a comparison between an actual flow experiment in a grid-type subassembly and the predictions by COBRA showed an agreement in flow distribution of $\pm$ 3% for the inboard and edge channels. Although the results for the corner channels showed a larger difference, it is believed that none of the corner channels will be a hot channel because of the following:

   a. The corner channel are designed for overcooling margin due to the slots in the grid support straps.

   b. The adjacent side channels are sufficiently cooled, which provides relief by mixing and conduction in case of overheating.

   c. The corner channels can transfer heat toward adjacent assemblies by conduction through duct wall and gap.

   COBRA runs have indicated that even with a high intra-subassembly power gradient the hot channel will always be located in one of the inboard channels. As a result of the comparison mentioned above, a factor of 1.03 is applied to this channel.

6. Local Channel Closing Due to Hot Bow--Preliminary bowing calculations have indicated that the maximum local reduction in rod spacing, (S = pitch-diameter) would be of the order of 10% between grids. Since COBRA cannot handle a wave type channel, an average reduction in rod spacing over the total length of 10% was assumed (see Figure 7-2).

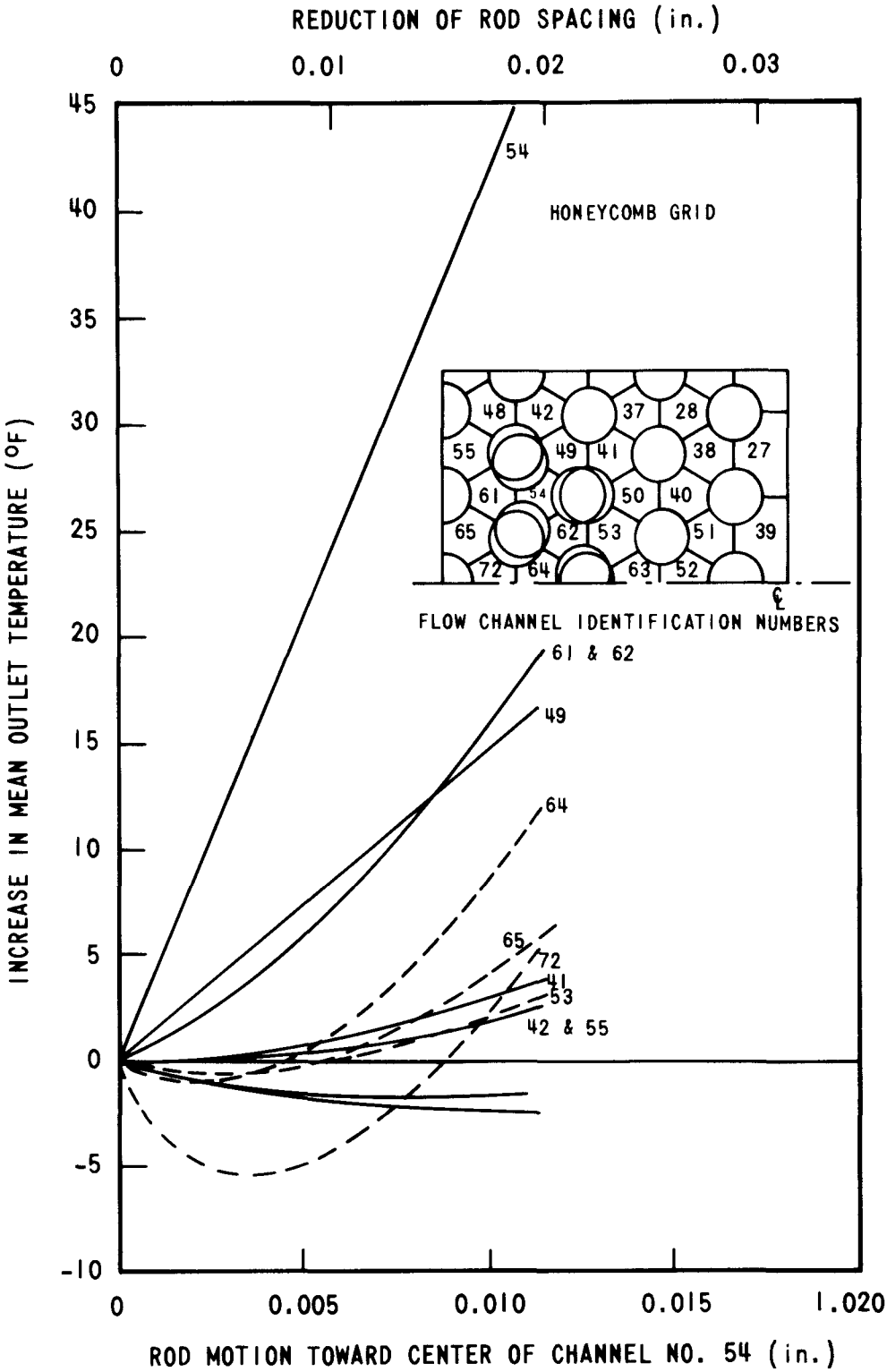

Figure 7-2. Effect on Channel Outlet Temperature of Simultaneous Displacement of Four Rods Towards the Center of Channel No. 54 By "COBRA" Code

3937-35

It is realistic to assume that all three fuel rods forming the hot unit cell flow channel will bow towards that channel of higher temperature. Based on this assumption, a maximum total average flow area reduction of 9.5% can be expected over the fuel rod length. The subchannel analysis for this channel results in an enthalpy rise of 5% when mixing and conduction with adjacent channels are taken into account.

For the influence on the film heat transfer coefficient, the maximum local pitch deviation has to be taken into consideration. Although the dependence on flow is negligible for the existing Peclet number range of interest, the p/d variation is significant in its effect on the heat transfer coefficient. At the location of maximum bowing (10% reduction in rod spacing), a decrease of 8% in the heat transfer coefficient was calculated using the reference design correlation.

$$Nu = 14.27 - 33.86 \left(\frac{P}{D}\right)^{-13.41} + 0.01345 \left(\frac{P}{D}\right)^{1.152} (Pe)^{0.8}$$

where: Nu = Nusselt number

Pe = Peclet number

$\frac{P}{D}$ = Pitch to fuel rod diameter ratio

7. Circumferential Temperature Variation on the Cladding--The circumferential temperature variation of the cladding due to variation in heat transfer around the fuel rod in low p/d fuel rod arrays without grids was calculated according to Reference 1. An increase of 20% in film temperature drop at the location of closest local rod spacing was evaluated. The presence of grids will produce additional local increase in film temperature drop whose magnitude, while not yet determined, was estimated to be 10%. A more precise estimate of this will be derived later in this program. It is reasonable to assume that the circumferential temperature variation disappears toward the fuel surface because of conduction within the cladding and the relatively high gap resistance. Therefore, a factor of 1.30 should be applied for the evaluation of the cladding hot spot temperature only. For fuel temperature determination, a value of 1.10 is assumed at this time.

3.1.1.2 Statistical Uncertainties

1. Power Level Measurement--Based upon FFTF recommendation, a calibration error of 9% in power measurement was assumed. This is based on an evaluation of sensor accuracy, sensor placement with respect to the location of maximum value, and sensor drift. Combination of these effects determines the maximum deviation in power level with regard to the assembly long term behavior (e.g., creep, swelling, corrosion, etc. behavior).

2. Orificing Uncertainty and Assembly Tolerance Effect on Flow Maldistribution--These effects influence each other. In a highly orificed assembly, the assembly tolerance effect is less dominant because the pressure drop within the assembly is only about 50% of the total Δp. This assembly is most sensitive to an uncertainty in orificing. For the near center assembly, which has little orificing however, the maldistribution is caused only by variation in assembly geometry. Since there are no experimental and manufacturing data available at the present design stage, an allowance for 5% flow variation between assemblies is provided with a 3σ confidence level.

3. Unit Cell Flow Area--Based on a statistical evaluation of critical fuel assembly tolerances and their effect on coolant channel flow area due to cold bow, pitch, and diameter variations, the following data which are valid as average values over the total channel length are used:

   Standard deviation of rod spacing = $\pm$ 4 mils

   Standard deviation of rod outside diameter = $\pm$ 1 mil

   Using a Monte Carlo approach which has been developed under Westinghouse proprietary work, a deviation of 3.65% for the channel flow area variation was calculated. With a 3σ area reduction of 11%, the corresponding enthalpy rise was evaluated as 4% using the subchannel analysis code COBRA, assuming 2% mixing plus conduction. The effect on the heat transfer coefficient was calculated to be 7.5%.

4. Fuel Fissile Content--Two values have to be evaluated. The first number of interest is the maximum deviation of the plutonium content of the individual pellet. This value is determined from the specified engineering tolerance on the PuO_2 variation and the measurement uncertainty. Both variations represent a 3σ value. Combining the two uncertainties statistically, a local variation of 3.5% in plutonium content per pellet is obtained with a confidence level of 99.87% (3σ) that this variation will not be exceeded. The second quantity of interest is the maximum deviation of fissile content per coolant channel which is formed by 3 fuel rods. The specifications require assuming that the maximum deviation (3σ) of the mean of each batch is 1% of the nominal value. The batch size will be approximately 5000 pellets; one fuel rod will contain approximately 140 pellets. To evaluate the deviation in fuel fissile content per channel which will not be exceeded with a probability of 99.87% (3σ), the following four events have to be analyzed.

   a. Probability that the mean of the batch where the pellets for one fuel rod were taken deviates from the nominal value.

   b. Probability that the mean of the random sample of pellets needed for one fuel rod drawn from the population of the pellets of one batch deviates from the mean of that batch.

c. Probability for a special arrangement of three fuel rods within the fuel assembly.

d. Probability of a total length variation due to a stackup of length tolerances.

A numerical analysis showed that a variation of 3 standard deviations in fuel fissile content per channel corresponds to a value of approximately 2%. The uncertainty values adopted are the FTR reference design values.

5. Cladding Thickness and Conductivity--A maximum deviation of 2 mils in cladding thickness is specified. Based on a cladding thickness of 15 mils, a 3σ variation of 12% in cladding ΔT is calculated. In a Westinghouse proprietary study the standard deviation of the cladding conductivity was evaluated as 0.6%. Combining these two effects statistically, a combined uncertainty value for cladding thickness and conductivity of 1.12 at a 3σ confidence level is obtained. These are the reference FFTF Reactor Design Values.

6. Heat Transfer Coefficients--The following heat transfer coefficients are considered:

   a. Coefficient of heat tranfer between cladding and coolant defined as film heat transfer coefficient,

   b. Coefficient of heat transfer between cladding and fuel surface defined as gap conductance.

   The film heat transfer coefficient is believed to have an uncertainty band of 15% at hot spot locations and conditions. The nominal gap conductance of 1200 Btu/hr $ft^2°F$ as evaluated for a 5 mil cold diametral gap in Westinghouse proprietary studies, has been assigned a $\pm$ 20% maximum variation to accommodate for the uncertainties (pellet and cladding diameter, gas composition and content, pellet eccentricity, etc.).

7. Uncertainty in Fuel Thermal Conductivity--The thermal conductivity of mixed-oxide fuel as a function of temperature is not yet known with desired accuracy, especially in the high temperature region close to the melting point. Besides the temperature dependence, the thermal conductivity also depends on the fuel density and the plutonium content. Both properties are subject to change slightly from batch to batch. Another uncertainty is the change in thermal conductivity with burnup. The combined effects of the above mentioned uncertainties are estimated to give a maximum reduction of 10% in the thermal conductivity of mixed-oxide fuel. This is the reference FTR design value.

8. Coolant Properties--The specific heat and the density of sodium are parameters used in the energy and momentum balance for the heated coolant channels to determine the local coolant temperatures. It is assumed that the correlations describing the temperature dependence of density and specific heat given by polynominal fits introduce a combined uncertainty of 4% at a 3σ confidence level.

3.1.2 Subchannel Analysis

The sensitivity of coolant temperature rise to subchannel closing was examined by COBRA code analysis. The temperature change resulting from rod spacing (P-D) reduction was plotted in Figure 7-2 for the conservative case of simultaneous motion of four rods towards the center of flow channel 54. The magnitude of temperature rise change obtained for channel 54 agrees with the assumption of a hot channel factor of about 1.05 for a 10% spacing change between the three rods forming the flow channel.

The grid support strap produces a partial blockage of the side flow channels similar to that effected by the grid straps in the inboard coolant channels. The relative magnitude of the grid loss coefficients of side and inboard channels affects the flow distribution and particularly the temperature gradients across the rows of the rods which are adjacent to the duct wall facing the central assembly. The effect was studied of varying the flow resistance of the edge channels (the loss coefficient) while keeping that of the inboard and corner channels constant. For a 0.050-inch rod to duct spacing, Figure 7-3 shows the influence on flow rate and rod bundle pressure drop of side channel loss coefficient; Figure 7-4, the influence on selected flow channel outlet temperatures; and Figure 7-5, the temperature gradients across rows of rods. Figure 7-6 identifies the flow channels in the 1/12 portion of the assembly adjoining the central assembly. Increasing the edge channel coefficient decreases and even reverses the temperature gradient across the rods. As expected, this is accompanied by an increase of overall pressure drop. The current design of the support grid strap (0.020-inch thickness), which has a loss coefficient of approximately 4.0, appears satisfactory. Manufacturability tests may dictate use of a heavier grid strap. Use of a 25 mil thick strap would produce additional pressure drop. This is not relieved by larger rod to duct spacing as long as the duct size is unchanged. Figures 7-7 and 7-8 give values for 54.5 mils spacing. The temperature gradient is affected but not the assembly pressure drop.

3.2 Preliminary Mechanical Design

3.2.1 Effect of Honeycomb Grid Axial Spacing on Flow Induced Vibration

In the previous quarterly progress report,[2] the equations were developed for parallel flow induced fuel rod vibration according to the modified Burgreen correlation.[3] The results of this analysis gave the allowable fuel rod axial load and grid span length for a maximum fuel rod vibration amplitude of 0.001 inch.

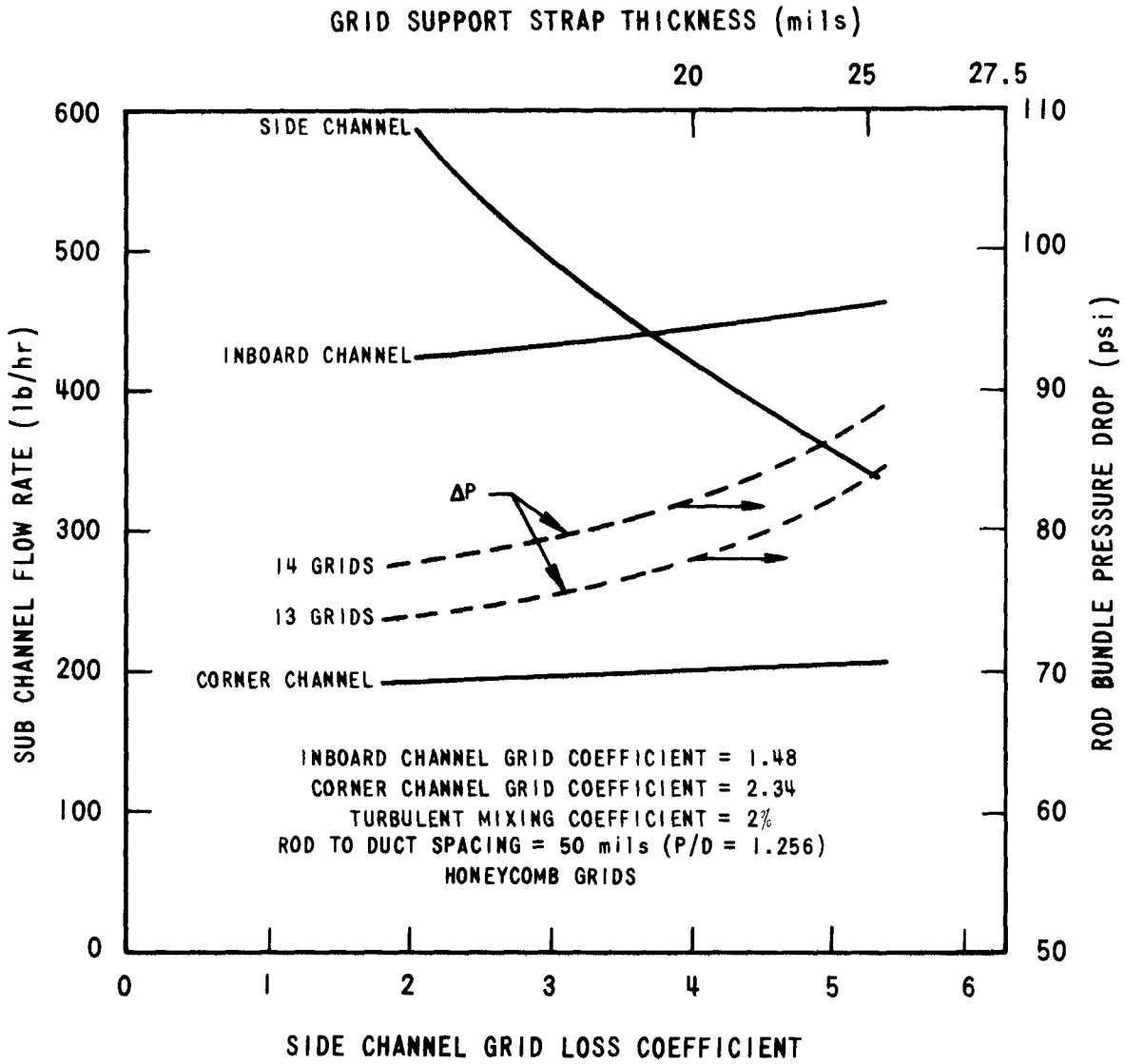

Figure 7-3. Variation of ΔP and Sub Channel Flow Rates at Core Outlet with Side Channel Grid Loss Coefficient - By "COBRA" Code

3937-34

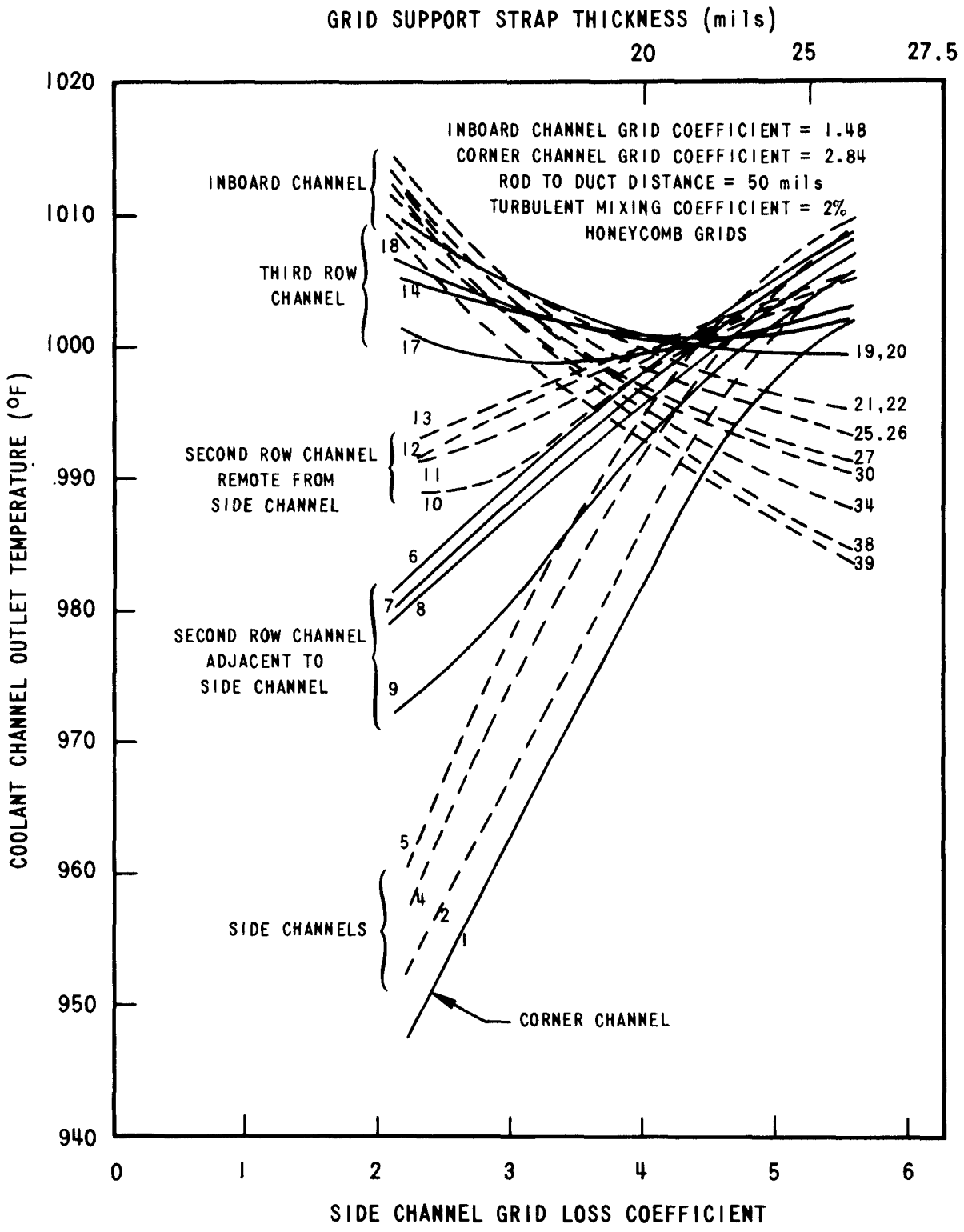

Figure 7-4. Effect of Side Channel Grid Loss Coefficient on Channel Outlet Temperatures - By "COBRA" Code

3937-33

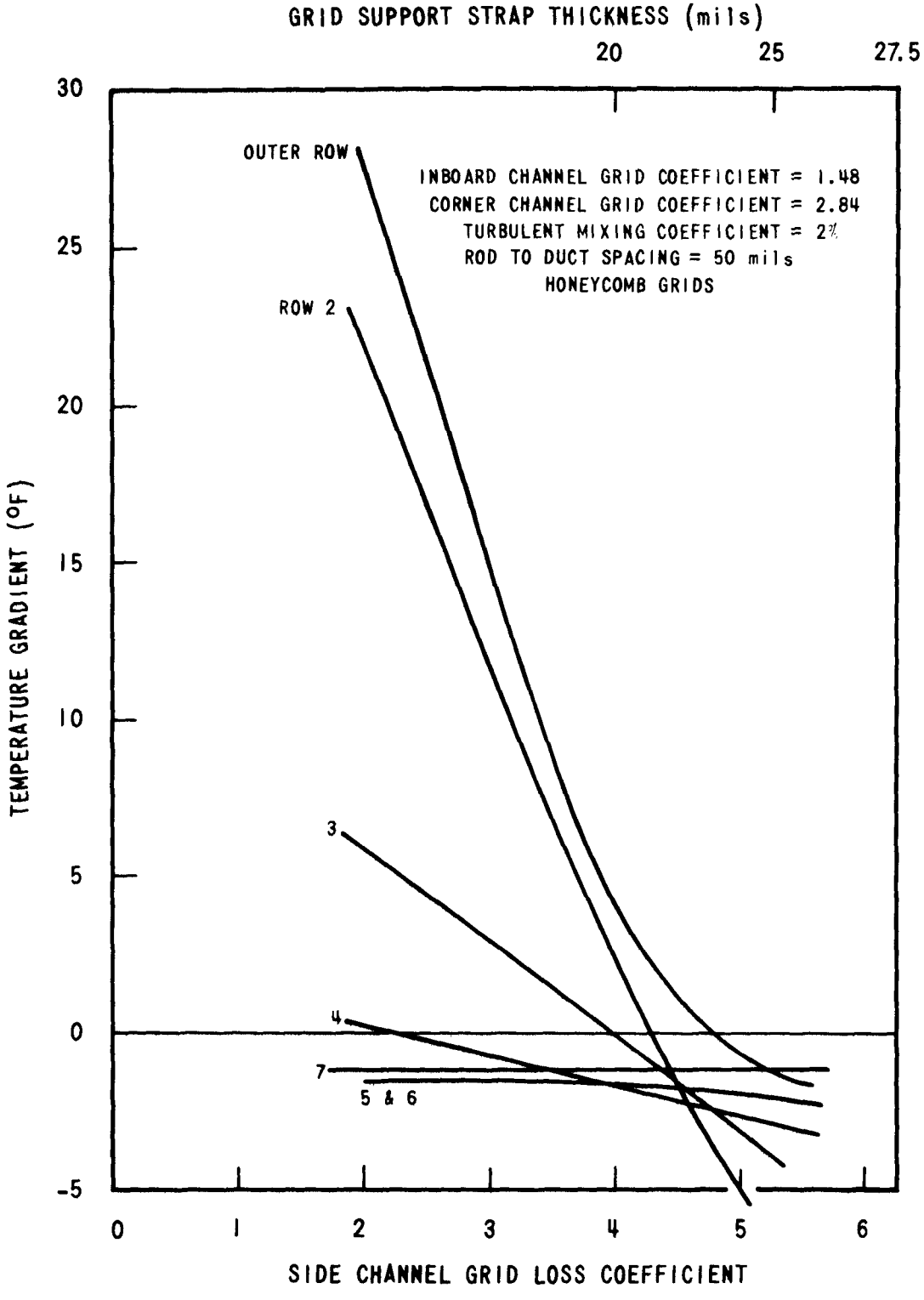

Figure 7-5. Mean Temperature Gradient Across Rows of Fuel Rods Versus Side Channel Grid Coefficient - By "COBRA" Code

3937-42

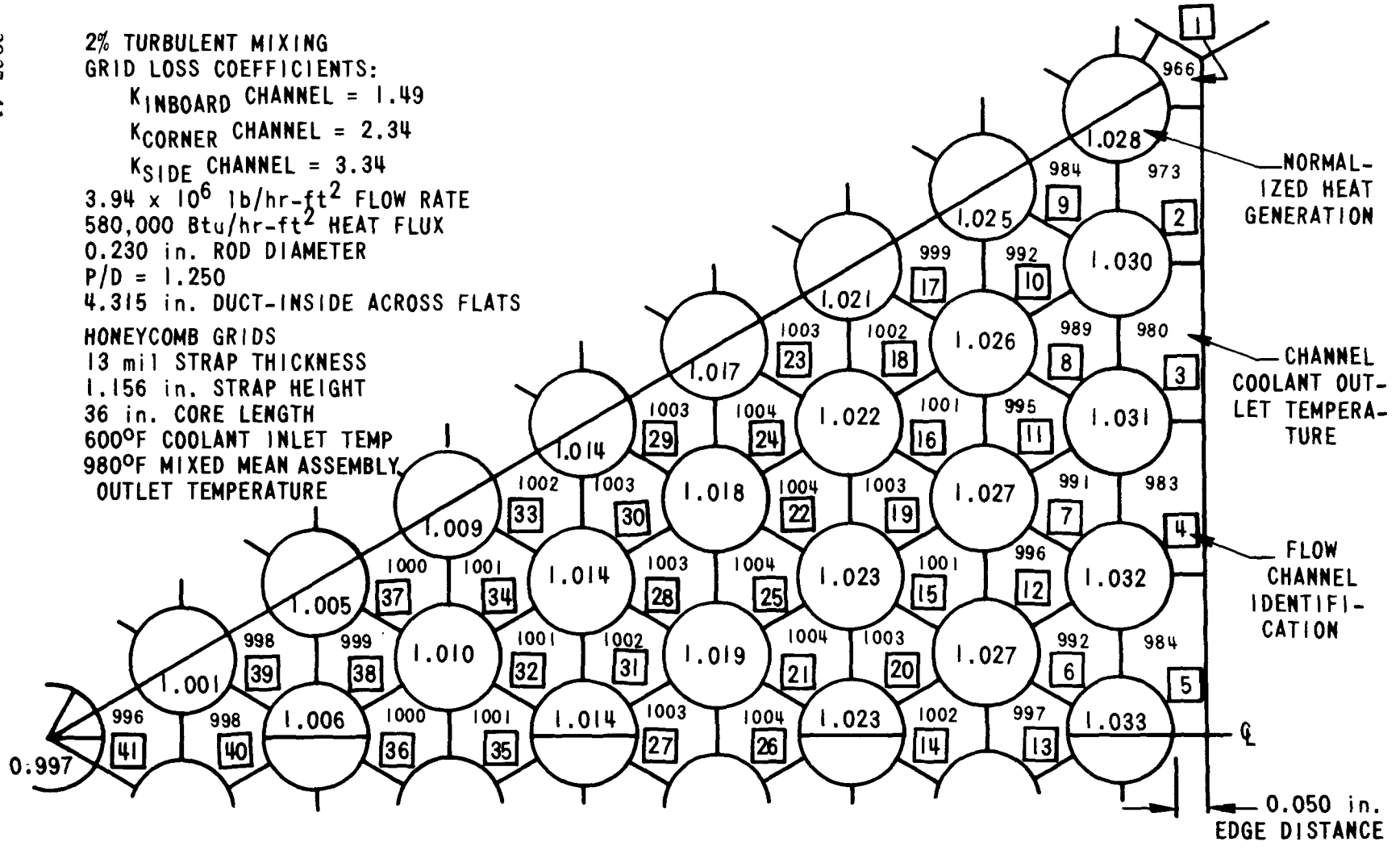

Figure 7-6. 1/12 Segment Adjacent to Central Assembly

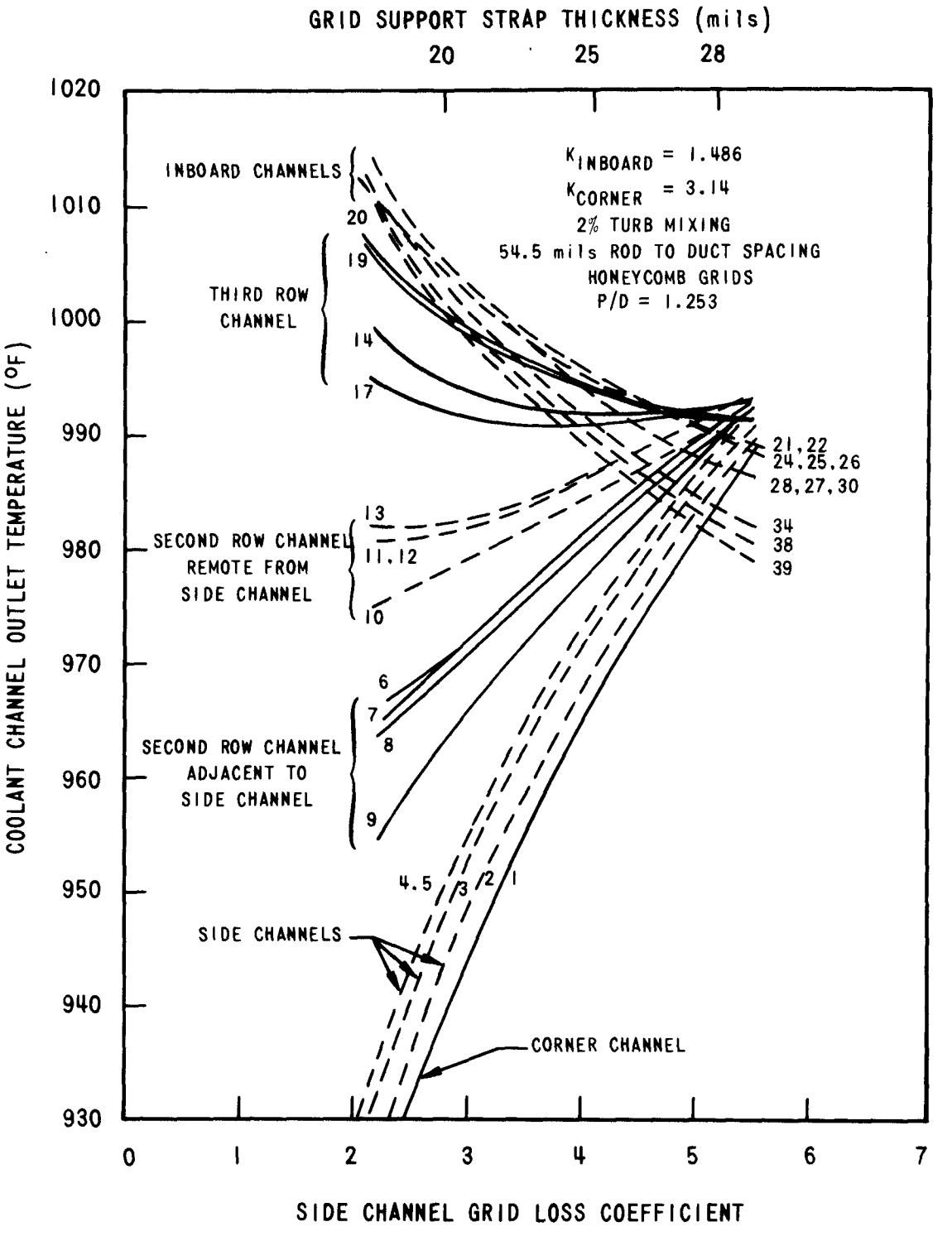

Figure 7-7. Effect of Side Channel Grid Loss Coefficient on Channel Outlet Temperature - By "COBRA" Code

3937-40

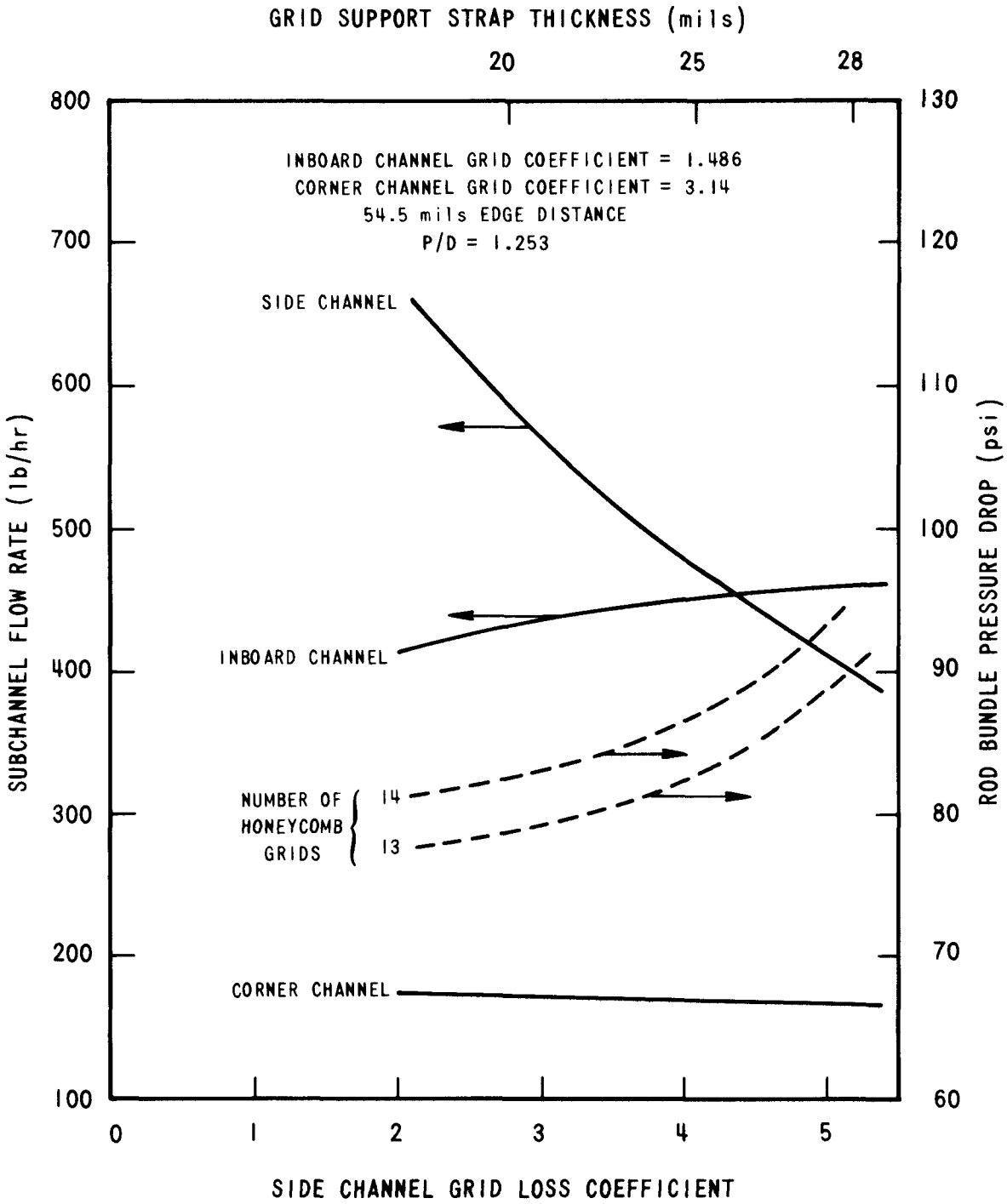

Figure 7-8. Variation of Pressure Drop and Subchannel Flow Rates at Core Outlet with Side Channel Grid Loss Coefficient - By "COBRA" Code

3937-39

Additional analyses of flow induced vibration have been performed for the honeycomb grid design to determine the true critical fuel rod, buckling load at end of life and its effect on fuel rod vibration. The critical fuel rod buckling load which is proportional to the cladding modulus of elasticity (E) and an area moment of inertia (I) has decreased at end of life due to the following effects:

1. Wastage of the cladding material due to sodium corrosion, fretting wear, and fuel-cladding reaction which reduces the area moment of inertia of the fuel rod and also enhances the following effect.

2. Creep straining of the cladding due to fission gas pressure and axial loading reduces the effective elastic modulus.

The cladding material wastage allowance was obtained from the cladding strain analysis for three standard deviations variation in cladding material properties. It has been shown that the critical buckling load at end of life can be reasonably predicted by using an effective elastic bending modulus, E_B, based upon the cladding state of stress and strain at end of life.[4] For this analysis, the equivalent elastic bending modulus, E_B, has been approximated as the tangent modulus to the cladding stress-strain curve at end of life.

$$\frac{1}{E_B} = \left[\frac{1}{E} + \frac{1}{E_{CR}}\right]_{EOL} \qquad (1)$$

where: E = Young's modulus

E_{CR} = Effective creep modulus, the ratio of the Von Mises equivalent cladding stress to the Von Mises equivalent primary and secondary thermal creep strain.[5]

The effective fuel rod bending stiffness (E_B I) is shown in Figure 7-9 for three standard deviations variation in material parameters at the end of the 545-day design life.

The fuel rod actual axial loading was calculated for the honeycomb grid design on the basis of the following conservative assumptions:

1. All three dimples within the honeycomb grid cell contact the fuel rod at end of life.

2. The coefficient of friction between the fuel rod and grid dimple is 1.0.

3. Grid dimples within the fuel rod axial core region exert a maximum radial force of 1.5 pounds each on the fuel rod.

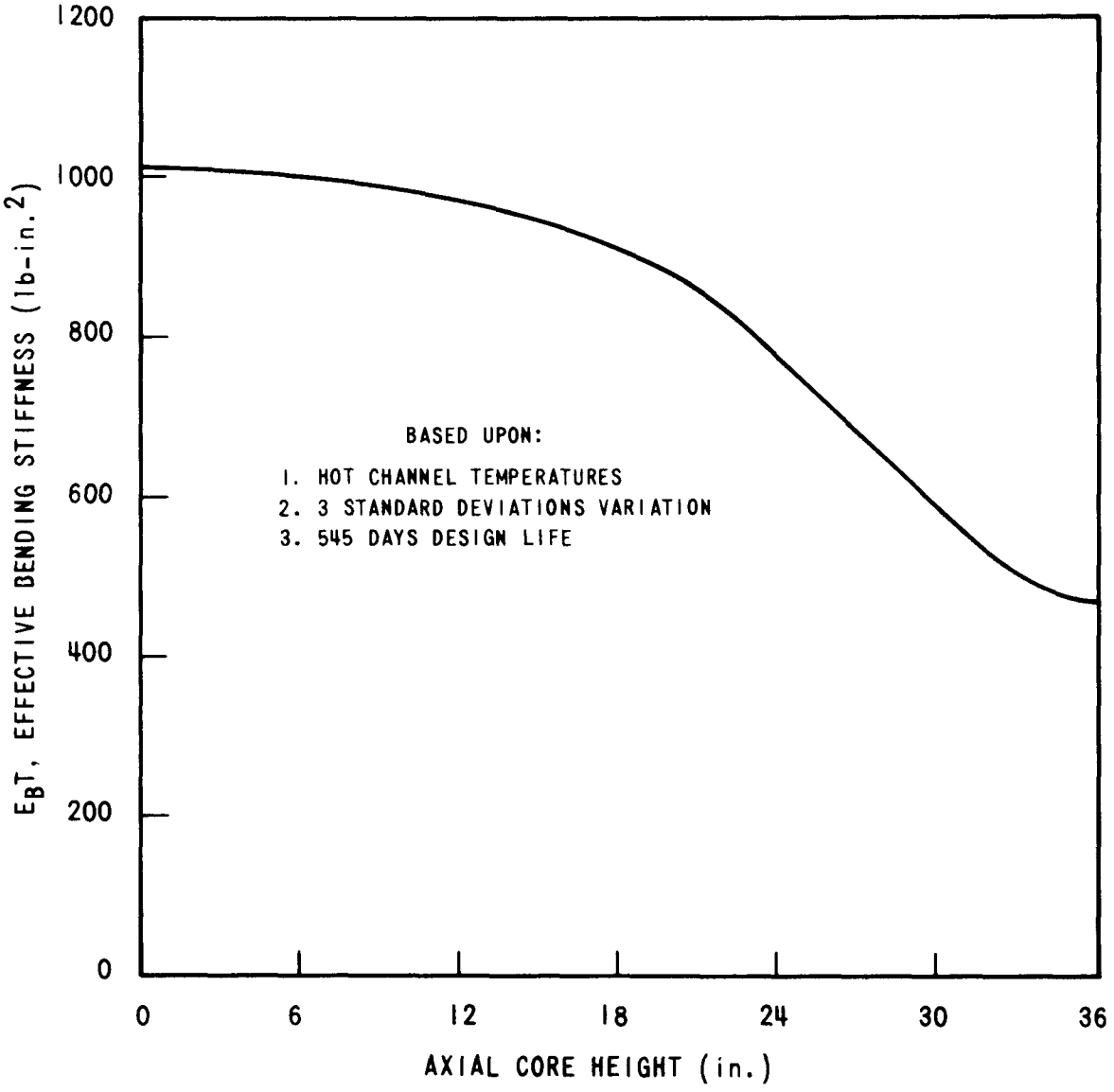

Figure 7-9. Fuel Rod Effective Bending Stiffness

3937-38

4. Grid dimples outside the fuel rod axial core region exert a maximum radial force of 0.5 pounds each on the fuel rod.

The buckling parameter, P/P_{CR}, is defined as follows, assuming that the grid provides pinned end fuel rod support:

$$P/P_{CR} = \frac{P \quad L^2}{\pi^2 (E_B I)_{EOL}} \qquad (2)$$

where:

- P = actual fuel rod axial load (lb)
- P_{CR} = critical buckling load (lb)
- L = grid span length (in.)
- $(E_B I)$ = effective fuel rod bending stiffness ($lb\text{-}in^2$)

For the fuel rod grid spacing and axial loading shown in Figure 7-10, the comparison of actual grid span length and the grid span length for 0.001 inch vibration is presented in Table 7-2.

The preceding analysis indicates that the assumed grid span lengths will restrict the fuel rod amplitude of self-excited vibration due to sodium coolant flow to values less than the allowable limit of 0.001 inch. Moreover, the analysis indicates that longer span lengths would be allowable if fuel rod vibration were the only criteria for specifying span length. As will be shown in the succeeding sections, fuel rod bowing will be the determining factor for grid span length in the axial core region.

Table 7-2 Honeycomb Grid
Fuel Rod Vibration Analysis

Grid Span (Grid No's.)	3σ Limit Buckling Parameter $(P/P_{CR})_{EOL}$	Length For 0.001 Inch Vibration (in.)	Actual Grid Span Length (in.)	Actual Vibration Amplitude (mils)
B - 1	0.179	7.945	7.0	0.677
1 - 2	0.129	8.064	6.0	0.403
2 - 3	0.121	8.082	6.0	0.400
3 - 4	0.109	8.110	6.0	0.396
4 - 5	0.103	8.124	6.0	0.394
5 - 6	0.101	8.128	6.0	0.393
6 - 7	0.099	8.133	6.0	0.392
7 - 8	0.082	10.197	6.0	0.196
8 - 9	0.070	10.231	6.0	0.194
13 - 14	0.048	10.295	7.0	0.306

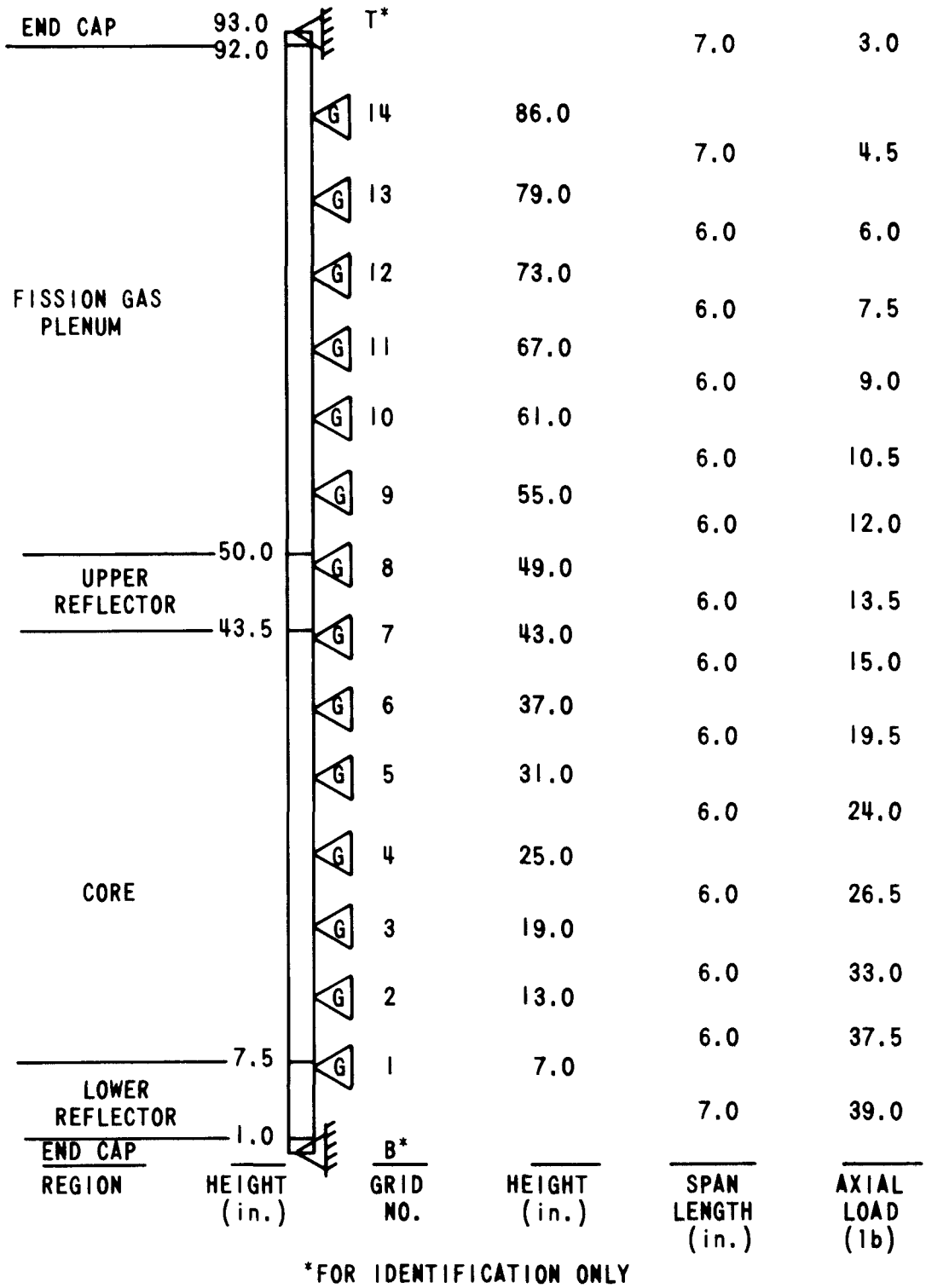

Figure 7-10. Fuel Rod Grid Spacing and Honeycomb Grid Loading

3937-37

3.2.2 Pre-Irradiation Channel Spacing

During manufacture and assembly of the grid-type test assembly components, dimensional variations will arise. The primary effect of such variations is the deviation of the fuel rod from its true position in the reactor core. If this deviation is excessive, the resulting flow channel closure could adversely affect the reactor core thermal performance. The allowable limit on the standard deviation of the pre-irradiation linear channel spacing is given in the Design Requirments as 0.004 inch.

Using statistical methods, the grid-type test assembly design tolerances are combined to predict the variation in linear channel spacing. The analysis is based upon the assumptions that two adjacent fuel rods will have equal and opposite deviations from true position and that the design tolerances are normally distrubuted within $\pm$ 3 standard deviations about the mean value. The grid-type test assembly tolerances that are considered in the statistical analysis are:

1. Fuel rod outside diameter
2. Effective grid cell pitch (includes initial gap and tolerance on grid cell dimple inscribed circle)
3. Fuel rod straightness
4. Lateral grid displacement
5. Grid off-perpendicularity
6. Grid dimple misalignment

A parametric analysis was performed with the PREBOW computer code to determine which of the above parameters most significantly affects the variation in pre-irradiation linear channel spacing. This analysis indicates that fuel rod straightness and grid cell effective pitch variations are the parameters which most significantly affect pre-irradiation linear channel spacing variation. Figure 7-11 shows the effect of effective grid cell pitch variation while Figure 7-12 shows the effect of fuel rod straightness variation on the linear channel spacing standard deviation.

On the basis of the parametric study and the honeycomb grid manufacturing feasibility study, reference design tolerances were selected. Table 7-3 shows the reference design tolerances and the statistical variations in linear channel spacing, fuel rod bow, and flow channel area for the honeycomb grid design and the assumed grid spacing.

The maximum linear channel spacing standard deviation for the 6-inch grid span length is 17% less than the design limit, while for the 7-inch grid span length it is 9% less than the design limit.

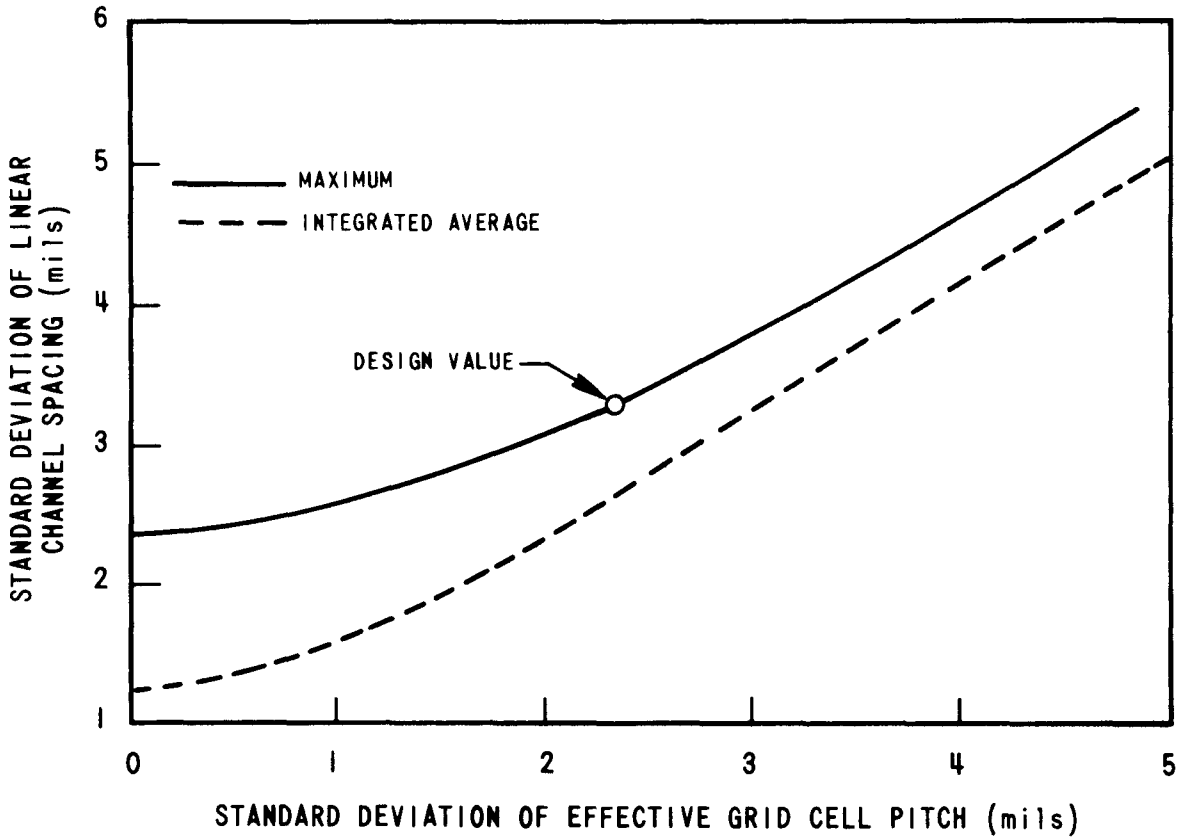

Figure 7-11. Relationship Between Standard Deviations of Pitch and Linear Channel Spacing

3937-43

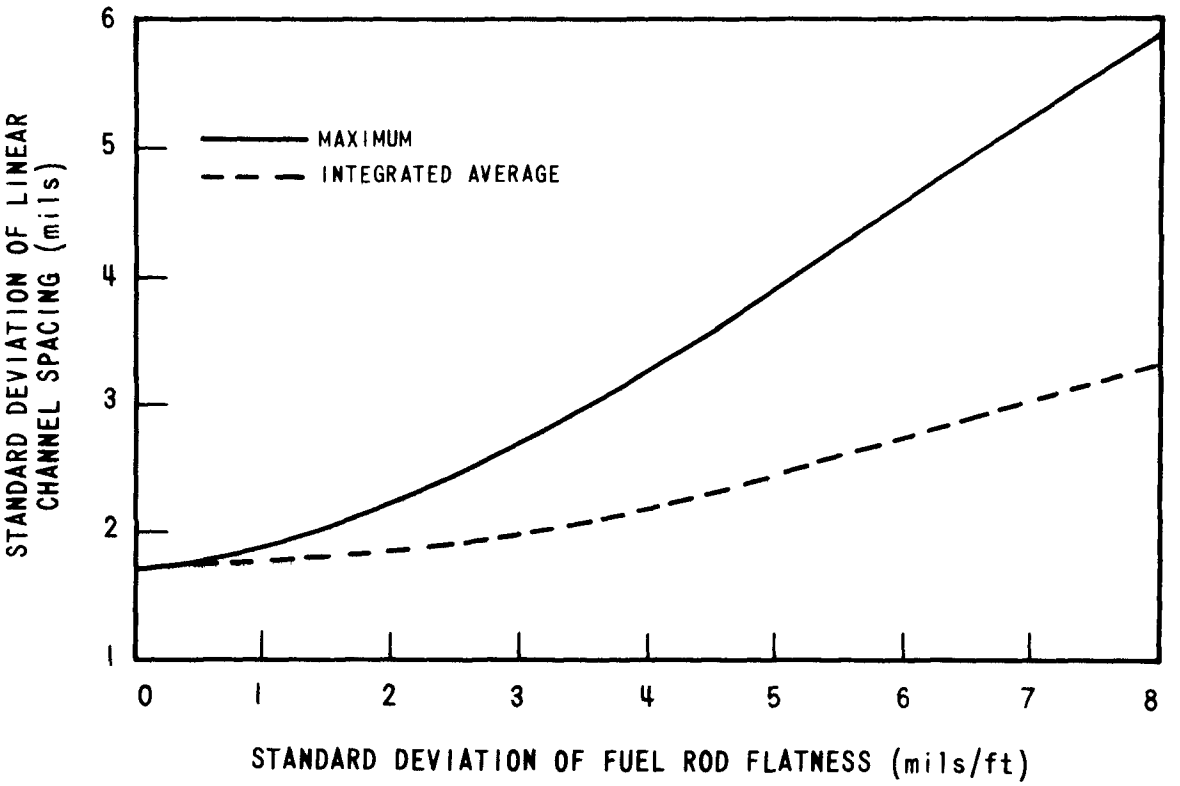

Figure 7-12. Relationship Between the Standard Deviation of Fuel Rod Flatness and Linear Channel Spacing

3937-44

Table 7-3. Honeycomb Grid Assembly Pre-Irradiation Channel Spacing Statistical Analysis

Parameter		Value
Fuel rod outside diameter tolerance (in.)		± 0.001
Effective grid cell pitch tolerance[(a)] (in.)		± 0.007
Fuel rod straightness (in./ft)		± 0.010
Lateral grid displacement		
for 6-in. grid span length (in.)		± 0.006
for 7-in. grid span length (in.)		± 0.007
Grid off-perpendicularity (degree)		± 0.5
Grid-dimple misalignment (in./in.)		± 0.002
For 6-in. grid span length		
Standard deviation of linear channel spacing (mils)	Maximum	3.334
	Integrated Average	2.636
Standard deviation of flow channel area ($in.^2$)	Maximum	6.618×10^{-4}
	Integrated Average	6.045×10^{-4}
Standard deviation of fuel rod bow (mils)		
	Maximum	1.667
	Integrated Average	0.834
For 7-in. grid span length		
Standard deviation of linear channel spacing (mils)	Maximum	3.622
	Integrated Average	2.729
Standard deviation of flow channel area ($in.^2$)	Maximum	6.878×10^{-4}
	Integrated Average	6.117×10^{-4}
Standard deviation of fuel rod bow (mils)		
	Maximum	1.945
	Integrated Average	0.973

[(a)] Includes effects of grid tolerances and fuel rod - grid cell gaps.

3.2.3 Thermal Stability Analysis

Previous work on fuel rod thermal stability included development of the equations for the Rapier and Jones thermal stability criterion modified to account for the effects of fuel rod axial loading.[2] The basic equation is,

$$\frac{A}{A + B} = M = M_S + M_{th} \tag{3}$$

where: A = magnitude of induced fuel rod bow

B = magnitude of initial fuel rod bow

M = total stability factor

M_S = buckling stability factor

M_{th} = thermal stability factor

Since the initial bow, B, is known, Equation 3 has been solved to determine the ratio of total fuel rod bow, A + B, to initial bow:

$$\frac{A + B}{B} = \frac{1}{1 - M} = \frac{1}{1 - (M_S + M_{th})} \tag{4}$$

Equation 4 shows that M is a measure of fuel rod stability, because when M = 1, the bowing amplification is infinite.

The thermal stability factor, M_{th}, is based upon the Rapier and Jones thermal stability factors, R and S.[2]

$$M_{th} = \frac{R}{\pi^2} \left[1 + \frac{4}{\pi^2} S\right] \tag{5}$$

These factors are defined for negligible conduction damping as:[6]

$$R = \frac{\alpha (T_m - T_c) H L^2}{R_o Y} \tag{6}$$

$$S = \frac{Q}{H} \frac{(\Delta T_c / \Delta L) L}{(T_m - T_c)} \tag{7}$$

where: α = coefficient of thermal expansion (in/in/°F)

T_m = mean cladding temperature (°F)

T_c = mean coolant temperature (°F)

L = grid span length (in.)

R_o = fuel rod outside radius (in.)

Y = flow channel width (in.)

$\Delta T_c/\Delta L$ = axial coolant temperature gradient (°F/in.)

H,Q = heat transfer constants

The flow channel width, Y, was based upon beginning of life dimensions assuming two adjacent fuel rods act equally to close the flow channel. Pre-irradiation bow is also considered in this dimension. The thermal stability factors, M_{th}, for the grid span lengths within the axial core region are shown in Table 7-4. Hot channel fuel rod and coolant temperatures, shown in Figure 7-13 were used for this analysis since they include hot spot factors based upon pre-irradiation bow. Outside the axial core region negligible heat generation was assumed; thus, the thermal stability factor is zero.

The creep buckling stability factor is given as:[2]

$$M_S = \frac{P}{P_{CR}} = \frac{P \quad L^2}{\pi^2 (E_B I)_{EOL}} \tag{8}$$

This factor is identical to the buckling parameter calculated for the fuel rod vibration analysis. The creep buckling stability factor, M_S, and the total stability factor, M, are given in Table 7-4. The total stability factor is a maximum near the core centerline, between grids 3 and 4. However, at this point the margin of safety for onset of fuel rod instability is still 240%. Thus, no fuel rod instability would be expected for the assumed grid spacing. Finally, the bowing amplification factor, calculated according to Equation 4 is presented in Table 7-4.

The initial fuel rod bow, B, is assumed to be the algebraic sum of the pre-irradiation fuel rod bow and the bowing induced by the maximum temperature gradients and end-of-life fluence gradients across the fuel rod. The pre-irradiation bow is calculated as three times the maximum standard deviation of fuel rod bow as given in Table 7-3. The temperature and fluence induced fuel rod bow has been calculated with the STASYS computer code and presented in a previous report.[2] The total fuel rod initial bow is then increased by the bowing amplification factor of Table 7-4 to determine the total fuel rod bow at end-of-life. Using statistical methods, the three standard deviation limit on linear channel spacing is calculated, and the additional flow channel closure due to fuel rod bow amplification is calculated as a percentage of the nominal flow channel width. The fuel rod bowing channel closing analysis is shown in Table 7-5. Table 7-5 also gives the allowable limit on flow channel closure specified in the 217-pin grid-type test assembly design requirements. For the worst case condition, the flow channel closure is only 60% of the allowable limit.

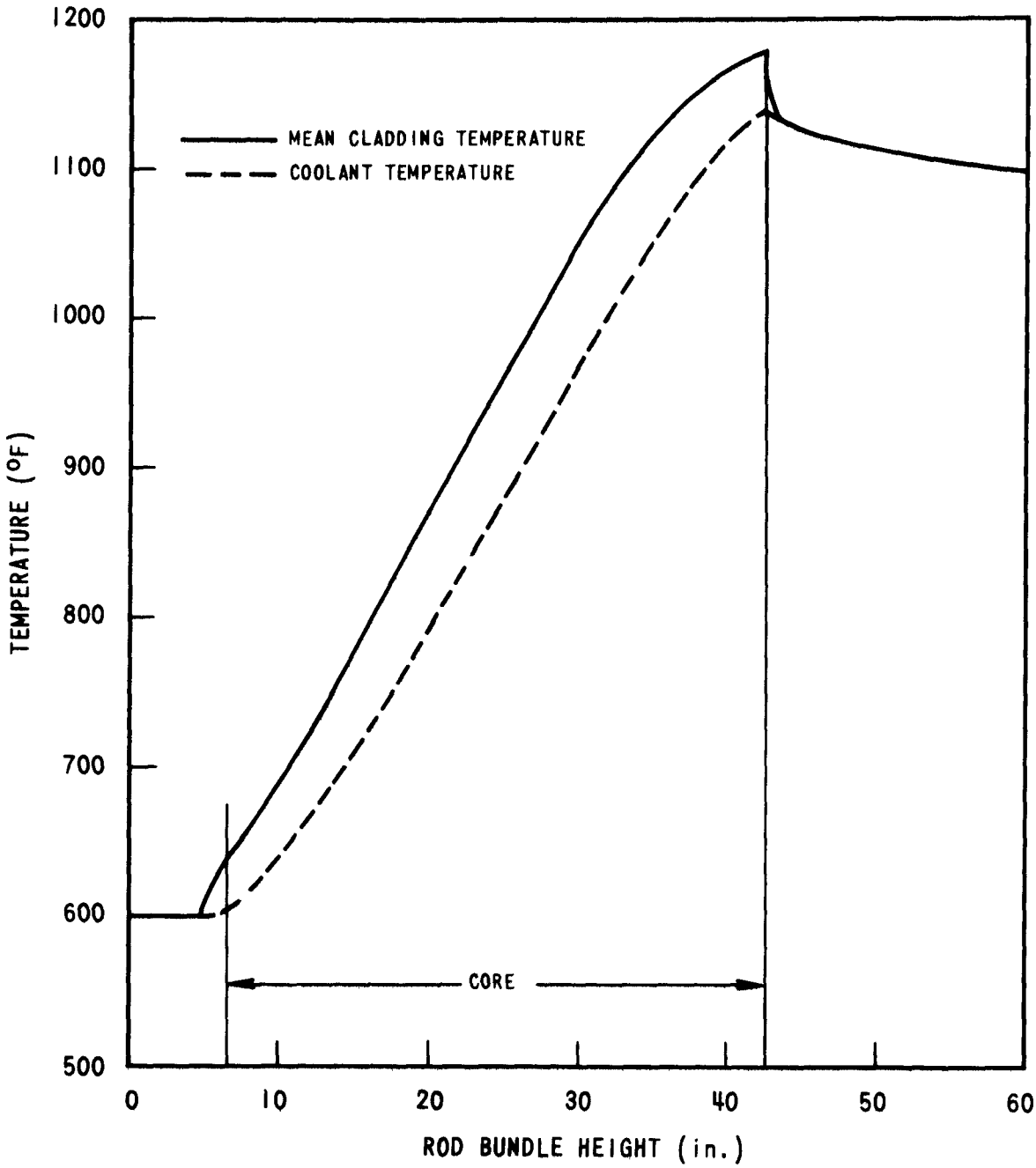

Figure 7-13. Axial Temperature Distribution in the Hot Channel

3937-45

Table 7-4. Fuel Rod Bowing Stability				
Grid Span Grid No's.	Thermal Stability M_{th}	Buckling Stability M_S	Total Stability M	Bowing Amplification Factor
B - 1	0.0	0.179	0.179	1.218
1 - 2	0.121	0.129	0.250	1.333
2 - 3	0.141	0.121	0.262	1.355
3 - 4	0.184	0.109	0.293	1.414
4 - 5	0.183	0.103	0.286	1.401
5 - 6	0.156	0.101	0.256	1.344
6 - 7	0.061	0.099	0.160	1.190
7 - 8	0.0	0.082	0.082	1.089
14 - T	0.0	0.032	0.032	1.033

However, the grid span length should not be increased significantly in the core region because the flow channel closure increases rapidly for small changes in grid span length. For example, if the grid span length between grids 4 and 5 were increased from 6 to 7 inches, the total flow channel closure would increase from 12.18 mils to 22.88 mils. Therefore, the maximum grid span length in the axial core region should be limited to approximately 6 inches.

3.2.4 Fuel Rod Thermal Ratcheting

Under certain combinations of steady-state and cyclic thermal loadings, there is a possibility of large distortions of the fuel rod developing as a result of ratcheting; that is, the deformation increases by a nearly equal amount for each thermal cycle. Excessive fuel rod distortion could produce failure due to cladding strain rupture. From Section 3.3.4 of Reference 7, the limiting value of the maximum cyclic thermal stress permitted in a fuel rod loaded by steady-state internal fission gas pressure in order to prevent cyclic growth in diameter is determined as follows:

Let y' = maximum allowable range of thermal stress computed on an elastic basis, divided by the yield strength, S_y.

x = maximum membrane stress due to pressure divided by the yield strength, S_y.

Table 7-5. Fuel Rod Bowing Coolant Channel Closing

Grid Span (Grid No's.)	Maximum Pre-Irradiation Bow (mils)	Thermal & Fluence Induced Bow (mils)	Initial Fuel Rod Bow (mils)	Total Fuel Rod Bow @ EOL (mils)	Total Flow Channel Closure (mils)	Additional Flow Channel Closure (%)	Allowable Flow Channel Closure (%)
B - 1	5.84	0.07	5.91	7.20	11.39	2.93	20
1 - 2	5.00	0.29	5.29	7.05	11.20	4.31	10
2 - 3	5.00	0.02	5.02	6.80	10.89	3.77	10
3 - 4	5.00	0.23	5.23	7.40	11.64	5.08	10
4 - 5	5.00	0.58	5.58	7.82	12.18	6.01	10
5 - 6	5.00	0.22	5.22	7.02	11.16	4.24	10
6 - 7	5.00	0.07	5.07	6.03	9.94	2.12	10
7 - 8	5.00	1.00	6.00	6.53	10.56	3.19	20
14 - T	5.84	2.65	3.49	8.77	13.41	6.45	20

Then, for linear variation of temperature through the fuel rod cladding:

$$\left.\begin{aligned} y' &= 1/x \text{ for } 0 < x < 0.5 \\ y' &= 4(1-x) \text{ for } 0.5 < x < 1.0 \end{aligned}\right\} \quad (9)$$

However, since inelastic fuel rod thermal creep is known to be present, the above elastic technique is not valid. In the absence of specific rules for inelastic thermal stress ratcheting, the following modification was made.

Assume y' = maximum allowable range of thermal strain divided by the yield strain

$$y' = \frac{\varepsilon_T}{\varepsilon_y} \quad (10)$$

x = maximum pressure induced elastic and thermal creep strain divided by the yield strain.

$$x = \frac{\varepsilon_E + \varepsilon_c}{\varepsilon_y} \quad (11)$$

ε_y = elastic yield strain based upon the yield stress at temperature, S_y, and the elastic modulus, E.

$$\varepsilon_y = S_y/E \quad (12)$$

Equations 10, 11, and 12 are then used directly in the original thermal ratcheting criteria, Equation 9.

This modified thermal ratcheting analysis was performed at the peak burnup of 125,000 MWd/Tonne, 545.5 full power days residence time. The thermal strain range was conservatively estimated as the total thermal strain magnitude; this assumes full thermal stress reversal for each temperature cycle. The end-of-life fuel rod cladding strain components were obtained from the cladding strain analysis for conservative 3σ material properties. Table 7-6 shows the modified thermal ratcheting parameters for various locations in the axial core region of the fuel rod.

Table 7-6 shows that only at the high temperature core outlet region where thermal-induced creep strain becomes significant does the thermal strain range approach the limt for fuel rod diametral growth. However, the margin of safety is still 60%. Therefore, fuel rod failure due to thermal stress ratcheting is not expected to occur. However, the validity of the modified thermal stress ratcheting criteria that was used in the preliminary analysis should be determined by further testing at simulated reactor operating conditions.

Table 7-6. Fuel Rod Modified Thermal Ratcheting Analysis

Axial Core Height (in.)	ε_y Yield Strain (%)	$\varepsilon_E + \varepsilon_c$ Elastic & Thermal Creep Strain (%)	ε_T Thermal Strain Range (%)	x	y'_{MAX}	y'_{ACT}	Margin of Safety
0	0.0793	0.0305	0.0221	0.385	2.60	0.279	8.33
9	0.0772	0.0337	0.0431	0.436	2.29	0.558	3.10
18	0.0748	0.0377	0.0518	0.504	1.98	0.692	1.86
27	0.0744	0.0478	0.0448	0.643	1.43	0.602	1.37
36	0.748	0.0653	0.0237	0.873	0.508	0.317	0.60

3.3 Proposed Irradiation Tests in EBR-II on Non-Fueled Grid Cells

A test description of "Proposed EBR-II Irradiation Tests on Grid Cells of the 217 Pin Grid Type Fuel Assemblies" was written and submitted to Mr. J. H. Kittel, Experiment Manager, EBR-II Project, Argonne National Laboratory, Argonne, Illinois. Comments on the proposed tests and needed out-of-reactor services were solicited at this time from EBR-II project personnel at Chicago and Idaho prior to our submitting an official approval-in-principle request to RDT.

The latest test capsule design specifies three cylindrical capsules specially designed to fit inside of a Mark-B subassembly as shown in Figures 7-14 and 7-15. These proposed test capsules will have a diameter of approximately one inch and will provide adequate cross-sectional area for testing grid specimens of seven complete grid cells. Each capsule will contain approximately 10 test specimens stacked vertically, thus providing for 30 test specimens in a proposed three capsule Mark-B subassembly.

Preliminary thermal analysis showed that the inside of the capsule can be maintained at the desired temperature level of 1200°F by a double wall construction with helium filling an annular gap of about 25-mil thickness. This assumes stainless steel construction throughout. Insertion of tantalum would require a marked decrease in gap width.

Detail design work was initiated on the grid test specimens and capsules. The test grids will be of typical LMFBR-FFTF design with several design clearances between the grid cell dimples and simulated fuel rods. The test arrangement will accommodate a reasonably large variety of controlled design conditions and will utilize prototype test specimens to obtain useful data.

Tests are contemplated on test specimens with either hexagonal honeycomb grid cells or rhomboidal shaped grid cells, the latter being typcial of line-of-sight grids. The effects of irradiation on spring relaxation will be tested by means of pre-stressed spring specimens. The spring test specimens will have elastic characteristics which will be typcial of proposed grid spring and dimple designs. Test specimens will include both cold worked and annealed Type 316 stainless steel in order to determine their relative merits in fast flux environments.

The anticipated testing time is based on the present EBR-II operating power of 62.5 Mw and a row 2 or 3 position of the Mark-B test subassembly in the reactor. The first of the test capsules will be removed and its contents examined after 18 months of irradiation, the second after 25 months, and the third after 41 months. These times will correspond to accumulated fast fluences of approximately 1×10^{23}, 1.4×10^{23}, and 2.3×10^{23} n/cm^2, respectively. The latter fast fluence (2.3×10^{23} n/cm^2) is representative of the anticipated total fast flux environment to which grids will be subjected, and consequently, should result in useful data on lifetime performance effects on the various grid specimens.

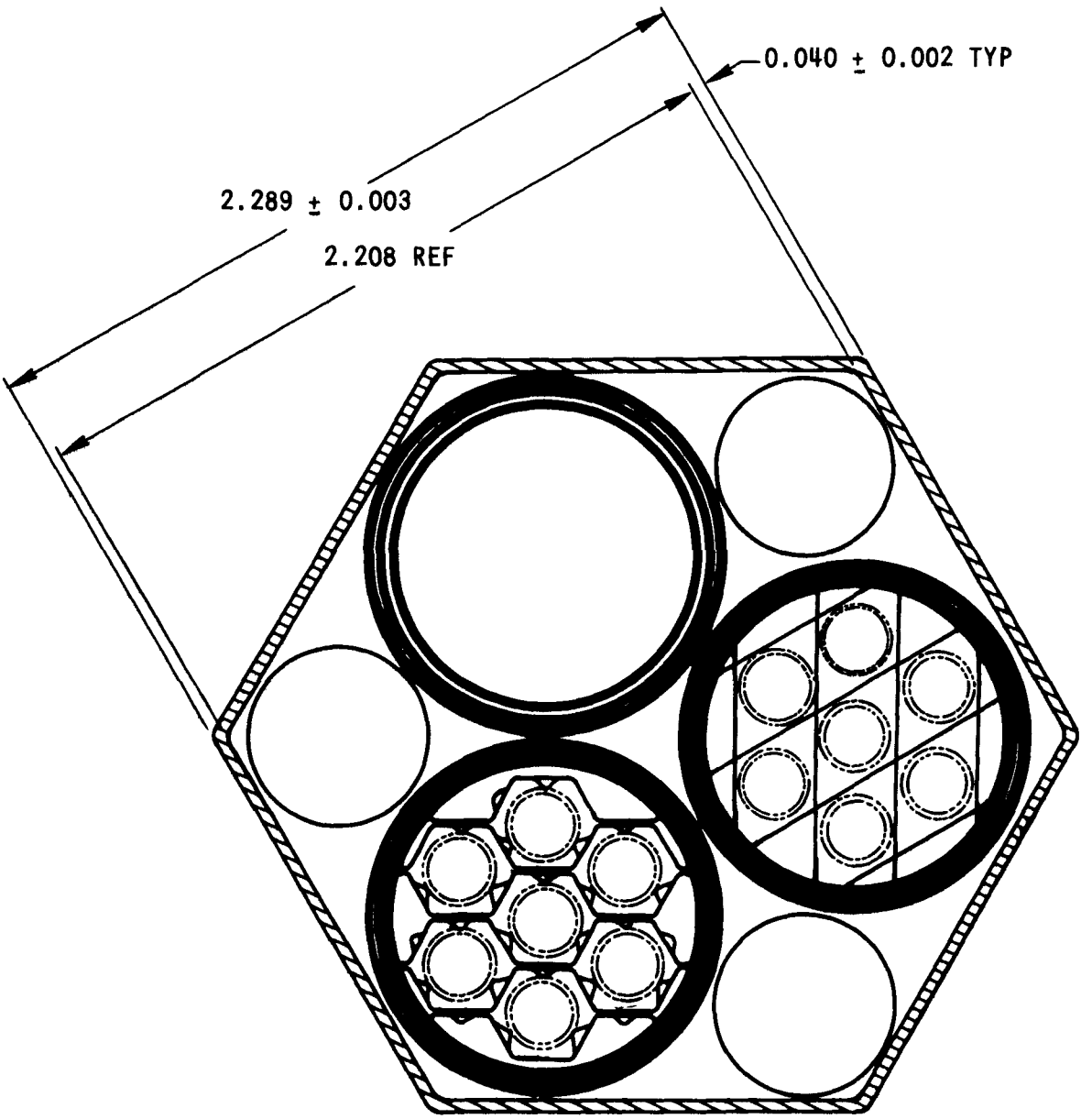

Figure 7-14. Capsule Installation for Irradiation Testing of LMFBR-FFTF Grids in EBR-II Mark B Subassembly

3937-46

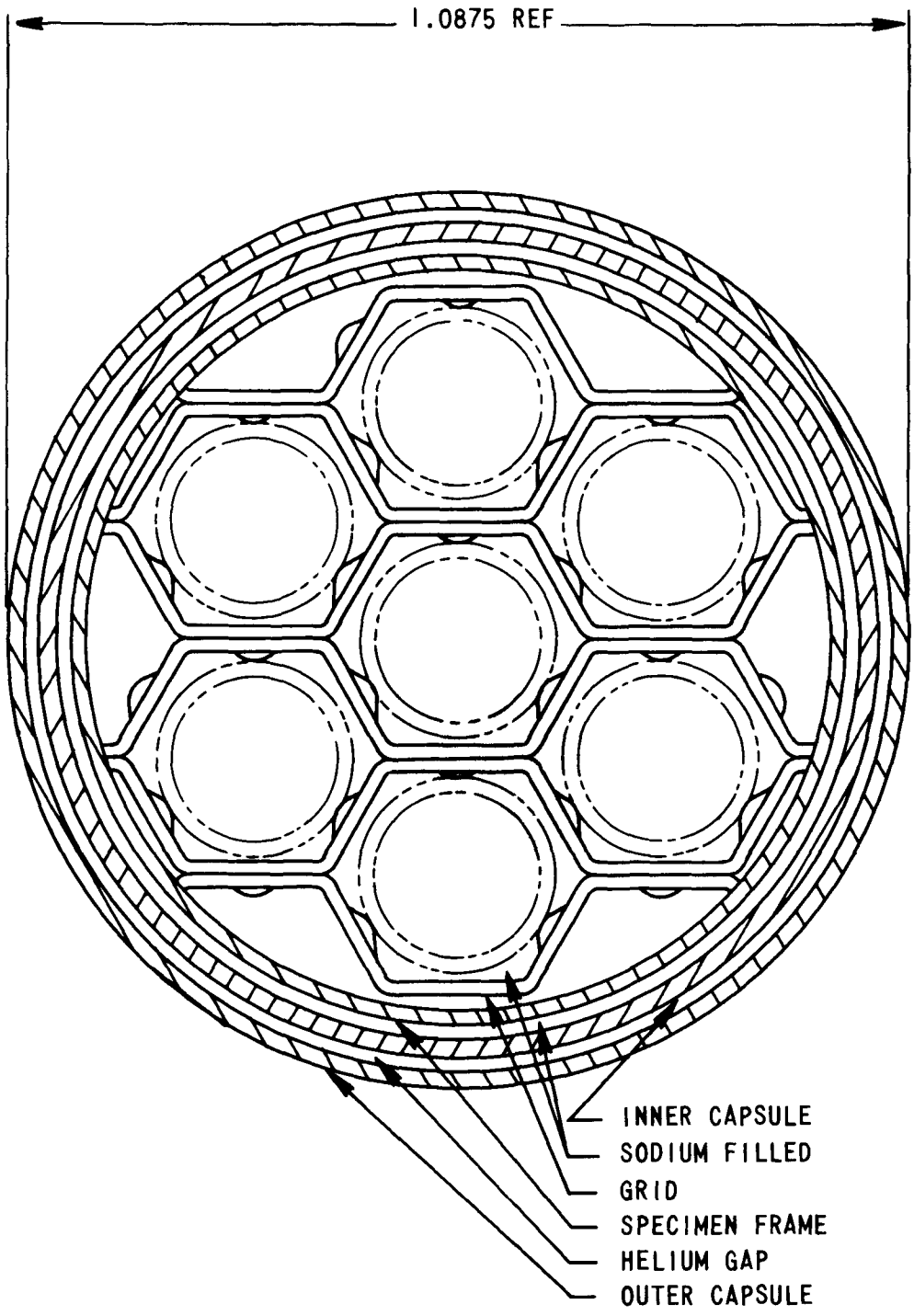

Figure 7-15. LMFBR-FFTF Hexagonal Grid Specimen EBR-II Irradiation Test

3937-47

4.0 REFERENCES

1. O. E. Dwyer and H. C. Berry, "Effects of Cladding Thickness and Thermal Conductivity on Heat Transfer to Liquid Metals Flowing In-Line Through Bundles of Closely Spaced Reactor Fuel Rods," Nucl. Sci. Eng. 40, pp. 317-330 (1970).

2. "Oxide Fuel Element Development Quarterly Progress Report for the Period Ending June 30, 1970," WARD-4135-11, September 1970.

3. D. Burgreen, "Vibration of Rods in Parallel Flow", Nucleonics 17, No. 8, pp. 78-79 (1959).

4. "Evaluation of Compliant Grid-Type Fuel Rod Spacers for FTR Fuel Assembly," WARD-3684-5, November 1968.

5. C. R. Soderburg, "Interpretation of Creep Tests for Machine Design," Trans. ASME 58, pp. 733-743 (1936).

6. A. C. Rapier and T. M. Jones, "Thermal Bowing of Reactor Fuel Elements," J. Nucl. Energy Pt A/B 19, pp. 145-191 (1965).

7. ASME Boiler and Pressure Vessel Code, Section III: Nuclear Vessels, 1968.

SECTION 8

OFBA-313 FABRICATION, DEVELOPMENT, AND TESTING OF LMFBR FUEL ASSEMBLY

E. C. Bishop, D. N. Elliott, A. Krebs, J. F. Patterson, and S. A. Shiels

1.0 OBJECTIVES

The objectives of this program are to evaluate the wear damage caused by those grid-pin interactions induced in a fuel pin assembly typical of WSA-3 design when operating in dynamic sodium, and to evaluate the effect of varying the dimple circle diameter on the wear damage (WSA-3 will be the first 37-pin grid subassembly to be inserted in EBR-II). Similar evaluations will be performed on a 37-pin subassembly which will utilize the final grid design proposed for the first 217-pin subassembly designed for irradiation in FFTF.

2.0 PRIOR WORK

Changes in the program plan necessitated that data be obtained on the effect of varying the diametral gap. Therefore, grids had to be produced with various dimple circle diameters within each grid. Variations in fit were also required along the length of each rod. Many of the rods will see the nominal diametral gap along their entire length, while others see varying diametral gaps.

Eleven grids were fabricated and carefully inspected using 100-to-1 magnification ratio in the Optical Comparator Inspection Procedure. After inspection and measurement of each cell, the grids were hand worked to produce the required dimple circle diameters in accordance with the grid design. The grids were reinspected after hand working and all dimple circle diameters were within 1 mil of the required value except for a few cells which were accepted with deviations within 2 mils.

Forty dummy fuel pins were fabricated. The grids and liners were inserted into the inner can, all machining on the subassembly was completed, and the components were readied for final assembly.

3.0 CURRENT PROGRESS

3.1 Subassembly Fabrication

The dummy pins were indexed 1 to 37 and were loaded in numerical order. Figure 8-1 shows a typical grid map on which the pin number, the corresponding grid cell number, the dimple circle diameter and the diametral gaps are shown. The loading sequence was such that the pin numbers are not always the same as the grid cell number. The pins were pulled into position using a threaded locating rod which screwed onto the top end plug. Loading was

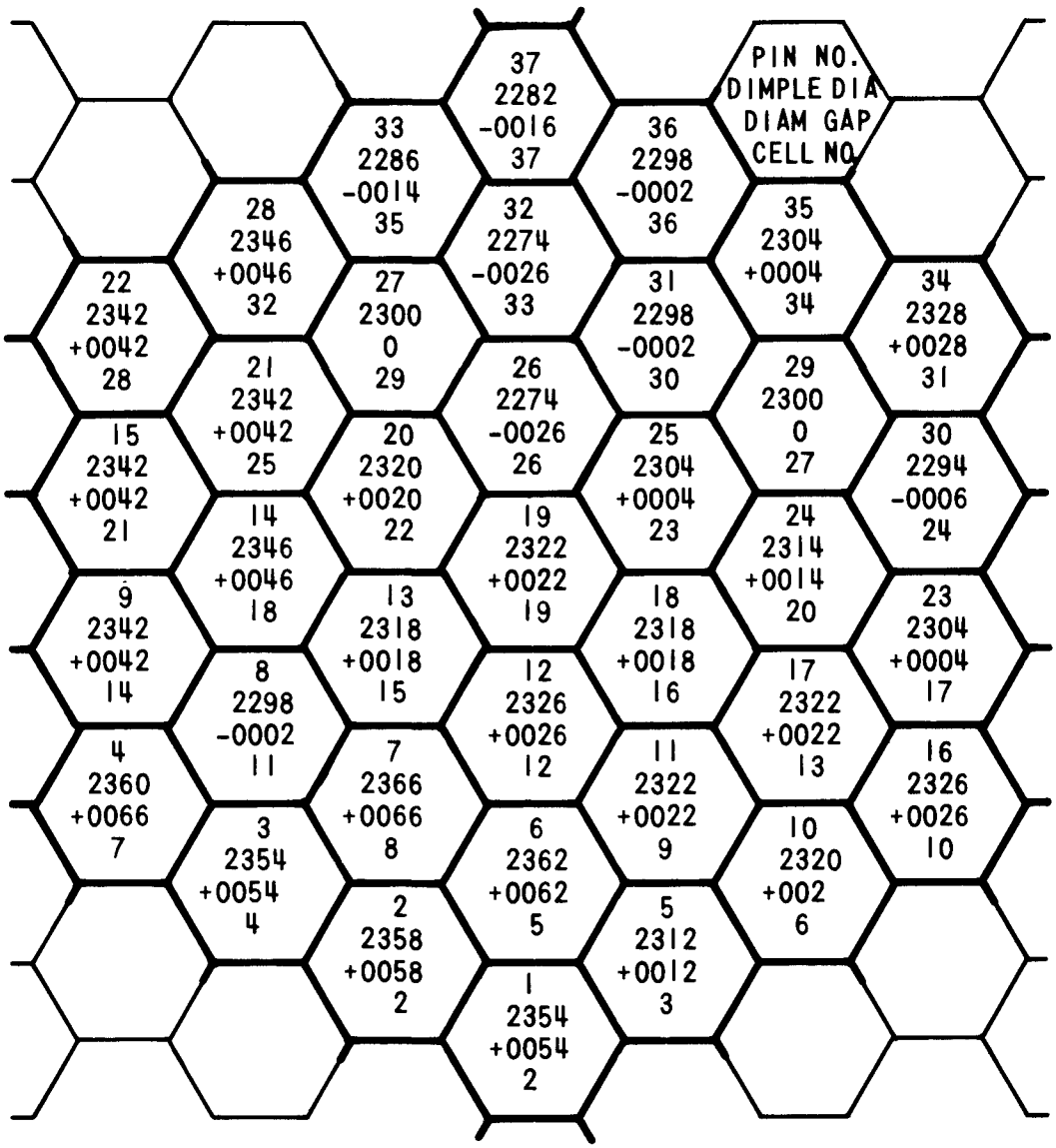

FIRST TEST ASSEMBLY
WSA-3 TYPE
NOMINAL PIN DIA - 0.230 in.
GRID NUMBER 3
POSITION - 46.41 in.
GRID ASSEMBLY NO. 22

Figure 8-1. Final Grid Dimensions

3937-16

carried out with the pins rotated 60° off the final position.

The loading force was measured in every case using a 50 lb spring balance attached to the loading rod. Loading forces varied from 1-1/2 lb total to in excess of 100 lb. The pins were rotated into the correct attitude while protruding about 4 inches from the can.

The bottom end grid was attached and the entire pin cluster was moved the last four inches using a specially designed jig. A load of about 200 lb together with light tapping of the end plug was sufficient to complete the loading.

The fabrication of the assembly was completed and fully documented in accordance with established fabrication and quality assurance (RDT2-2T) procedures.

3.2 Test Facility Fabrication and Installation

The DFAT test section was removed from the GPL-1 test cubicle and readied for modification. It was found, however, that protrusions of the thermocouple penetration welds would prevent insertion of the test assembly. A new test section was therefore fabricated. Modification was completed, subassembly was placed in the test section, and the final closure weld was made.

The new air blast cooler shown in Figure 8-2 was completed late in the reporting period. Both the test section and the cooler have now been installed in the GPL-1 cubicle. Figure 8-3 shows the installation and Figure 8-4 the piping schematic. The assembly is ready for tests.

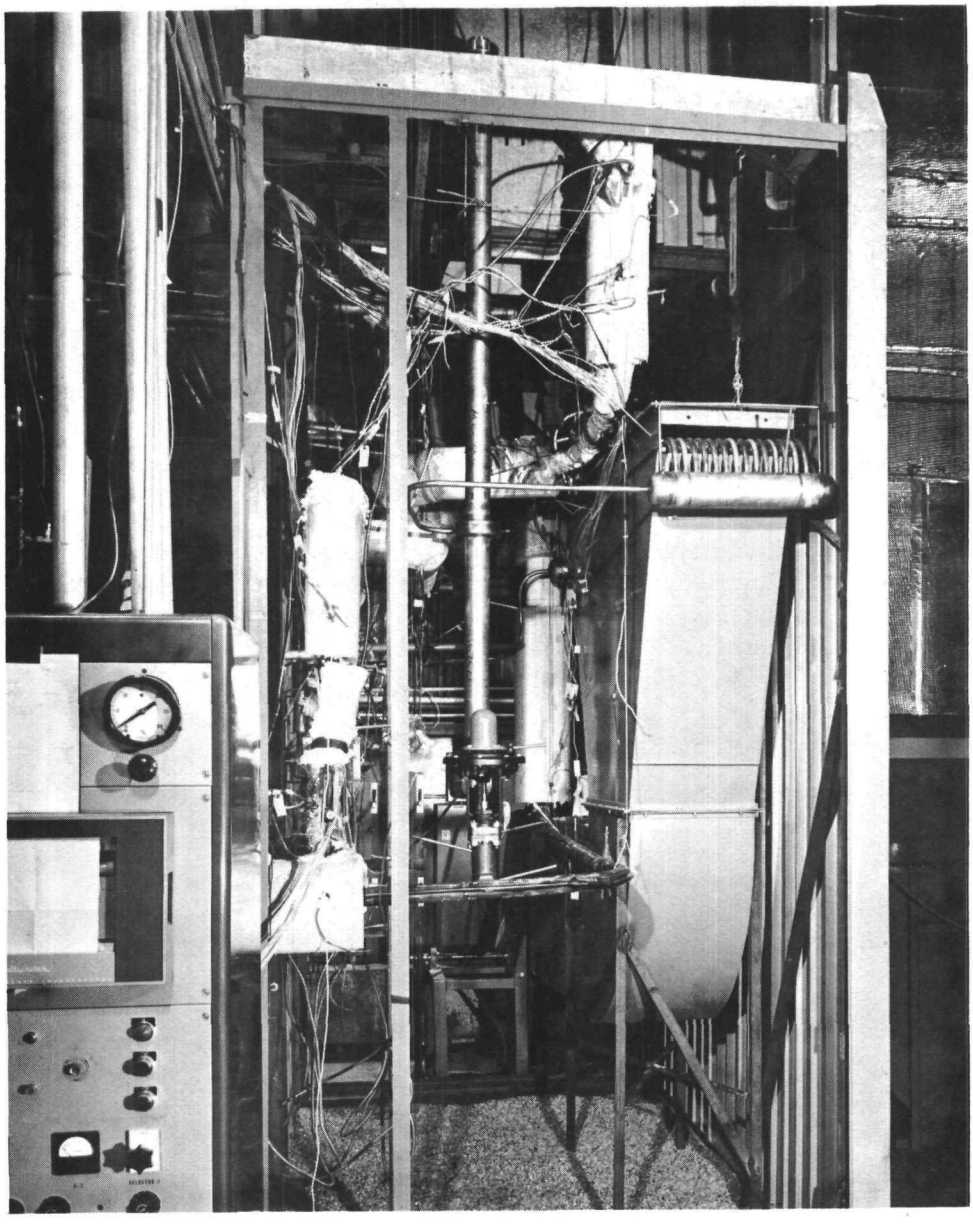

Figure 8-2. Air Blast Cooler for Sub Assembly Fretting Test

3937-17

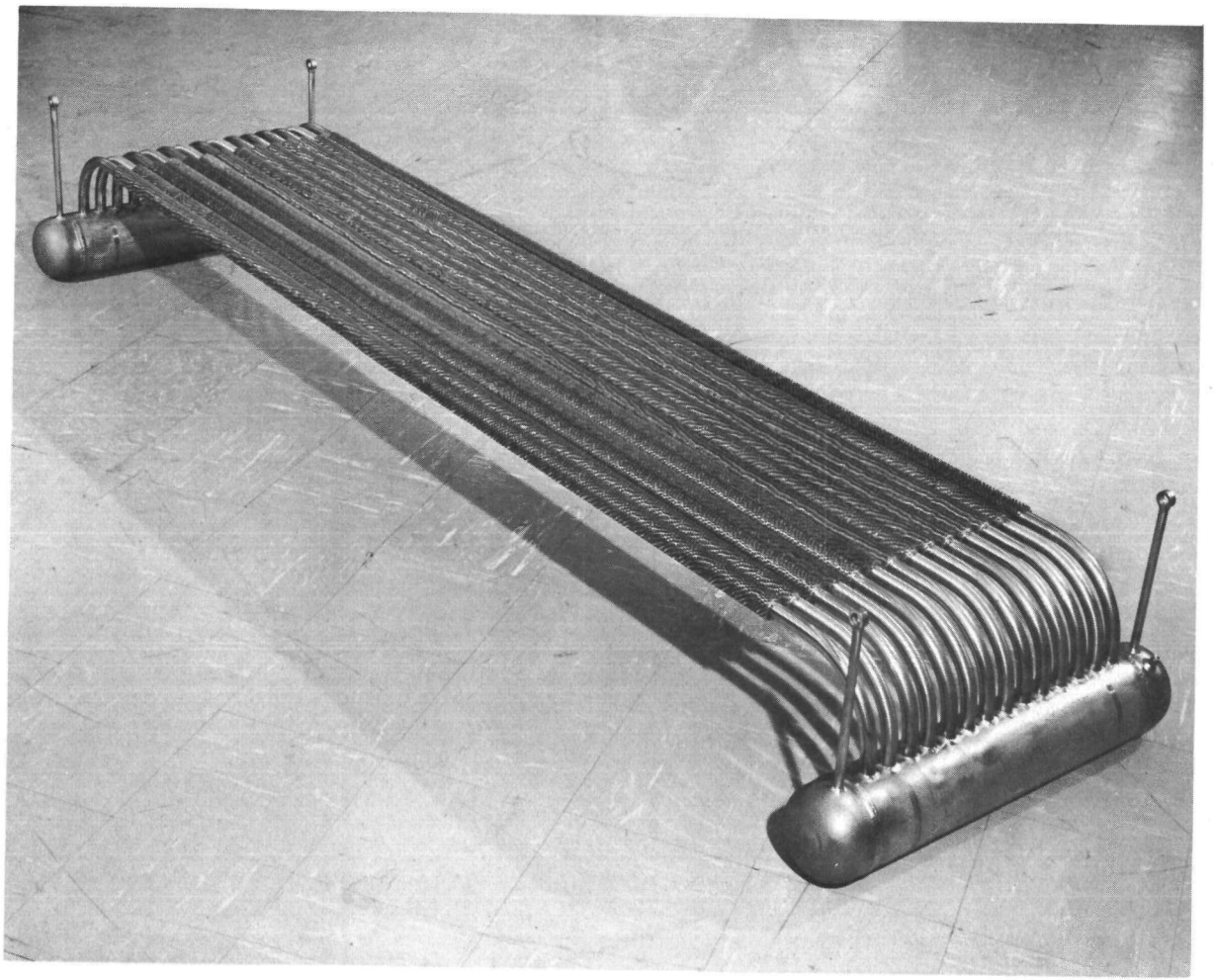

Figure 8-3. Sub Assembly Fretting Test Installation

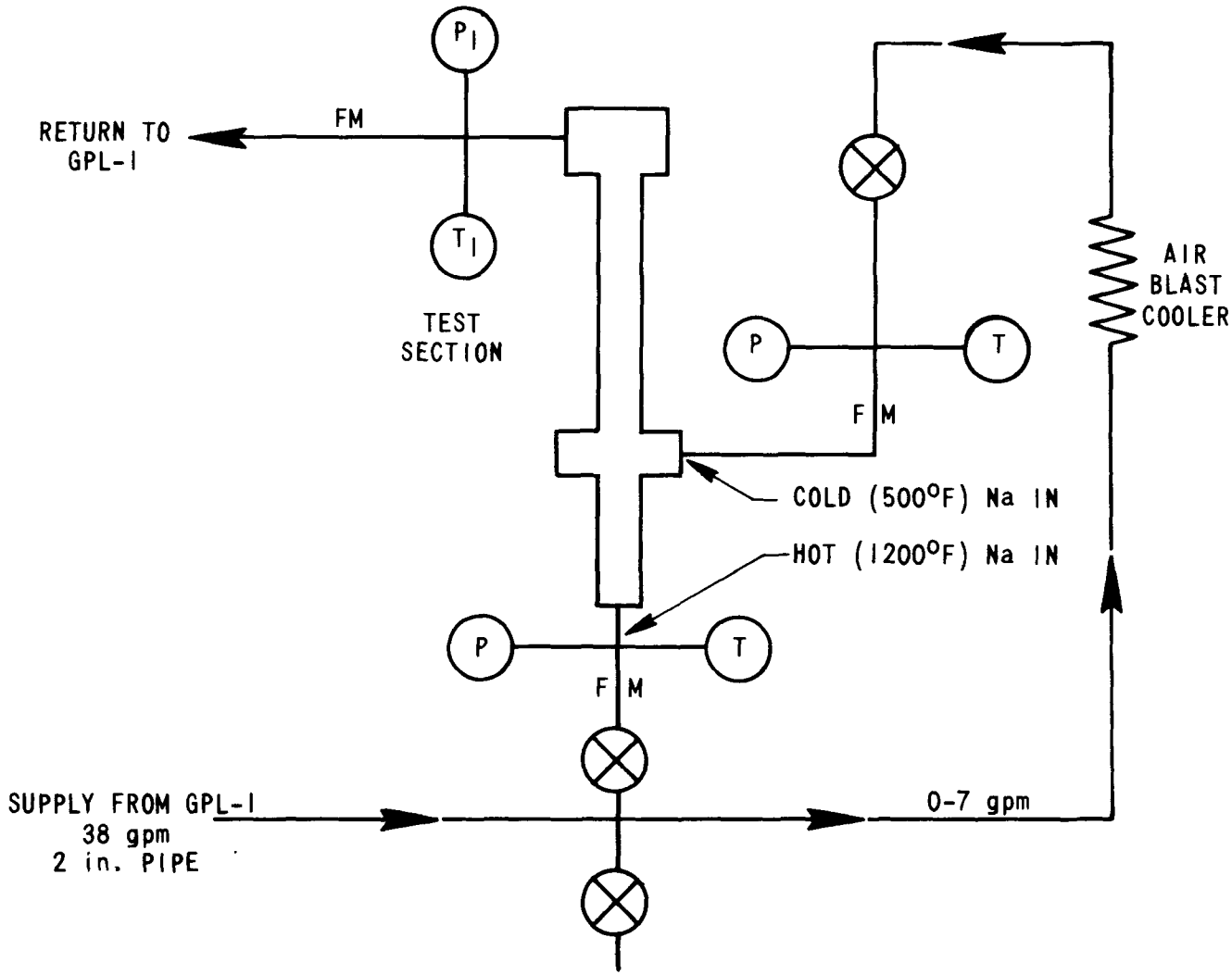

Figure 8-4. Piping Schematic for the Subassembly Fretting Test

SECTION 9

OFBA-410 FABRICATION DEVELOPMENT OF EBR-II GRID-TYPE SUBASSEMBLIES

E. C. Bishop, D. N. Elliott, T. A. Galioto, W. E. Ray, and W. L. Wilson

1.0 OBJECTIVES

The objectives of this task are to develop fabrication procedures and produce 37-pin EBR-II subassemblies based on the PFR honeycomb grid design. The scope will be limited to grids, cans, and end fittings. Fuel pins will be prepared under OFBA-510 to -513, and all tooling and fixture design, fabrication, and procurement will be funded under OFBA-411. The subassembly fabrication effort covered by this task will include the following:

1. Establish optimum welding parameters for grid fabrication.
2. Determine the optimum welding procedures for fabrication of can welds and can-to-grid joints.
3. Determine fabrication and assembly procedures for attaching any fittings required to support and locate the subassemblies in EBR-II.
4. Prepare simulative samples of all joints and evaluate the effects of fabrication and heat treatment operations on the mechanical properties of the joints.
5. Identify suitable inspection criteria for assessing subassembly components.
6. Fabricate the simulative models for design verification testing.
7. Provide mechanical test data and component characterization.
8. Fabricate subassemblies for insertion in EBR-II.
9. Provide input to hazards reports on component reliability.

2.0 PRIOR WORK

During the last reporting period, grids and liners were fabricated for the WSA-3 flow test subassembly and welded into an inner can using gas tungsten arc spot welding. A bottom grid support and outer can were also made and the flow test subassembly was loaded with dummy fuel pins. Flow test end fittings were attached to complete the first subassembly made under this contract.

3.0 CURRENT PROGRESS

3.1 Materials

To facilitate procurement of various size strip materials for subassembly fabrication, a 500 lb coil of 0.039 x 12.5 inch Type 316 stainless steel strip was purchased from Allegheny Ludlum, after having selected a heat with 0.04 to 0.06 Wt% carbon and less than 0.05 Wt% nitrogen. Sections of this coil will be rolled and slit to size as required and should eliminate problems previously experienced with a re-roll mill supplying out of specification material. A purchase order has been placed with Hamilton Precision Metals to roll two 50 lb lots of material to 0.010 and 0.020 inch thickness, 20% cold worked strip to be used for grid fabrication.

3.2 Grid Fabrication

During the current period, 20 inner grid assemblies have been fabricated for use in welding trails and for WSA-3. A procedure specification has been issued to control the fabrication of inner grid assemblies. This specification covers detailed fabrication steps such as welding parameters and sequence, as well as quality control requirements to assure that weld strength and size requirements are fulfilled. Minor difficulties were experienced when burred pins on the inner grid assembly welding fixture were replaced. The new pins had the same overall diameter as the old pins but were found to flatten some of the strap dimples during assembly. It was determined that the old pins had small grooves adjacent to the dimples and had an effectively smaller diameter than the new pins. This problem was resolved by grinding flats on the new pins.

A procedure specification for support strap assembly fabrication has been issued,and 20 of these assemblies were welded, machined, and inspected during the current period.

Several grid assemblies have been made using various weld detail joint designs in an attempt to optimize the weld geometry and strength reserve at the joints between the inner grid and support strap assemblies. From the standpoint of weld strength, elimination of crevices, and appearance, it would be preferable to weld the complete length of inner grid strap protruding into each slot of the support strap assembly. However, because of the thermal distortion associated with this welding, the amount of heat input has to be minimized to maintain the grid peripheral pitch and dimple circle diameter tolerances. Dimensional inspection of these trial grid assemblies determined the maximum size of peripheral welds that could be made without producing unacceptable pitch distortions. Mechanical testing indicated that weld strengths at this joint location are adequate and WSA-3 grid assemblies are now being welded in accordance with a procedure specification that has been written and issued for this application.

SECTION 9

OFBA-410 FABRICATION DEVELOPMENT OF EBR-II GRID-TYPE SUBASSEMBLIES

E. C. Bishop, D. N. Elliott, T. A. Galioto, W. E. Ray, and W. L. Wilson

1.0 OBJECTIVES

The objectives of this task are to develop fabrication procedures and produce 37-pin EBR-II subassemblies based on the PFR honeycomb grid design. The scope will be limited to grids, cans, and end fittings. Fuel pins will be prepared under OFBA-510 to -513, and all tooling and fixture design, fabrication, and procurement will be funded under OFBA-411. The subassembly fabrication effort covered by this task will include the following:

1. Establish optimum welding parameters for grid fabrication.
2. Determine the optimum welding procedures for fabrication of can welds and can-to-grid joints.
3. Determine fabrication and assembly procedures for attaching any fittings required to support and locate the subassemblies in EBR-II.
4. Prepare simulative samples of all joints and evaluate the effects of fabrication and heat treatment operations on the mechanical properties of the joints.
5. Identify suitable inspection criteria for assessing subassembly components.
6. Fabricate the simulative models for design verification testing.
7. Provide mechanical test data and component characterization.
8. Fabricate subassemblies for insertion in EBR-II.
9. Provide input to hazards reports on component reliability.

2.0 PRIOR WORK

During the last reporting period, grids and liners were fabricated for the WSA-3 flow test subassembly and welded into an inner can using gas tungsten arc spot welding. A bottom grid support and outer can were also made and the flow test subassembly was loaded with dummy fuel pins. Flow test end fittings were attached to complete the first subassembly made under this contract.

3.0 CURRENT PROGRESS

3.1 Materials

To facilitate procurement of various size strip materials for subassembly fabrication, a 500 lb coil of 0.039 x 12.5 inch Type 316 stainless steel strip was purchased from Allegheny Ludlum, after having selected a heat with 0.04 to 0.06 Wt% carbon and less than 0.05 Wt% nitrogen. Sections of this coil will be rolled and slit to size as required and should eliminate problems previously experienced with a re-roll mill supplying out of specification material. A purchase order has been placed with Hamilton Precision Metals to roll two 50 lb lots of material to 0.010 and 0.020 inch thickness, 20% cold worked strip to be used for grid fabrication.

3.2 Grid Fabrication

During the current period, 20 inner grid assemblies have been fabricated for use in welding trails and for WSA-3. A procedure specification has been issued to control the fabrication of inner grid assemblies. This specification covers detailed fabrication steps such as welding parameters and sequence, as well as quality control requirements to assure that weld strength and size requirements are fulfilled. Minor difficulties were experienced when burred pins on the inner grid assembly welding fixture were replaced. The new pins had the same overall diameter as the old pins but were found to flatten some of the strap dimples during assembly. It was determined that the old pins had small grooves adjacent to the dimples and had an effectively smaller diameter than the new pins. This problem was resolved by grinding flats on the new pins.

A procedure specification for support strap assembly fabrication has been issued,and 20 of these assemblies were welded, machined, and inspected during the current period.

Several grid assemblies have been made using various weld detail joint designs in an attempt to optimize the weld geometry and strength reserve at the joints between the inner grid and support strap assemblies. From the standpoint of weld strength, elimination of crevices, and appearance, it would be preferable to weld the complete length of inner grid strap protruding into each slot of the support strap assembly. However, because of the thermal distortion associated with this welding, the amount of heat input has to be minimized to maintain the grid peripheral pitch and dimple circle diameter tolerances. Dimensional inspection of these trial grid assemblies determined the maximum size of peripheral welds that could be made without producing unacceptable pitch distortions. Mechanical testing indicated that weld strengths at this joint location are adequate and WSA-3 grid assemblies are now being welded in accordance with a procedure specification that has been written and issued for this application.

3.3 Liner and Inner Can Fabrication

Procedure specifications have been issued to cover both liner and inner can fabrication. Both components have a similar fabrication sequence in that they are first machined and then have spacers attached to position them in the subassembly. Liners and the inner can for WSA-3 have been machined and inspected. Spacers have been attached to the liners and the liner flanges are being ground to improve concentricity and location of these components in the grid assemblies and inner can. The inner can spacer design has been modified to minimize the possibility of inner can swelling distorting the outer can. Spacers for the new design have been machined and inspected.

Samples of the inner can and liners have been thermally cycled three times between ambient temperature and 1100°F to determine the dimensional stability of these components. The small dimensional changes that resulted from thermal cycling were within the tolerance ranges of all dimensions. Length and across-flats dimensions were virtually unaffected; whereas, bow and twist measurements indicated that the thermal cycling improved the dimensional consistency of these components.

3.4 Subassembly Fabrication

Following completion of flow measurements, reported under OFBA-411, and WSA-3 flow test subassembly was disassembled, and all of the components were cleaned. The subassembly was then reassembled after dummy fuel pin markings had been carefully documented. This subassembly was shipped to EBR-II site where it was disassembled and inspected. EBR-II personnel will use the subassembly to develop handling and cleaning procedures in preparation for irradiating the WSA-3 fuel assembly.

SECTION 10

OFBA-411 SUBASSEMBLY DESIGN AND HARDWARE

F. C. Engel, R. A. Markley, J. F. Patterson, and D. Spencer

1.0 SUBTASK 1. SUBASSEMBLY HARDWARE

2.0 OBJECTIVES

The objectives of this subtask are to design and fabricate tooling necessary for forming grid and subassembly components. Mechanical design of subassembly hardware, consistent with the design analysis of OFBA-311, is also included in this subtask.

3.0 PRIOR WORK

Mechanical design of all WSA-3 subassembly hardware and tooling fixtures was completed. Manufacture and procurement of the fixtures were completed including the grid and liner inserting tools. Major checkout, modification, and trial operations of the grid strap forming tool were completed. A grid was produced with all cells having dimple circle diameters within the range 0.232 ± 0.008. The permanent grid tool shims were ground to the same size as the temporary shims which were used for this grid. All tooling was made workable for WSA-3 and was used to manufacture the flow test mockup.

4.0 CURRENT PROGRESS

All objectives of Subtask 1 except for grid fabrication follow-on have been met and previously reported for WSA-3. Hardware design will be initiated in accordance with the schedule for WSA-4.

5.0 SUBTASK 2. FLOW TESTING

6.0 OBJECTIVES

The objectives are to plan, conduct, and evaluate out-of-pile flow tests intended to characterize hydraulic parameters of 37-pin subassemblies.

7.0 PRIOR WORK

A housing was designed to permit mounting of the 37-pin assembly in the thermofluids water loop. Detailed construction drawings were issued to the ARD model shop. The housing was manufactured and fitted in the water loop. The orifice was chosen by flow testing orifices with different size holes until the correct hydraulic characteristics were obtained.

The subassembly was hydraulically characterized using analytical methods, and these results were compared with the tests. Flow distribution tests were completed and compared with the results of the COBRA code established under OFBA-311.

8.0 CURRENT PROGRESS

The results of the flow tests of the WSA-3 mockup subassembly were evaluated and written for an internal memorandum and the WSA-3 data package. Most of the results were also reported in the April-June 1970 quarterly (WARD-4135-11). All objectives for Subtask 2 have been met for subassembly WSA-3.

SECTION 11
OFBA-510 PELLET FABRICATION

M. G. Bale, B. Riley, H. H. Scott, T. W. Wallace, and N. G. Wolcott, Jr.

1.0 OBJECTIVES

The objectives of this task are to demonstrate a process capable of producing mixed uranium-plutonium dioxide fuel of the required isotopic, physical, and chemical form to meet all aspects of OFBA-310 and -311; to demonstrate the capability for all necessary and pertinent support analytical determinations in the control of process variables and requirements defined by fuel specifications; and to fabricate mixed uranium-plutonium dioxide fuel for all phases of the contract and irradiation program.

2.0 PRIOR WORK

Initial work on the fabrication of mixed-oxide fuel was directed toward meeting O/M control, fuel homogeneity, and density specifications. Milling trials, binder additions, and pressing operations were investigated to determine the role of these variables on final pellet characteristics.

Fabrication of WSA-3 pellets was initiated using 2 kg fuel batches. Such quantities of material were sufficient to produce 1000 to 1200 pellets and these filled two or three sintering boats. With these larger quantities, problems were encountered in O/M control. An analysis of available data indicated that the binders added to the pellets were not being completely removed during the low temperature portion of the cycle and carbon residues were reducing the mixed-oxide at the sintering temperature. In such cases, the final O/M control was accomplished by refiring pellets in argon/5% hydrogen atmosphere containing 1000 ppm moisture.

3.0 CURRENT PROGRESS

3.1 Investigation of Process Variables

Two major problem areas were identified during the previous period, internal pellet cracking and O/M control. A third potential difficulty, moisture pickup on fired pellets, was also considered for investigation.

3.1.1 O/M Control

In early work, low O/M values on fired pellets were corrected by refiring batches with additional moisture in the sintering gas. Evaluation of the reactions occurring suggested a convenient method of obtaining a satisfactory O/M value from the first sintering run. During the binder burnout

period, 1500 ppm moisture is added to the sintering gas to produce an oxidizing atmosphere. This is maintained up to 1200°C, at which point the temperature is held for six hours. This temperature is selected as a compromise that provides minimal pellet sintering with maximum diffusion of oxygen into and carbon monoxide out of the pellet. After the hold, insufficient carbon remains to affect the O/M, and the sintering gas moisture is reduced to affect final control of the oxygen content. This technique has been used very effectively for batches containing up to 1/2 Wt% binder. For higher percentages, somewhat lower O/M values are occasionally obtained indicating the 1500 ppm moisture additions and six hour holds are close to critical values. These are affected, however, by other variables, such as furnace boat load, open porosity of the pellets, rate of sintering at 12000°C.

3.1.2 Internal Pellet Defects

Various fabrication processes were suspected of causing pellet defects; notably, binder type, binder addition method, preslugging pressure, pressing pressure, and sintering cycle. It is probable that all contribute to varying degrees, but that the problem is accentuated by the small diameter of the pellet. No specific cure has yet been found, since any one batch of powder is found to behave differently to another batch when prepared under similar conditions. Such difficulties have been met, however, by running one or two binder trial experiments with every batch prior to committing the bulk of the material. Acrawax, stearatex, and carbowax are commonly investigated at the 0.5, 1, and 2 Wt% levels, being added before or after preslugging. The densities of the fired pellets are measured, the pellets are ground, densities rechecked, and pellet condition carefully noted. The best binder condition can be selected for each lot with pressing conditions set to give the correct pellet length and density. In some cases, it has also been possible to optimize on pellet shrinkage, thus maximizing the number of pellets produced from a quantity of powder and minimizing grinding losses.

3.1.3 Fired Pellet Moisture Absorption

Various reports indicated that fired pellets can absorb moisture from surrounding atmospheres necessitating a drying operation prior to loading. In order to evaluate this problem and to determine the water release between 200°C and 600°C a number of pellets of various densities were tested. Most of the pellets showed total contents of less than -30 ppm, and those analyzed in two steps, at 200°C and then at greater than or equal to 600°C, show less than 12 ppm moisture release above 200°C. It is anticipated that most of the fuel for WSA-3 can be loaded without a final drying operation though the capability and procedure for this work are available if required. It is probable that differences in the pore structure of pellets from different batches of material affect the absorption rate though no correlation between open porosity and moisture content has yet been obtained.

A detailed Operating Procedure was written for operation of the CEC moisture analyzer used in the fabrication line for process observation. Experience has shown that familiarity with the day to day operating characteristics of this instrument in a room atmosphere glove box (10% to 40% relative humidity) is required in order to achieve accurate analyses on single fired pellets.

3.2 Fuel Fabrication

Fuel for the WSA-3 experiment was fabricated during this period. As detailed above, the fabrication process was modified to produce quality fuel with good control of chemical properties. Details of processing conditions for relevant batches are given in Table 11-1. With one exception, Batch 42, the standard ARHCO PuO_2, was recalcined at 700°C for 15 minutes in an effort to decrease particle agglomeration and improve homogeneity.

It has been observed that mixed batches of UO_2 and calcined PuO_2 generally sinter to 93% T.D. at 1650°C without milling. When milling is used to improve homogeneity, the material readily sinters to 95% T.D. or higher. Control of the lower density, 90% T.D., has thus been somewhat difficult, and larger percentages of binders were initially added to reduce sinterability. This, however, resulted in poor O/M control and wide density variation. Somewhat better control has recently been obtained using 1/2 Wt% binder and sintering at lower temperatures as, for example, Batch UP-41. All pellet densities were measured for potential fuel use with the results recorded under Task OFBA-513. Figures 14-3 and 14-4 (Section 14) illustrate the continued improvement in density control.

3.3 Raw Material Procurement

Both PuO_2 and UO_2 were received during the quarter. Approximately 10 kg of plutonium were obtained as nitrate at the beginning of the period. This was processed to oxide with 900g being calcined at 425°C, 900g at 575°C, and the remainder at 750°C. These temperatures were selected to permit comparative studies of powder variables with fabrication procedures and results. This work is currently planned to follow WSA-4 and WSA-5 fuel fabrication. 20 kg of fully enriched UO_2, shipped from UNC, was found to satisfy all chemical specifications. High iron and chromium contents (see OFBA-511, Section 12) were judged to be due to stainless steel impurities and were not thought to be deleterious to the project. Powder properties were also within specification, but it was found that the material would not sinter readily. Pellets pressed at green densities up to 65% T.D. would not sinter above 70% T.D. at 1650°C for four hours suggesting reworking of the powder was required. Additional oxidation/reduction cycles or considerable milling may be necessary to meet the 92% T.D. sinterability specification.

Natural UO_2 is available for the requirements of WSA-4 and for the insulator pellets required in future subassemblies.

3.4 Additional Work

3.4.1 AEC Audit

Toward the end of the period, all glove boxes were cleaned for a physical inventory. Twenty-six oxide containers representing all stages of the fabrication operation were check weighed and sampled for the AEC Audit.

Table 11-1. Processing Conditions for WSA-3 Fuel Pellets

Batch	Weight (kg)	Mill Time (hr)	Binder Type	Binder Amount (%)	Preslug (tsi)	G.D. (%)	Sintering Temp. (°C)	Sintering Time (hr)	Sintering Gas [a] ppm to °C	T.D. (%)
UP-34	2	24	Acrawax	1.5	5	46	1650	4	1000	95
UP-36	1.6	50	Acrawax	0.5	8	46	1650	4	1000 to 1200 70 to 1650	95
UP-37	1.6	16	Acrawax	1.5	8	46	1650	4	1000 to 1200 70 to 1650	80-90
UP-39	1.6	16	Acrawax	1.5	8	45	1500	4	2000 to 2000	
UP-39-4	(Refire)						1600	4	1600 70 to 1600	90
UP-39-5	(Refire)						1450	12	70	90
UP-40	1.6	16	Acrawax	0.5	8	45	1650	4	1500 to 1200 70 to 1650	96
UP-41	1.6	24	Stearatex	0.5	8	45.5	1550	4	1500 to 1200 70 to 1550	89-92
UP-42	1.6	16	Acrawax	1.0	6	44	To Be Completed			

[a] Sintering gas is 4 scfh Ar-5% H_2 with moisture added. The ppm value refers to quantity of water added up to the quoted temperature.

These have since been packaged and shipped for analysis to the New Brunswick (New Jersey) Laboratories.

3.4.2 Operating Procedures

Sufficient confidence had been obtained in the best use of equipment to write effective Operating Procedures. Forty-one operating procedures were prepared and reviewed with the Quality Control Group. Additional procedures will be written as respective operations are required for fuel processing.

SECTION 12

OFBA-511 OXIDE FUEL CHARACTERIZATION AND EVALUATION

J. Y. Chang, P. M. French, W. R. Jacoby, and P. D. Shalek

1.0 OBJECTIVES

The principal objectives of this task are to develop characterization techniques and to characterize and evaluate the uranium dioxide and mixed uranium-plutonium dioxide (powders and pellets) developed and fabricated under Task OFBA-510. Product characterization is required for control and performance evaluation objectives.

A secondary objective is to determine the various physical and mechanical properties (e.g., thermal conductivity, expansion, etc.) of these materials at each compositional change. These are necessary to complement the fabrication process (OFBA-510) and the irradiation programs (OFBA-310 and -311). This task will require some National Laboratory support.

2.0 PRIOR WORK

Sampling procedures and tentative specifications were established for the various materials to be UNC fuel characterized in the mixed-oxide fuel program.

An investigation was made of the effects of various process variables upon sintered fuel homogeneity of test batches of $(U,Pu)O_2$ pellets. Three types of basic inclusions were observed in this material, and studies were conducted to determine their nature and source.

Oxygen-to-metal determinations on trial batches of $(U,Pu)O_2$ resulted in changing the sintering atmosphere from a N-6%H_2 atmosphere to a high-moisture content Ar-5%H_2 atmosphere. Results for average particle size and BET surface area on milled powders showed the effectiveness of the wet milling operation. Extensive autoradiographic and metallographic examinations were conducted to investigate particle size and distribution and homogeneity in $(U,Pu)O_2$ fuels. Detailed characterizations of the first large batch of fuel resulted in establishing better processing conditions for subsequent mixed-oxide batches.

3.0 CURRENT PROGRESS

3.1 General

Concurrent with other tasks in this program, a complete review of written procedures was intiated during this period. Where required, these procedures were upgraded and new ones identified and written. Twenty-six procedures relevant to OFBA-511 were issued.

3.2 Analytical Chemistry

The raw materials for the fuel to be used in WSA-5 were characterized during this period. Acceptance analyses for the Pu nitrate from ARHCO showed it to be satisfactory from a chemical standpoint. The nitrate was converted to PuO_2 by Westinghouse Nuclear Fuels Division via the oxalate route and calcined at three different temperatures: 425, 575, and 750°C. The resulting materials appear to be satisfactory in all respects. They contain <320 ppm total metallic impurities, the highest individual being Ca at 70 ppm. Boron values varying from < 1 to 9 ppm were unexpected (since the nitrate tested at 2 ppm B) but not considered prohibitive, since the pellet specification for B is 10 ppm. Nitrogen was somewhat high at 66-101 ppm, but fabrication experience has shown that firing in Ar-5%H_2 with >1,000 ppm H_2O will minimize this impurity. As expected, certain chemical and physical attributes varied with the calcination temperature. This data is summarized in Table 12-1.

Table 12-1. Variation of Chemical and Physical Properties of PuO_2 Powders with Calcination Temperature

Calcination(a) Temperature (°C)	C (ppm)	Loss On Ignition (%)	BET Surface Area (m^2/g)	Fisher Avg. Part. Dia. (μm)	Bulk Density (g/cc)	Tap Density (g/cc)
425	612	1.06	25.8	1.83	1.82	2.59
575	547	0.84	13.5	1.68	1.71	2.47
750	248	0.31	5.7	2.38	2.12	3.07

(a) 2.5 hours in air

The fully-enriched UO_2 obtained from UNC (produced by the ADU process) was judged satisfactory from a chemical standpoint, although Fe, at 500 ppm, was just at the specification limit and Cr, at 250 ppm, was slightly over the limit (200 ppm). The 2.05 O/M and 6.15 m^2/g surface area values obtained for this material were quite different from those determined for the fully-enriched UO_2 from NUMEC which was used for WSA-3 fuel.[1] The O/M of this latter material was 2.355, and the surface area 3.56 m^2/g. The UNC material, however, did not meet the sinterability specification and will probably have to undergo further processing (see OFBA-510, Section 11).

From the end of the last period until the present the method of adjusting O/M of large $(U,Pu)O_2$ fuel batches progressed systematically through the following stages.

Stage 1. Initially, moisture contents of 150-400 ppm approximately the theoretical required for the desired 1.95-1.99 O/M, were maintained in the Ar-5%H_2 sintering gas during a series of fires until satisfactory values were obtained. O/M values as low as 1.91 were observed after

the initial firing, due to the reducing effects of the 1.5% binder content. For refires, the boat cover was removed. This method produced substantial O/M gradients (1.929-1.989, for example) throughout the boat. In order to monitor these gradients, O/M samples were selected from positions known to produce extreme values due to the gas-flow pattern. This method of sampling is still in effect.

Stage 2. In the first significant change to the process, pellets in a covered boat were exposed to higher moisture (1000 ppm), and a three-hour hold at 1000°C for binder burnout was added to the cycle. Somewhat higher initial O/M values resulted. Subsequent refirings in an open boat, still using 1000 ppm H_2O, raised the values to the specification range, but still left small to moderate O/M gradients. The ranges varied from ± 0.009 to ±0.034.

The burnout temperature of 1000°C was selected based on draw trials on green pellets heated to 500 and 1000°C. [2] The data indicated that from 1% binder in the green pellet, 1000 ppm C remained after heating to 1000°C for one hour. This level of residual C is significant, since calculations show that it is sufficient to reduce $(U,Pu)O_{2.00}$ to $(U,Pu)O_{1.92}$ when CO_2 is the reaction product.

Stage 3. In the next modification to the process, the burnout step was conducted at 1200°C for six hours and followed by cooling, removal of the boat lid, and sintering; all with 1000 ppm H_2O in the furnace gas. Such a cycle produced oxidation above the specification range (i.e., O/M > 1.99), and the pellets had to be reduced by refiring in relatively dry gas containing 50-70 ppm H_2O. The O/M gradient appeared to be minimized by this approach from a higher value.

Stage 4. The final stage combined the burnout and reducing steps from State 3 above into one firing cycle through the use of a domed boat lid which served as a radiation shield while allowing reasonably efficient gas access to the pellets. For pellets containing only 0.5% binder, specification O/M was attained in one firing. For those batches containing 1.5% binder, 2000 ppm H_2O was used during the burnout step to initially overoxidize the pellets, and sometimes a reducing refire was required. It should also be noted that 0.5% binder was used in the fabrication of nominally 95% dense pellets and 1.5% binder with nominally 90% dense pellets. Data for recent batches adjusted by this stage (Table 12-2), shows the O/M gradients are apparently no longer a problem.

Care must be taken not to carry the initial overoxidation step too far, as the reduction of $(U,Pu)O_{2+x}$ occurs at a considerably slower rate than its oxidation.

Table 12-2 Recent O/M Data for $(U_{0.75}Pu_{0.25})O_2$
Potential Fuel Batches for Use in WSA-3

Batch Number	Nominal Density (% Theoretical)	Mean O/M (for 4 analyses)	2σ (C = 0.7979 for 2σ calculation)	Range of Values
UP-36-1	95	1.979	0.0098	1.976-1.985
UP-36-2	95	1.983	0.0163	1.977-1.991
UP-37-1	90	1.989	0.0073	1.985-1.991
UP-39-5	90	1.986	0.0054	1.983-1.988
UP-40-1	95	1.988	0.0130	1.981-1.993
UP-40-2	95	1.981	0.0181	1.976-1.991
UP-41-1	90	1.979	0.0098	1.974-1.983
UP-41-2	90	1.992	0.0038	1.990-1.993

Wide density ranges (up to 10% T.D.) were observed at an intermediate step in the firing of low-density fuel batches UP-37 and UP-39. Because the highest densities occurred at the front of the boat where oxidation first takes place, O/M may exert a significant effect on the sintering rate of $(U,Pu)O_2$.

Extensive chemical characterization was done on batches UP-34-2, 36-1, and 36-2, which had previously been identified as potential pin material on the basis of O/M and density measurements. The analyses completed (Pu,U, C, N, Cl, F, and TMI) were consistent among batches and showed the materials to be generally well within specification limits. One exception was an acceptable, but significantly higher, Pu assay for UP-34-2 (23.1% vs desired 22.3%). This is the only batch to have shown such a deviation.

A Zr impurity pickup (from the ball-milling media) of approximately 700 ppm was detected in pellets from the above batches, seemingly independent of milling time. This value was considerably higher than expected from earlier experience. The specification for Zr, however, was set at 1000 ppm in view of the overall low metallic impurity content of the fuel. An investigation was begun to determine if Zr, in solid solution, might be responsible for an observed increase [2] in the $(U,Pu)O_2$ matrix microhardness.

Moisture determinations, run on production batches UP-36-1 and UP-36-2 at the time of loading, indicate that there will be no moisture adsorption problem with the high density (95% T.D.) fuels. Values ranging from 4 to 20 ppm were obtained. Total gas release values of 0.013-0.022 cc/g were also well within specification.

3.3 Metallography and Autoradiography

Considerable effort was spent in evaluating the effects of different binder additions and pelletizing procedures on the sintered microstructures of pellets. The large testing batch examined had 19 different fabrication conditions, the variables being shown in Table 12-3.

Table 12-3 Fabrication Variables for Test Batch

Binder	Time of Binder Addition	Green Density (% Theoretical)	Sintered Density (% Theoretical) Preslug Pressure	
			4 tsi	8 tsi
Acrawax	Before Preslug	49.5	95.7	93.7
	After Preslug	46.0	90.0	--
		47.0	92.4	90.4
		48.5	91.8	91.2
		50.0	91.6	--
		53.0	--	92.0
Carbowax	Before Preslug (Wet)	45.5	89.2	87.8
		50.5	88.3	89.8
	After Preslug	47.0	92.5	88.2
		50.5	93.2	92.0
P.V.A.	Before Preslug	44.0	--	88.2

Note: 1% binder added, material sieved through 35 mesh after preslugging.

In general, variation in binder type (Acrawax, Carbowax, or polyvinyl alcohol) has very little effect on the amount of microcracking. Acrawax, however, did produce a much finer pore structure than the other two binders. This confirms a recent observation [2] regarding the first large-scale batch UP-31 where an Acrawax/Carbowax mixture was employed and two discreet groups of voids were observed. The small group of voids, 1-20μm in size, were obviously due to the Acrawax addition and the large group (50-90μm) to the Carbowax.

The structure of pellets made with Carbowax were sensitive to the relationship between preslugging pressure and green density, whereas the relationship was of lesser importance when Acrawax was used. Thus, with

Carbowax, a preslugging pressure of 8 tsi in conjunction with pressing to a low green density (45-47% theoretical) has a tendency to produce more microcracking than preslugging at 4 tsi with a high green density (50-5 % theoretical). If a preslugging pressure of 8 tsi is used, the green density must be kept higher than 50.5% theoretical to prevent corner and general microcracking throughout the pellet.

Fewer cracks and more even porosity distributions were obtained when Acrawax was added before rather than after preslugging as shown in Figure 12-1. The amount of Acrawax added also had a marked effect on pellet structure, 0.5% additions to preslugged granules giving sound pellets but 1.5% additions produced badly cracked ones.

A successful chemical etching technique was developed using an HNO_3 (20 mils) - HF (0.03 ml) - H_2O (80 ml) - $Cr(NO_3)_3$ (0.1 g) solution with several of the above experimental pellets. The samples are placed in a leak-tight desicator and etchant applied by means of an eyedropper. Etching times of approximately 90 minutes are required at room temperature in the closed container. The technique gives a more consistent etch than the one previously described, [3] with grains as small as 1μ being clearly delineated (see Figure 12-2).

Detailed metallographic examination has been initiated on pellets selected from Batches UP-31 through UP-40. Fabrication details are provided in Task OFBA-510, Section 11. Data on the various attributes available indicate fuel from batches UP-34, -36, and -40 will be acceptable for use in high density pins. For metallographic examination, four samples which were visually acceptable for use in pins were taken from each sub-batch; e.g., UP-36-1 and UP-36-2. The pellet density distribution histograms (see Task OFBA-513, Section 14) were also used in the selection and the samples chosen to represent the entire density distribution of visually acceptable ground pellets.

Pellets from batches UP-36-1 and UP-36-2 have a well-sintered structure as illustrated in Figure 12-3, with very similar porosity distributions. The chamfered corners are well preserved, and no cracking was detected. This material had 0.5% Acrawax added to the preslugged granules, and this is manifested in a slightly patterned pore structure due to some concentration of binder at the surface of the granules.

Although the porosity distributions are virtually identical in samples from UP-36-1 and -2, there is some difference in grain size. Measurements by the linear intercept technique show the average grain size of UP-36-1 to be 3.8μm, while UP-36-2 is 12.6μm. The average pore sizes being virtually identical. Details are given in Tables 12-4 and 12-5.

A small number of metallic inclusions were observed in both sub-batches of UP-36, but their size (< 25μm x < 7μm) and volume (<0.5 v/o) are not considered significant. Autoradiography on batch UP-36 samples indicates excellent homogeneity, comparable with coprecipitated material. [2] (see Figure 12-4)

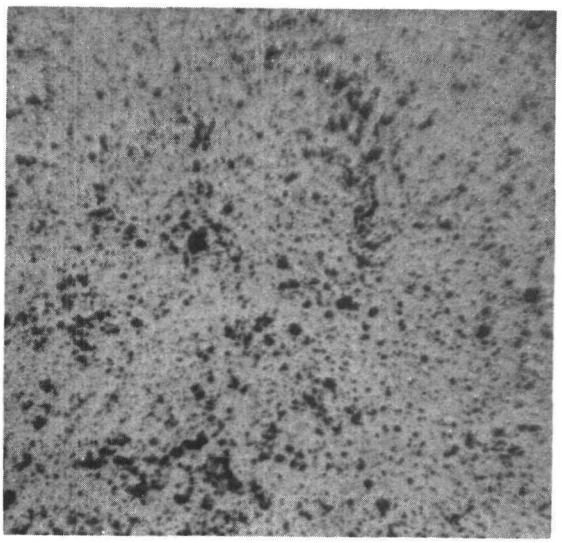

(a) 1% ACRAWAX ADDED TO $(U,Pu)O_2$ POWDER MIX. NOTE UNIFORM POROSITY DISTRIBUTION.

AS POLISHED.

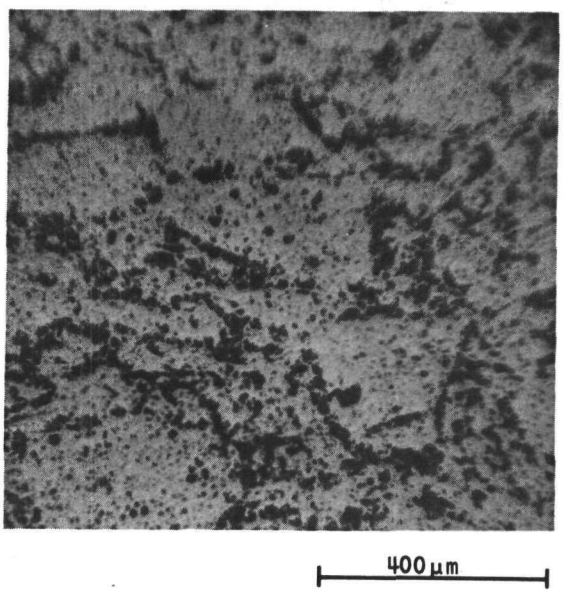

(b) 1% ACRAWAX ADDED TO $(U,Pu)O_2$ GRANULES. NOTE LARGE VOLUME OF POROSITY IS CONCENTRATED AT GRANULE SURFACES.

AS POLISHED.

Figure 12-1. The Effect of Adding Binder to the Powder Versus Granules on Sintered Pellet Microstructure

3937-20

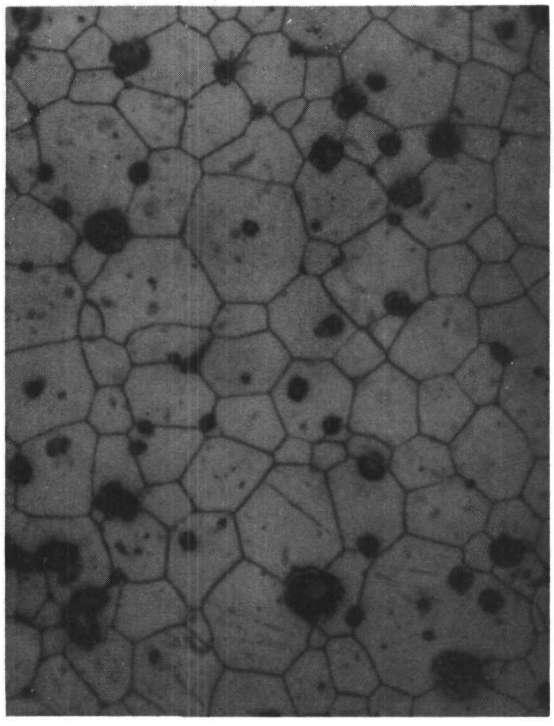

50 µm

THIS IS NOMINALLY 95% DENSE MATERIAL. NOTE GOOD GRAIN BOUNDARY DELINEATION.

AVERAGE GRAIN SIZE: 13 µm

Figure 12-2. $(U,Pu)O_2$ Pellet Used in Chemical Etching Trials

3937-21

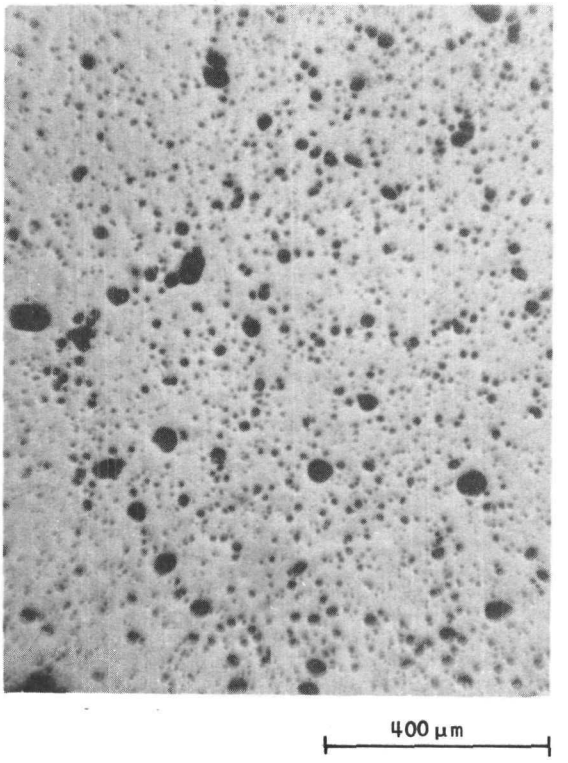

Figure 12-3. Porosity Distribution in an As-Sintered $(U,Pu)O_2$ Pellet from Batch UP-36-2

3937-22

Table 12-4 Grain and Pore Size Data for Nominally 95% Dense $(U,Pu)O_2$ Fuel Pellet Batches for Use in WSA-3

Batch Number	Average Pore Size (μm)	Pore Size Range (μm)	Average Grain Size (μm)	Grain Size Range (μm)
UP-34-2	20	1 ∿ 75	4.3	1 ∿ 15
UP-36-1	25	1 ∿ 75	3.8	1 ∿ 15
UP-36-2	26	1 ∿ 75	12.6	3 ∿ 35

Table 12-5 Green and Pore Size Distributions for Nominally 95% Dense $(U,Pu)O_2$ Fuel Pellet Batches for Use in WSA-3

Batch Number	Grain Size Distribution Size (μm)	Grain Size Distribution No. of Grains per cm^2 ($x10^{-4}$)	Pore Size Distribution Size (μm)	Pore Size Distribution No. of Pores per cm^2 ($x10^{-2}$)
UP-34-2	15-20	8	50-80	4
	5-8	158	25-30	58
	1-5	261	1-25	1960
UP-36-1	10-13	26	50-80	23
	5-8	289	25-30	93
	1-5	184	1-25	1787
UP-36-2	20-25	1		
	15-20	26		
	10-15	42	50-80	3
	5-10	34	25-30	45
	1-5	16	1-25	1080
	< 1	9		

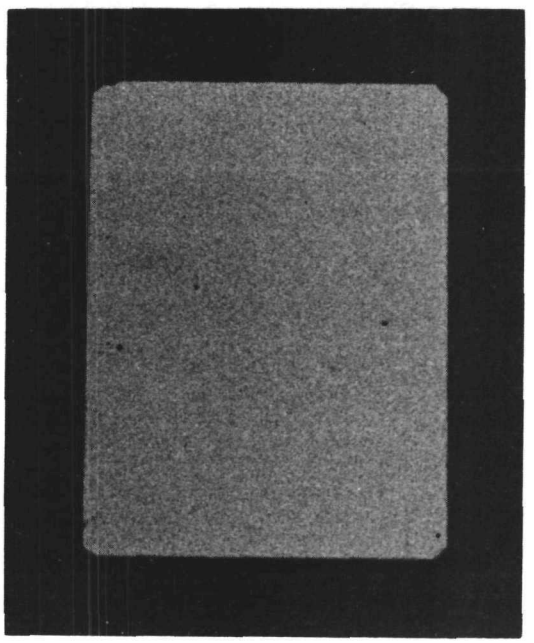

Figure 12-4. Typical Autoradiograph of Pellet from Batch 36-2

3937-24

The porosity distributions in batch UP-34-2 (Figure 12-5) is different from that observed in pellets from UP-36-2 (Figure 12-3), being much more concentrated along the granule surfaces. Details of grain and pore size measurements are given in Tables 12-4 and 12-5. The differences in fabrication account for the observed porosity distribution. In batch UP-34, 1.5% Acrawax was added to the powder prior to preslugging; while with batch UP-36, 0.5% Acrawax was added to the preslugged granules. Autoradiography has been completed on batch UP-34-2; the results indicate satisfactory homogeniety similar to that shown for batch UP-36.

3.4 Immersion Density

Immersion density data on pellets from various high density $(U,Pu)O_2$ fuel batches are given in Table 12-6. Four pellets per batch were sampled, and the data represents duplicate runs on each pellet. The immersant was dried xylene. With batches UP-31 through -36, there is virtually no open porosity in the pellets which confirms metallographic observations. Preliminary metallographic examination of pellets from batch UP-40 indicates some degree of interconnection as indicated by the immersion density data on this batch.

Table 12-6 Immersion Density Data for Nominally 95% Dense $(U,Pu)O_2$ Fuel Pellet Batches for WSA-3

Batch Number	Geometric Density (% Theoretical)	Immersion Density (% Theoretical)	Open Porosity (%)	Closed Porosity (%)
UP-34-2	95.4	96.5	0.1	3.4
UP-36-1	94.7	96.7	0.1	3.2
UP-36-2	94.8	97.0	0.2	2.8
UP-40-1	95.8	97.6	0.7	1.7
UP-40-2	95.8	97.0	0.7	1.5

4.0 REFERENCES

1. "Oxide Fuel Element Development Quarterly for the Period Ending December 31, 1969," WARD-4135-4, February, 1970.

2. "Oxide Fuel Element Development Quarterly Progress Report For the Period Ending June 30, 1970," WARD-4135-11, September 1970.

3. "Oxide Fuel Element Development Quarterly Progress Report for the Period Ending September 30, 1969," WARD-4135-1, November 1969.

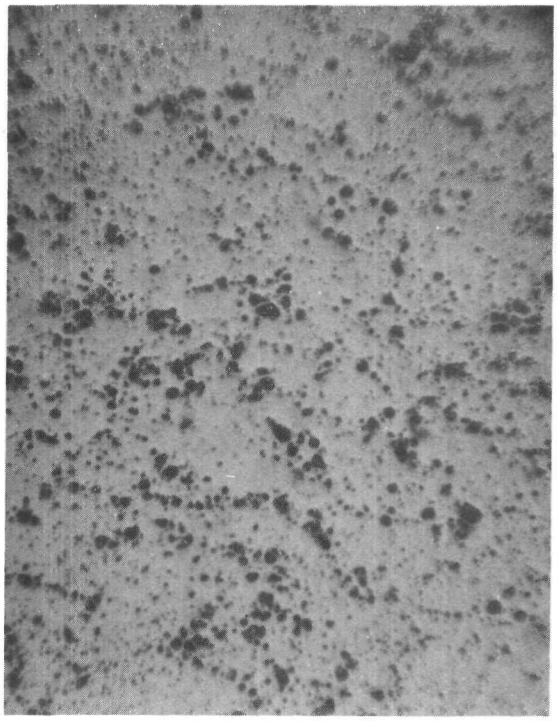

Figure 12-5. Porosity Distribution in an As-Sintered Pellet from Batch UP-34-2

3937-23

SECTION 13

OFBA-512 FUEL ELEMENT FABRICATION

R. C. DeKlever, W. R. Jacoby, R. K. McGeary, and D. P. Shapland

1.0 OBJECTIVES

The principal objectives of this task are to:

1. Fabricate and characterize 45 fuel pins for the WSA-3 irradiation experiment. The pins are about 5 feet long, and 37 will be fitted into a grid assembly for insertion in EBR-II. Eight pins will serve as standbys.

2. Develop and install the equipment needed, and establish procedures for operation for the increased length fuel pins.

3. Adapt methods for xenon tagging of fuel pins, and fabricate the WSA-3 pins containing the specified xenon gas additions.

4. Fabricate sodium encapsulated pins as requred for the WSA-5 experiment.

5. Fabricate unencapsulated pins for the WSA-4 grid assembly irradiation experiment.

2.0 PRIOR WORK

Fabrication and testing of all the fuel pins for WSA-1 was completed, and the assembly was shipped to EBR-II. Three glove boxes were made operational for fuel pellet loading and final pin fabrication of WSA-3. Fabrication of dummy fuel pins for flow testing and for the fretting tests have been completed and the pins delivered. Certified tubing has been received and fuel tube preparation and bottom end plug welding is under way for WSA-3. The xenon tagging apparatus has been constructed and trial runs performed. Results of analyses of gas samples have not been completed. The design of a new profilometer to survey the surface topography of fuel pins has been completed. Construction will begin next quarter.

3.0 CURRENT PROGRESS

3.1 WSA-3 37-Pin Grid Assembly

3.1.1 Pin Fabrication Status

The WSA-3 irradiation test assembly requires the fabrication of 45 fuel pins; 37 will be inserted in grids for testing, and 8 pins will serve as standbys.

All of the high density fuel pellets required for Group I and Group II Experiments (24 pins) have passed all inspection requirements and are available for loading into cladding tubing. Results of the inspection program are detailed in Task OFBA-513, Section 14. All 13 of the Group II fuel pins have been loaded with pellets, and fabrication is completed. The 11 Group I pins will be completed by October 15, 1970.

About half of the low density fuel pellets for Group III and Group IV Experiments (21 pins) have been manufactured and approved for loading. The status of pellet manufacturing is described in Task OFBA-510, Section 11. Fabrication of all 45 pins is expected to be completed by mid-November.

Fabrication of the WSA-3 fuel pins was preceded by fabricating two prototype pins in which all processing (including xenon tagging) and all evaluation tests were performed in the same manner to be used for the actual pins. No significant problems were encountered during loading, decontamination, or closure welding. Processing of the WSA-3 pins was then started with batches of 4 or 5 pins to produce the 13 pins of Group II. No defective pins or difficulties were encountered.

3.1.2 Procedures

Prior to pin fabrication, a process flow sheet was formulated in order to coordinate assembly and to insure that procedures had been established to cover each of the processing steps. Table 13-1 shows the fabrication process flow sheet and the applicable Procedure Number, and Table 13-2 lists all of the procedures. The process flow sheet indicated that certain procedures were lacking, and considerable time was directed to insuring that the fabrication steps were covered by applicable procedures. Having procedures ot cover each assembly step, operator error can be minimized and project coordination, record keeping, and quality control, efficiency can be increased.

3.1.3 Bayonet Fitting on Top End Plug

The fabrication of the hold-down assemblies and fuel tube assemblies has been completed. During the fabrication of the bayonet fitting in the top end plug for the WSA-3 fuel pins, it was observed that tacking the spiral pin in place, Figure 13-1 (a), produced unsatisfactory results. The spiral pin consists of 2, 1/4 wraps of 0.005 inch thick, 1/4-hard Type 302 stainless steel rolled into a tube of 0.094 inch outside diameter. Approximately 50% of all tacks on the spiral pins were rejectable due to cracks. Also, only a few pounds of force were required to displace the pin. These conditions were deemed unacceptable for inclusion in EBR-II.

A suggestion that the spiral pin be abandoned in favor of a solid Type 304 stainless steel wire, 0.094 inch in diameter, tacked on both sides, Figure 13-1 (b), was approved. The resulting tacks were free from cracks, and the wire could not be dislodged with a load sufficient to cause wire deformation. The solid wire was substituted for all top end plug bayonet fittings for the WSA-3 subassembly.

Table 13-1. Fabrication Process Steps for WSA-3

I. Fuel Tube Fabrication

	Procedure #
a. Machine tubing to length	3210
b. Temporarily mark tubing	3160
c. Inspect tubing	3210
d. Clean tubing	3220
e. Inspect as rec'd. end plugs	3130
f. Clean bottom end plugs	3230
g. Inspect components for cleanliness	3230, 3210
h. Weld bottom end closure	3240
i. Take preliminary radiographs	3520
j. Inspect weld radiographs	3520
k. Dress weld nugget	3550
l. Check straightness	3535, 3540
m. Helium leak test	3515
n. Die penetrant inspection	3510
o. Clean top end plugs and bayonet pins	3230
p. Tack bayonet pins in place	3250
q. Deburr and polish bayonet pin and tack	3250
r. Inspect tack and final dimensions	3250
s. Store all components	

II. Hold-Down Assembly Fabrication

a. Machine tubing to length	3210
b. Inspect	3210
c. Clean tubing	3220
d. Inspect as rec'd. spacer discs	3120
e. Clean spacer discs	3230
f. Clean springs	3230
g. Inspect all components	3270
h. Tuck weld spacer discs to spacer tube	3270
i. Clean and inspect	3270
j. Crimp springs to spacer discs	
k. Inspect and store assembly	3270

III. Fuel Loading

	Procedure #
a. Receive fuel with approved OP-10-01 O/M ratio	
b. Visually inspect fuel	3320
c. Weigh pellets	3320
d. Measure length and diameter	3320
e. Punch computer cards	3330
f. Computer run	3330
g. Select 18 pellets for chem. and metallography	3140
h. Select 15 pellets for archives and reserve	3140
i. Select fuel pellet stack	3340
j. Select insulator pellets	3340
k. Match smear density	3330
l. Load fuel stack	3410
m. Decontaminate, insert hold down	3420
n. Store	

IV. Fuel Pin Assembly Fabrication

a. Clean and inspect top end plugs	3120,3230
b. Xenon tag and weld top end closure	3450,3440
c. Take preliminary radiographs and inspect	3520
d. Dress welds	3550
e. Check straightness	3535,3540
f. Helium leak test	3515
g. Die penetrant inspection	3510
h. Stamp permanent density	3260
i. Final radiography bottom end plug	3520
j. Final radiography top end plug	3520
k. Fuel stack radiography	3520
l. Full length radiography	3520
m. Profilometry	3505
n. Final cleaning and polishing	3530
o. Final dimensional inspection	3535
p. Certify for shipment	3555
q. Load and ship	

Table 13-2 Operating Procedures For Fuel Element Fabrication

No.	Procedure
3110	Procurement Document Review
3120	Receiving Inspection
3130	Material Identification and Control
3140	Archive Sample Selection and Disposition
3150	Control of Nonconforming Items
3160	Temporary Marking Methods
3210	Preparing Fuel Tube Ends for Welding
3220	Fuel Tube Cleaning
3230	Cleaning End Plugs and Other Metal Components
3240	Bottom End Plug Welding
3250	Tack Welding Top End Plug Bayonet Pin
3260	Fuel Pin Permanent Identification Marking
3270	Tack Welding Spacer Tube End Caps
3320	Measuring, Sorting, and Storage of Fuel Pellets
3330	Computer Deck Assembly for Pellet Calculations
3340	Pellet Selection Plan for Loading
3320	Measuring, Sorting, and Storage of Fuel Pellets
3330	Computer Deck Assembly for Pellet Calculations

No.	Procedure
3340	Pellet Selection Plan for Loading
3410	Fuel Insulator Pellet Loading into Tubes
3420	Radioactive Decontamination of Open Fuel Tube End
3440	Welding Top End Plug
3450	Xenon Tagging of Fuel Pins
3460	Welder, Equipment and Procedure Qualification
3505	Profilometry of Fuel Pins
3510	Dye Penetrant Inspection
3515	Helium Leak Testing
3520	Radiography of Fuel Pins
3525	Developing Radiographic Films
3527	Replacing and Replenishing Radiographic Fluids Process
3530	Final Polishing Fuel Pins
3535	Straightening Fuel Pins
3540	Straightening Welded End Plugs
3550	Inspection of Maximum Diameter of Welds and Weld Dressing
3555	Data Package Compilation

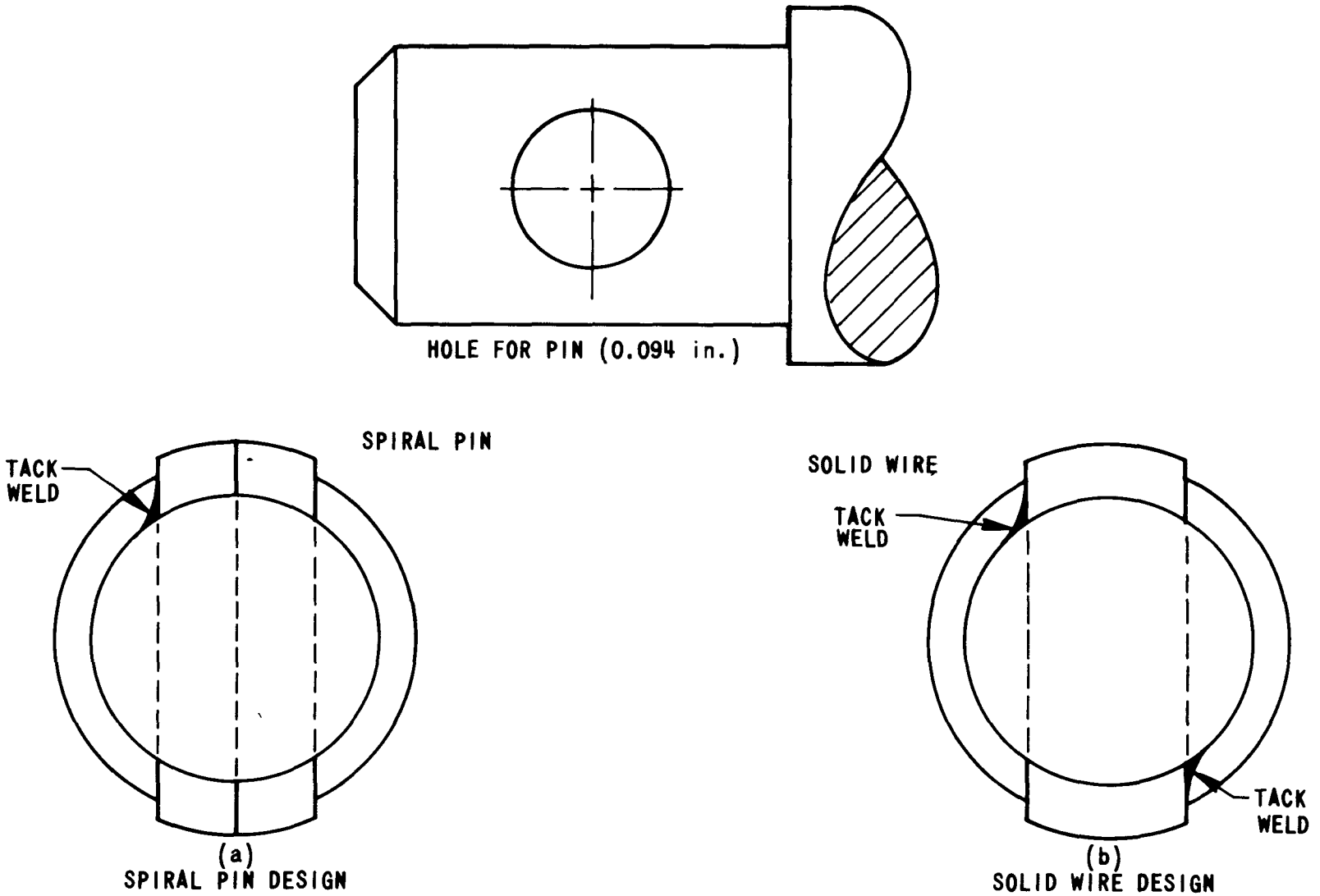

Figure 13-1. Comparison of Tacks Used for Spiral Pin and Solid Wire Bayonet Fittings for WSA-3 Top End Plug

3.1.4 Xenon Tagging

During the quarter, a total of 21 prototypical fuel rods were processed through xenon tagging and welding, then analyzed for xenon tag gas content. During these trials, the welding and xenon tagging equipment was commissioned for use.

Parameters established from xenon tagging development data were: 1) elapsed time required for the operator to insert the end plug after removing the apparatus, and 2) tagging fixture gas plenum backfill pressure after allowing an equilibrium tag mixture to be introduced into the evacuated fuel rod void volume. Table 13-3 summarizes the experimental data. The composition of the supply gas as sampled directly from the cylinder into the analyzing apparatus was 11.27 mole percent xenon. Samples 1 through 10 were processed as the first batch using the standard xenon tagging procedure. The relatively low xenon values detected in Samples 2, 3, and 6 were attributed to a leaking O-ring seal and bellows vacuum valve. The last three samples from the initial batch, 8 through 10, were processed in order to determine the optimum gas backfill pressure. As indicated by the experimental data and verified by calculation, the minimum allowable pressure asssuming negligible loss by gaseous diffusion is approximately 21 psig. Samples 11 through 17 were processed in exact accordance to the procedure in order to determine repeatability of the tagging process. Except for Sample 13, where the gas supply from the cylinder was depleted, all results were reasonably consistent yielding an average Xe in He content of 10.51 mole percent. This value is well above the minimum 8.4 mole percent xenon required by the specification. Samples 18 through 21 established the maximum allowable time that the upper end of the fuel rod could remain open after xenon tagging and prior to end plug insertion.

The atmosphere within the welding chamber for these trials was changed from pure helium to a binary mixture of 0.938 mole percent neon in helium. The matrix gas was doped in order to establish xenon loss and neon entry into the tube as a function of time. Figure 13-2 illustrates the rate of xenon tag gas egress and the corresponding neon ingress rate for an open end fuel pin with an effective open cross-sectional area of 0.0059 in^2. This plot indicates that the top of the fuel rod could remain open up to approximately 10 minutes before the minimum allowable (8.4 mole percent xenon) tag composition is reached. These data are based on an initial tag addition consisting of a 1.0 ml quantity of xenon which corresponds to 11.27 mole percent xenon in helium. The upper curve in Figure 13-2 shows the total xenon and neon[a] concentration in the completed fuel pin. The slight increase in concentration of the heavy gases indicates the helium carrier gas is lost more readily.

---

[a] Since the composition of the box gas was 0.938 mole percent neon in helium, the actual analytical values have been altered so as to show the effect if the initial Xe and Ne concentrations had been equal in the tubing and box atmospheres, respectively. Thus, the values plotted are the actual measured percent neon times the ratio 11.27/0.938.

Table 13-3 Summary Of Xenon Tag Development Work

Specimen Number	Mass Spec. Gas Analysis (Mole %)			Matrix Gas (Mole %)		Tagging Apparatus Removal Time (sec)	Time Required For End Plug Insertion (sec)	Remarks
	He	Xe	Ne	He	Ne			
Standard	88.67	11.27	--	--	--	--	--	Analysis of Supply Cylinder
1	87.10	11.12	--	99.9+	--	30	30	
2	91.20	8.35	--	99.9+	--	30	30	Leaking Seal Detected
3	96.89	2.83	--	99.9+	--	30	30	Leaking Seal Detected
4	89.05	10.74	--	99.9+	--	30	30	
5	88.94	10.67	--	99.9+	--	30	30	
6	99.33	0.44	--	99.9+	--	30	30	Leaking Seal Detected
7	90.50	9.02	--	99.9+	--	30	30	
8	89.84	9.60	--	99.9+	--	30	30	Gas Plenum Filled to 25 psig
9	91.38	8.13	--	99.9+	--	30	30	Gas Plenum Filled to 20 psig
10	92.37	7.24	--	99.9+	--	30	30	Gas Plenum Filled to 15 psig
11	89.29	10.54	--	99.9+	--	15	20	
12	89.42	10.58	--	99.9+	--	5	30	
13	99.08	0.69	--	99.9+	--	5	30	Gas supply in cylinder depleted during run
14	89.16	10.84	--	99.9+	--	10	25	
15	89.45	10.55	--	99.9+	--	5 min	25	
16	89.90	10.10	--	99.9+	--	1 min	23	
17	89.44	10.56	--	99.9+	--	1 min	15	
18	89.49	10.38	0.13	99.06	0.94	20	1 min	Teflon plug in place until end plug inserted
19	89.48	10.44	0.08	99.06	0.94	20	1 min	Teflon plug removed until end plug inserted
20	90.37	9.45	0.18	99.06	0.94	20	5 min	Teflon plug removed until end plug inserted
21	92.04	7.58	0.37	99.06	0.94	15	15 min	Teflon plug removed until end plug inserted

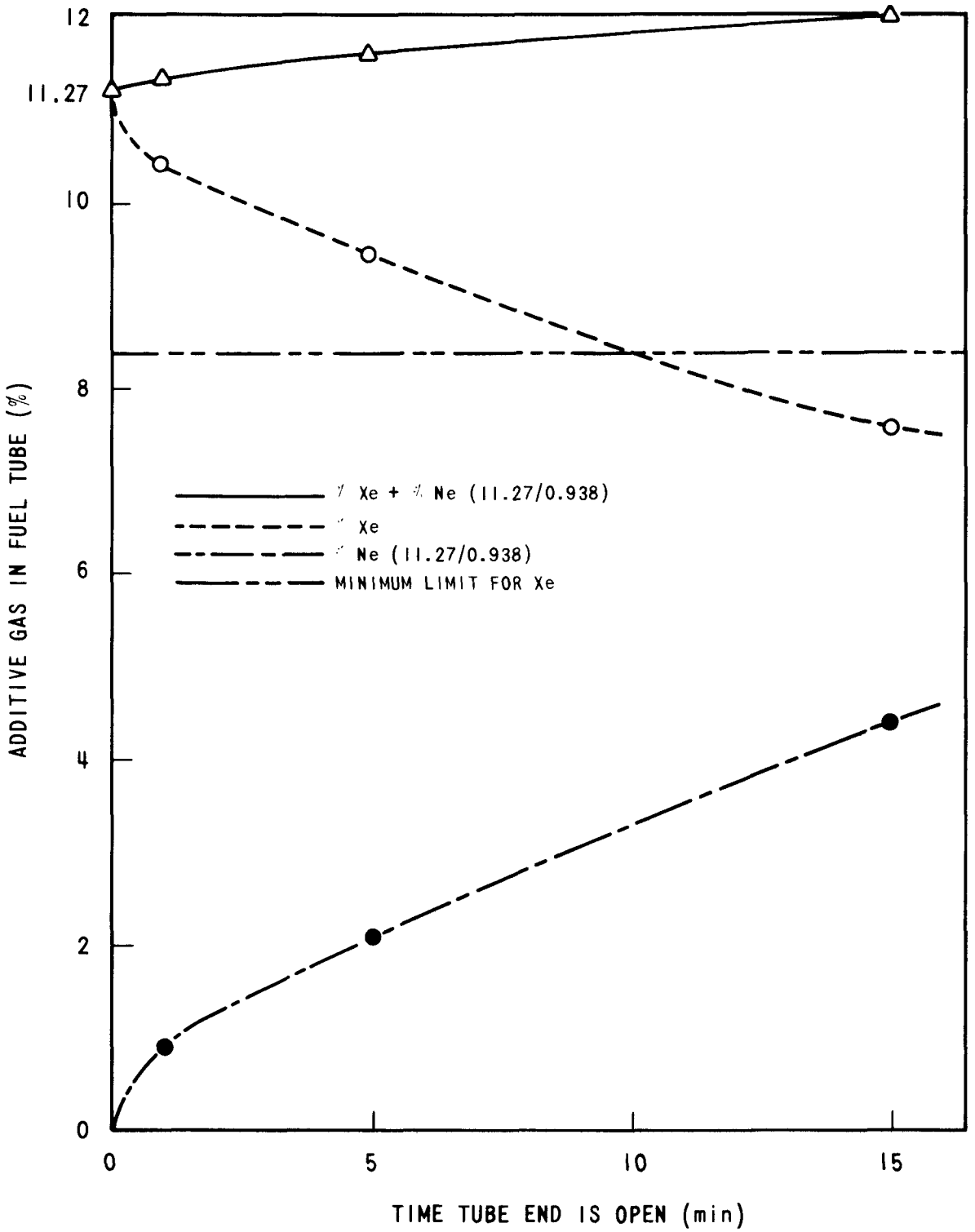

Figure 13-2. Rate of Xenon Loss and Neon Entry Into Open Ended Fuel Tube With 0.0058 in.^{2} Effective Area

3937-26

3.1.5 Top End Plug Closure Weld

Upon completion of the xenon tagging development work, a formal welding qualification was performed for the top end fitting welds. Five consecutive simulated top end fitting weld samples were welded and non-destructively and, subsequently, destructively examined in accordance with the requirements outlined in the EBR-II Experimenters Guide. All attributes of the weld quality were found acceptable.

Figure 13-3 shows the set-up used to make the final top end plug circumferential weld. The dead weight of the copper bar is used to overcome the two pound nominal load exerted on the top end fitting by the hold down spring inside the fuel pin. The conventional means for overcoming this load is a spring-loaded device with a foot that rotates with the end plug. Such a device is troublesome and can cause misalignment of the plug in the tube. The dead weight is trouble free and simple.

Xenon tagging and welding of the first fuel-bearing rod for WSA-3 was witnessed by W. J. Larson from EBR-II, Argonne National Laboratories (ANL). During this welding cycle, the initial archive sample was xenon tagged and welded, and the final sample will be tagged and welded immediately following the final WSA-3 fuel element weld.

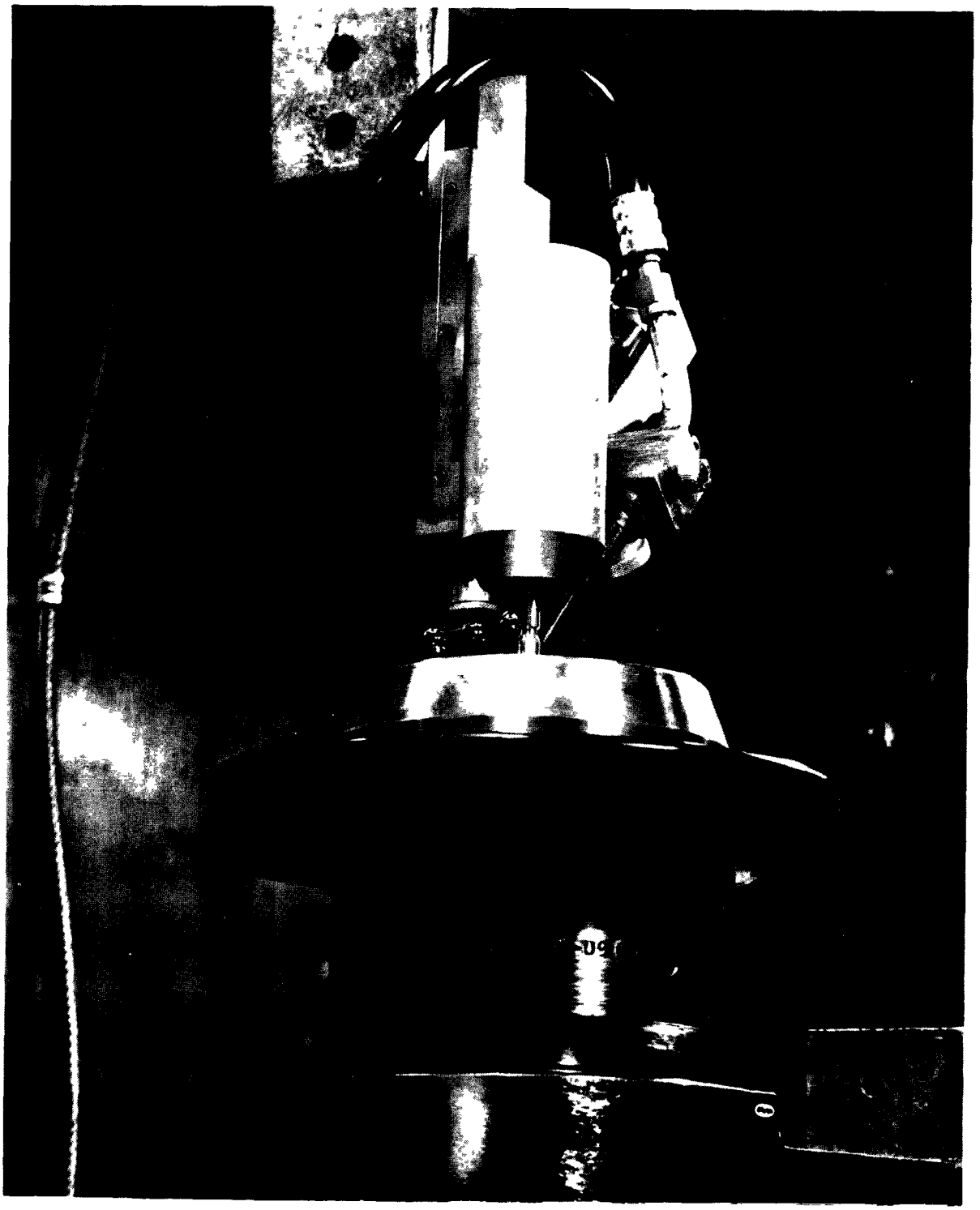

Figure 13-3. Welding Setup After Xenon Tagging Apparatus is Removed and Electrode and Dead Weight are Positioned

3937-27

SECTION 14

OFBA-513 PRODUCT CONTROL AND DOCUMENTATION

W. B. Bargerstock, W. R. Jacoby, and R. K. McGeary

1.0 OBJECTIVES

The objective of this task is to provide quality control for the entire fuel fabrication from raw material acceptance to final product identification. Included is responsibility for documentation of all data and information needed for final records from all phases of fabrication and material handling.

For the fiscal year on Tasks OFBA-510 and -512, at least 90 irradiation test pins for grid assemblies and up to 20 sodium encapsulated pins will be fabricated. Measurements of length, diameter, and weight for more than 7,000 fuel pellets will be keypunched and analyzed by use of a computer program in order to develop statistical information on fabrication and also to control the smear density allocation of pellets in cladding tubing. Fuel pin measurements and other pertinent data are to be collected and documented. Detailed reacords are to be kept for prototype pins, test samples, archive samples, as well as actual irradiation test pins.

2.0 PRIOR WORK

The objectives stated above have been exercised during the fabrication of the WSA-1 and WSA-2 test pins, two prototype assemblies of 37 pins each for the hydraulic flow test, for the materials fretting test, and for the initiation of the WSA-3 fuel pins.

Quality control and documentation procedures for control of the product of Tasks OFBA-510 and -512 have been established. The evaluation and control of hardware fabrication and careful record keeping have been considered essential for this program.

3.0 CURRENT PROGRESS

With the current loading of 13 WSA-3 fuel pins, the need for careful product control and documentation of results has increased. The computer program has now been used to calculate the pellet density and smear density over 4500 pellets for the WSA-3 fuel pins. Each of about 70 storage tubes in the glove box contain 60 pellets, the individual pellet identity and density of which are known. To assemble the loading stack of 54 pellets, specific pellets must be taken from the various storage tubes in accordance with computer generated smear density pellet allocation sites. To avoid errors of selection, careful documentation of pellet locations is required at all times. Location charts and pellet assignment charts are maintained. As an

inventory proof check, a white ceramic pellet is used to replace each fuel pellett as it is removed from its storage location. The characteristics of each of about 5300 pellets are maintained at present from 14 different fuel pellet batches.

Density histograms have been constructed for each batch. A typical histogram for a high density batch is shown in Figure 14-1 and for a low density batch in Figure 14-2. All of the high density fuel has been completed; the histograms for the five batches required to produce 24 pins have been smoothed and plotted in Figure 14-3. Most of the pellets are within ± 1% of a nominal value of 95.5% of theoretical density which meets specification requirements. For the low density fuel, six batches have presently been submitted for measurement. Smoothed histograms for these batches are shown in Figure 14-4. The density spread is considerably greater than for the high density pellets. The specification currently requires 90 ± 1% T.D. for usable pellets. About half of the quantity of acceptable pellets needed for 21 pins is available. Consequently, additional fuel batches are being made. The higher numbered batches shown in Figure 14-4 are the most recently fabricated, so that comparison of 41-1 with the 37 batches demonstrates that progress is being made in narrowing the density spread. Details of this work are covered in OFBA-510, Section 11.

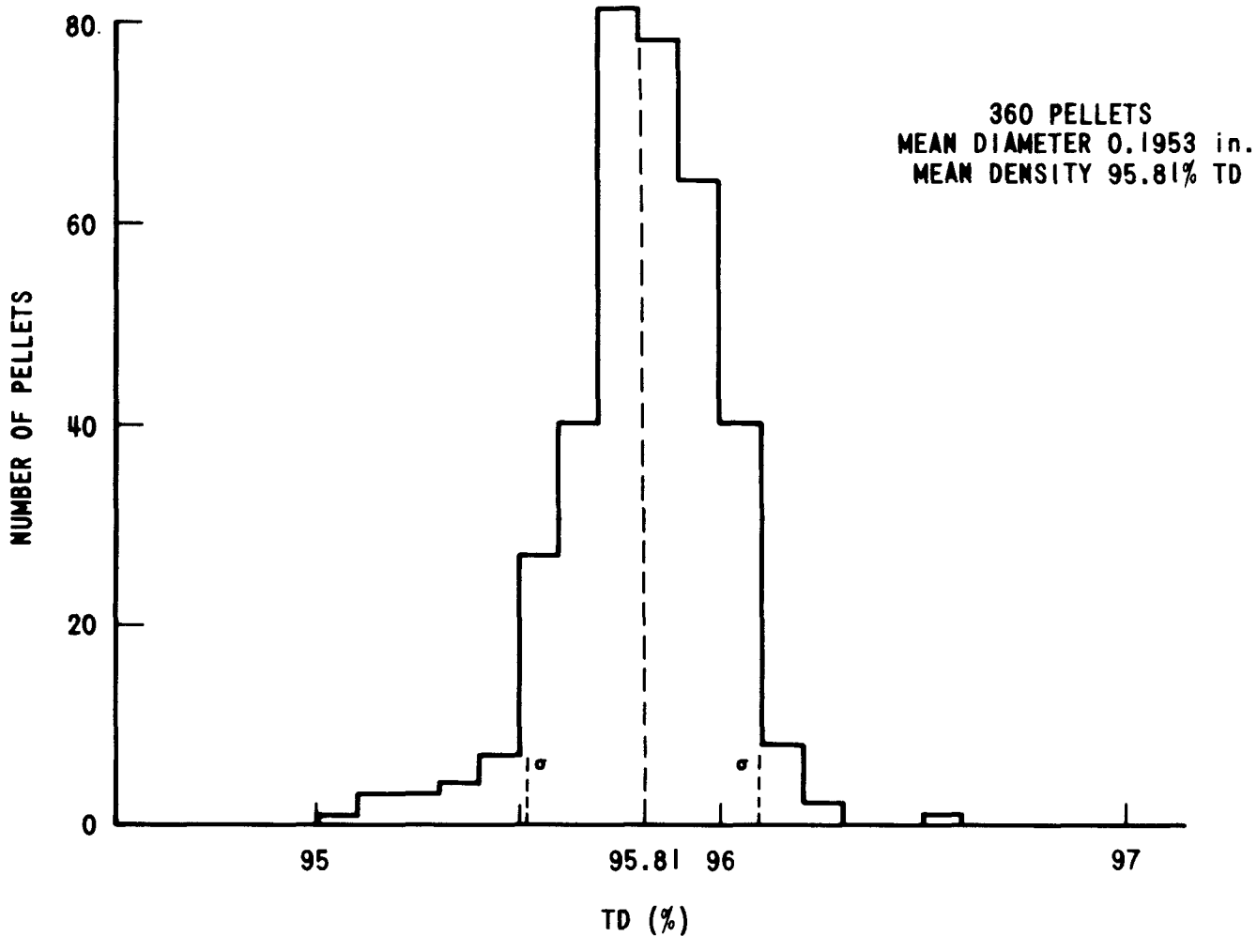

Figure 14-1. Total Pellet Population Distribution for Batch 40-2

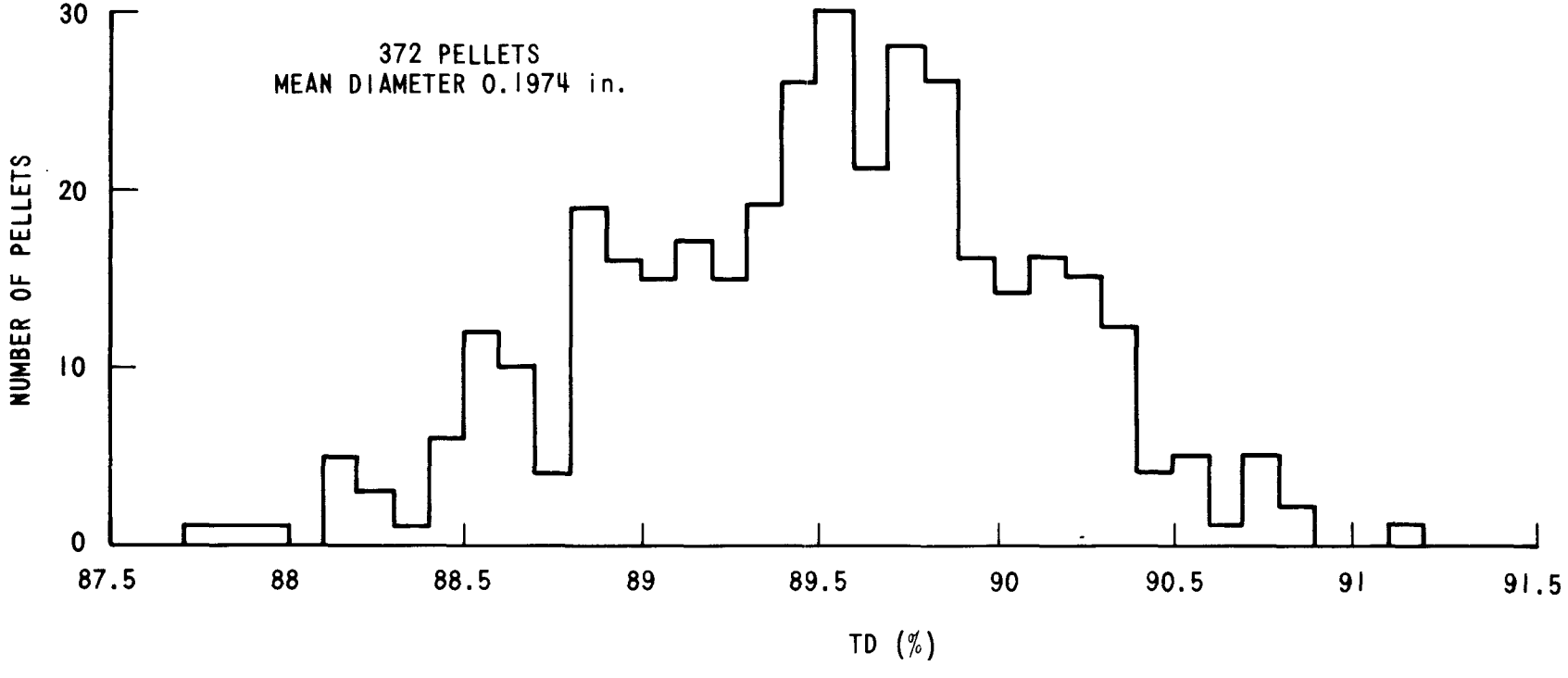

Figure 14-2. Total Pellet Population Distribution for Batch 41-1

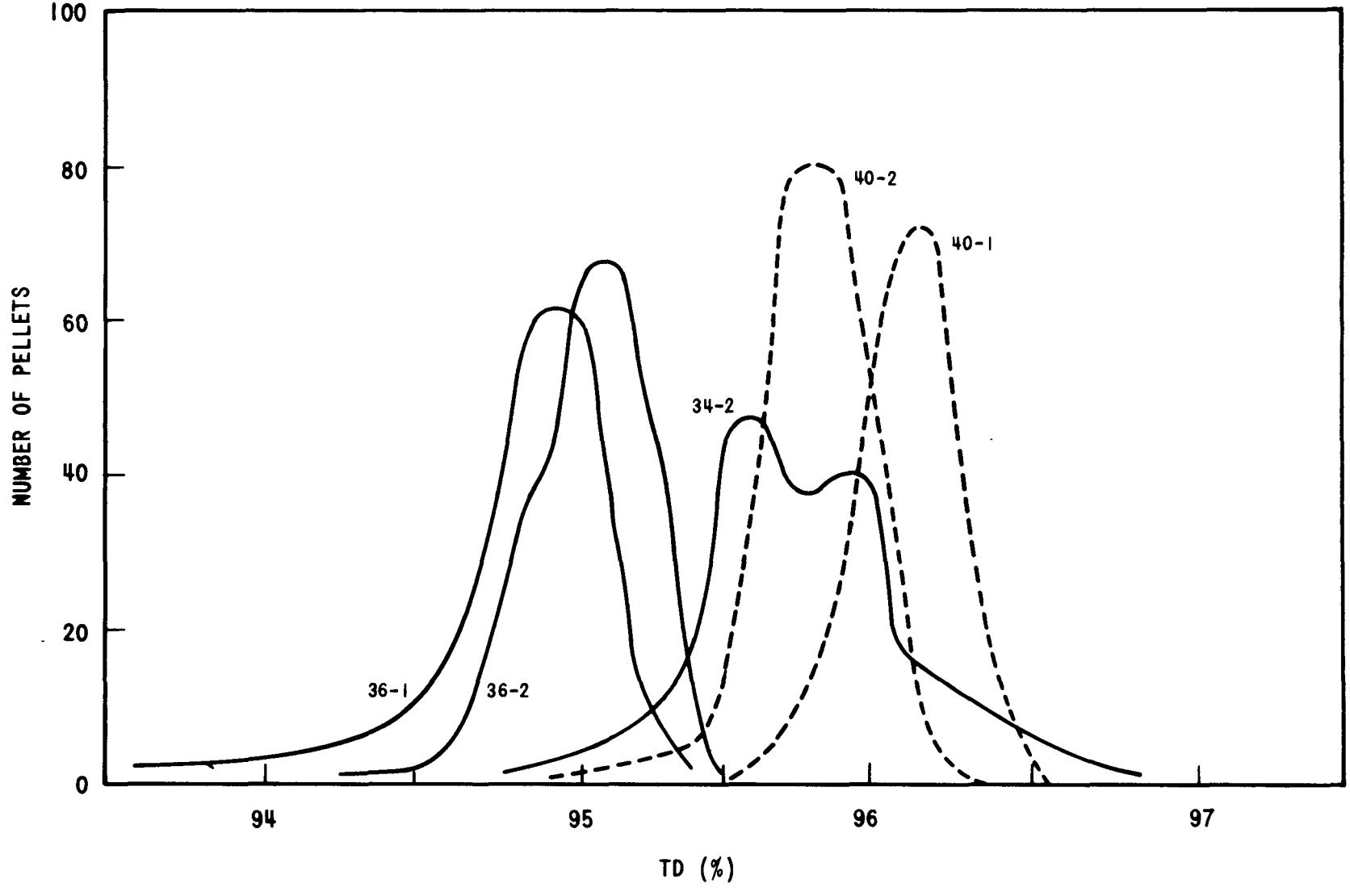

Figure 14-3. Density Distribution for the Group I and Group II Pellet Batches for WSA-3 Fuel Pins

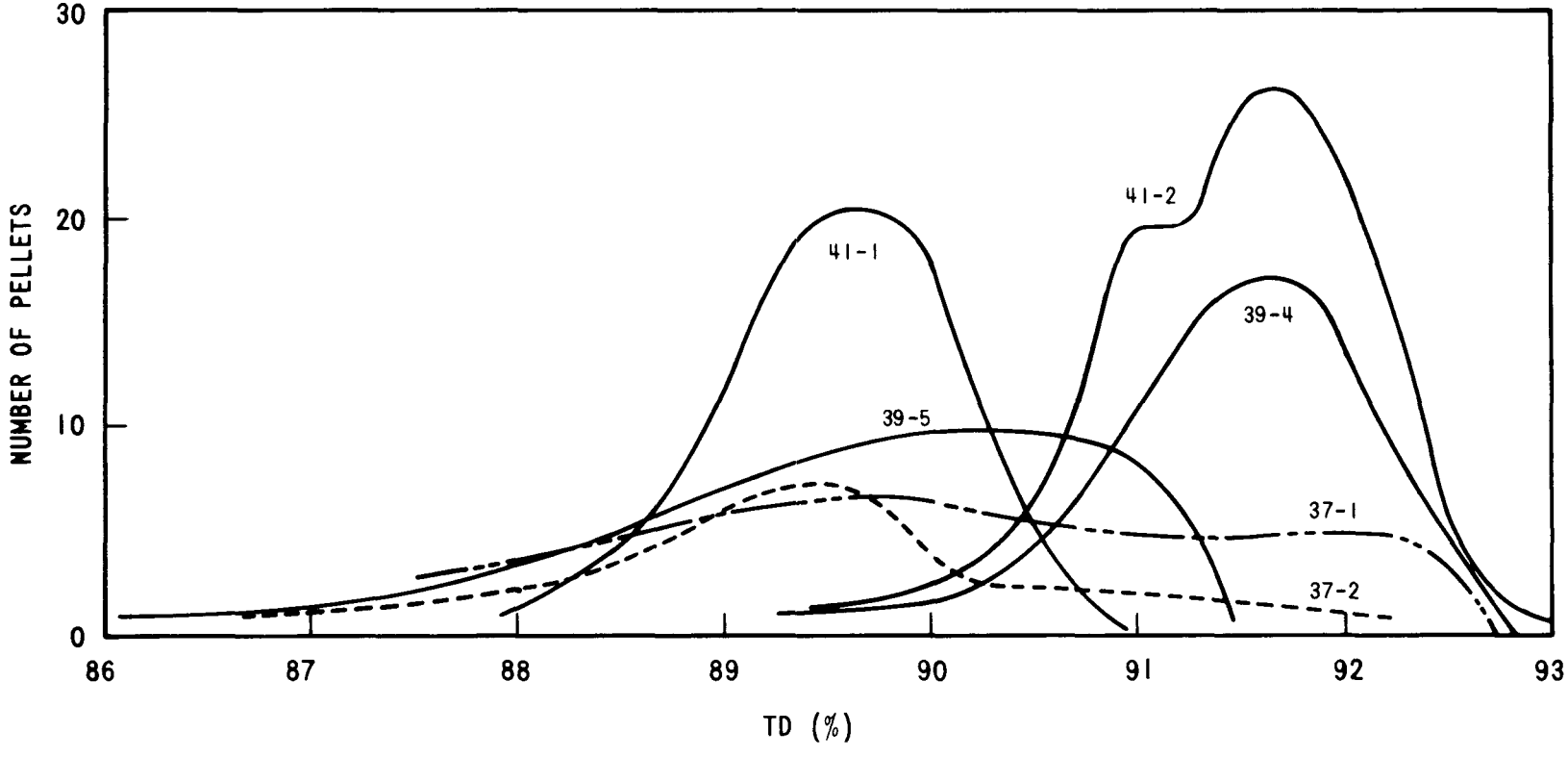

Figure 14-4. Density Distribution for the Low-Density (Groups III, IV) Fuel Batches for WSA-3 Fuel Pins

DISTRIBUTION LIST

Division of Reactor Development and Technology
U. S. Atomic Energy Commission
Washington, D. C. 20545
Attn: Director
Assistant Director, Engineering Standards
Assistant Director, Nuclear Safety
Assistant Director, Plant Engineering
Assistant Director, Program Analysis
Assistant Director, Project Management (2)
Assistant Director, Reactor Engineering (2)
Assistant Director, Reactor Technology
Chief, Fuels and Materials Branch (3)
Chief, Fuel Engineering Branch
Chief, Reactor Vessels Branch
Chief, Coolant Chemistry Branch
Chief, Core Design Branch

Assistant Director
Pacific Northwest Programs
U. S. Atomic Energy Commission
P. O. Box 550
Richland, Washington 99352

USAEC-RDT Site Office
Argonne National Laboratory
Building 2
Argonne, Illinois 60439

USAEC-RDT Site Office
P. O. Box 2108
Idaho Falls, Idaho 83401

USAEC-RDT Site Office
P. O. Box 1446
Canoga Park, California 90304

USAEC-RDT Site Office
310 DeGuigne Drive
Sunnyvale, California 94086

USAEC-RDT Site Office
P. O. Box 2325
San Diego, California 92112

USAEC-RDT Site Office
P. O. Box 154
Madison, Pennsylvania 15663

USAEC-RDT Site Office
P. O. Box X
Oak Ridge, Tennessee 37830

USAEC-RDT Site Office
P. O. Box 550
Richland, Washington 99352

Division of Naval Reactors
Chief, Nuclear Materials Branch
U. S. Atomic Energy Commission
Washington, D. C. 20545

U. S. Atomic Energy Commission - DTIE(3)*(50)**
P. O. Box 62
Oak Ridge, Tennessee 37831

Manager (2)
U. S. Atomic Energy Commission
New York Operations Office
376 Hudson Street
New York, New York 10014

Office of Asst. General Counsel for Patents
U. S. Atomic Energy Commission
Washington, D. C. 20545

Director (2)
LMFBR Program Office-ANL
9700 South Cass Avenue
Argonne, Illinois 60430

Director, Metallurgy Division (2)
Argonne National Laboratory
9700 South Cass Avenue
Argonne, Illinois 60439

Manager, FFTF Project (2)
WADCO
P. O. Box 1970
Richland, Washington 99352

FFTF Fuels Department (2)
WADCO
P. O. Box 1970
Richland, Washington 99352

---

* submitted with transmittal form AEC-426
**submitted for transmittal to recipients under UKAEA/USAEC and EURATOM/USAEC Fast Breeder Information Exchange arrangements.

Manager, Chemistry and Metallurgy Div.
Battelle Northwest Laboratory
P. O. Box 999
Richland, Washington 99352

Division Leader, Chemistry and Metallurgy Div. (CMB)
Los Alamos Scientific Laboratory
P. O. Box 1663
Los Alamos, New Mexico 87544

Director, Metallurgy and Materials Science Division
Brookhaven National Laboratory
Upton, New York 11973

Director, Metals and Ceramics Division (2)
Oak Ridge National Laboratory
P. O. Box X
Oak Ridge, Tennessee 37820

Division Chief, M & S Division
NASA - Lewis Research Center
2100 Brook Park Road
Cleveland, Ohio 44135

Director
Atomics International
Liquid Metal Engineering Center
P. O. Box 309
Canoga Park, California 91305

Manager-Advanced Development Activity
General Electric Company
Knolls Atomic Power Laboratory
P. O. Box 1072
Schenectady, New York 12301

General Manager
Westinghouse Electric Corporation
Bettis Atomic Power Laboratory
P. O. Box 79
West Mifflin, Pennsylvania 15122

Director, LMFBR Technology Program
Atomics International
P. O. Box 309
Canoga Park, California 91304

Associate Manager, Materials Engineering Dept.
Battelle Memorial Institute
Columbus, Ohio 43201

Director, Nuclear Development Center
The Babcock and Wilcox Company
Atomic Energy Division
Lynchburg, Virginia 24501

Manager, Plutonium Chemistry and Ceramics Fuels Development
Nuclear Materials and Equipment Corporation
Leechburg, Pennsylvania 15656

Manager, Sodium Reactor Technology
General Electric Company
Breeder Reactor Development Operation
310 DeGuigne Drive
Sunnyvale, California 94086

Manager, Nuclear Laboratories
Combustion Engineering, Inc.
Nuclear Division
Prospect Hill Road
Windsor, Connecticut 06095

Laboratory Assistant Director
Gulf Energy & Environmental Systems, Inc.
P. O. Box 608
San Diego, California 92112

Manager, Research
United Nuclear Corporation
Research and Engineering Center
Grasslands Road
Elmsford, New York 10523

Head, Fuels and Materials
Atomic Power Development Associates
1911 First Street
Detroit, Michigan 48226

K-2 Group Leader
Reactor Division
Los Alamos Scientific Laboratory
P. O. Box 1663
Los Alamos, New Mexico 87544

Irradiations Coordinator
EBR-II Project
Argonne National Laboratory
P. O. Box 1096
Idaho Falls, Idaho 83401

Director
Vallecitos Nuclear Center
General Electric Company
P. O. Box 846
Pleasanton, California 94566

Experiment Manager
EBR-II Project
Argonne National Laboratory
9700 South Cass Avenue
Argonne, Illinois 60430